NTNU

Norwegian University of
Science and Technology

Feasibility investigation for the application of direct AC-AC conversion in offshore wind power based on a comparative evaluation

Kristian Prestrud Astad

Master of Science in Energy and Environment
Submission date: June 2010
Supervisor: Marta Molinas, ELKRAFT

Norwegian University of Science and Technology
Department of Electric Power Engineering

Problem Description

A comparative evaluation between a direct AC-AC converter system and an AC-DC-AC solution for multiple generator topologies in wind energy conversion systems. The comparative evaluation will be based on a detailed investigation of losses, silicon usage in conversion, size, and number of elements to be able to draw an approximate feasibility figure. Input to the master part of the work will be the conclusions drawn from the project part and improvements will be suggested out of the comparative evaluation.

Assignment given: 15. January 2010
Supervisor: Marta Molinas, ELKRAFT

Abstract

In this thesis a feasibility study of a direct AC-AC converter for wind power application has been performed. Two three-phase voltages are converted to a single phase square wave for input to a high-frequency transformer and then rectified. No DC-capacitor is present in the converter and bi-directional switches consisting of two reverse blocking IGBTs allow the direct AC-AC conversion. Efficiency, silicon usage, price and output quality of the converter were to be compared with a reference case and conclusions to be drawn from the obtained results. The price comparison could not be finalized due to lack of price data.

The efficiencies were found to be 97.7 % for both the converter setups while the silicon usage was 4.6 % lower for the direct AC-AC solution. A back-to-back converter was used as the reference case. The harmonic content was less in the back-to-back converter and DC-offsets in the phase currents caused power oscillations for both converters but they were higher in the direct AC-AC converter. The reference case needs more switches than the direct AC-AC solution if put in a split drivetrain configuration and DC-capacitors are also present in the former. The size is therefore expected to be lower for the AC-AC solution.

The obtained results was used to conclude that the direct AC-AC solution is a feasible solution for a split drivetrain configurated wind turbine with multiple generators.

The voltage of the square wave in the direct AC-AC converter needs to be two times higher than the DC-voltage in the reference case to obtain the same rated voltage in the generators when they are supplying power simultaneously. The switch voltage ratings must then be increased accordingly. Another application was proposed to better exploit the converter topology examined and to avoid the doubled voltage rating. An isolated power system with a time varying energy source such as a wind turbine needs an auxiliary power source to be able to supply the full load power when the other is unavailable. The double input converter can then control the two generators so that a constant output power is achieved. The square wave voltage amplitude can then be dimensioned from the load power only rather than for the total rated power in the two generators. It is therefore halved and the voltage stresses on the switches are similarly reduced.

Preface

This is my Master's thesis in Electric Power Engineering carried out at the Faculty of Information Technology, Mathematics and Electrical Engineering at the Norwegian University of Science and Technology(NTNU). A new direct AC-AC converter topology for wind power applications has been investigated and different approaches and methods have been undertaken to fully comprehend the operation and the feasibility of the converter.

Besides the knowledge I have gained during this work is also a growing awareness of the numerous parts of power engineering that I do not know anything about, yet. The curiosity and interest that made me choose this study program will still be a driver in my continued work in this field but now outside the university.

A great thanks goes to my supervisor and inspirer, Marta Molinas, who has been giving input to my thesis all the way from the very beginning and for encouraging me to present my work in a technical conference.

I would also like to thank Alejandro Garcés for always having time for my carefully and not so carefully considered questions.

My office was nothing more than the best I could have been a part of, thank you for the fun, laughter and from time to time some technical discussions.

I am also lucky to have a wife who has made the hard days easier.

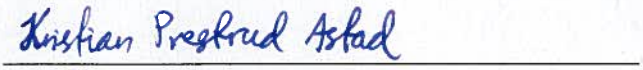

Kristian Prestrud Astad
Trondheim, Norway
June 10, 2010

Contents

List of Figures

List of Tables

1 Introduction

1.1 Motivation of the study

Wind power has been and is a major contributor to the generation of renewable energy. The size and rating of the turbines are increasing and research is performed to overcome problems with weight, cost and reliability. Wind turbines are placed offshore due to the fact that winds are higher there but long distances from shore introduce new challenges as transformers are needed to boost the voltage to provide a high transmission voltage. DC power transfer solutions are favored as they give the lowest losses for long distances. [6] Offshore converter stations or series connection of wind turbines with a DC output are then necessary for obtaining a voltage level sufficient for power transmission to shore.

In this thesis a feasibility study on a direct AC-AC solution for a specific generator setup with a low number of switches is to be performed. The AC-AC solution includes an active rectifier and a high-frequency transformer stage to make possible a DC series connection of the wind turbines. The two converter stages are further abbreviated the nine-switch converter or the 9SC in the rest of the document. This thesis is a continuation of my specialization project with the title "Double Input AC/AC Nine-Switch Converter for Wind Power Applications" [1] performed at the Norwegian University of Technology and Science(NTNU), autumn 09. Conclusions from the project are used as input for the continued research and highlights are listed in section 1.4.1.

The direct AC-AC solutions offers advantages such as no DC-capacitor present in the converter and less converter stages. This reduces the weight and component number and may offer a lower maintenance demand. The AC output can be fed into a transformer and provide isolation between the generator and the grid. The possibility of a high-frequency output from the converter gives the ability to greatly reduce the size of the transformer as size and frequency are inverse proportional. However there are possible trade-offs connected to the mentioned advantages. The undertaken feasibility study tries to unveil all features of the converter and give a conclusion regarding its applicability in offshore wind turbines.

1.2 Double input AC-AC nine-switch converter

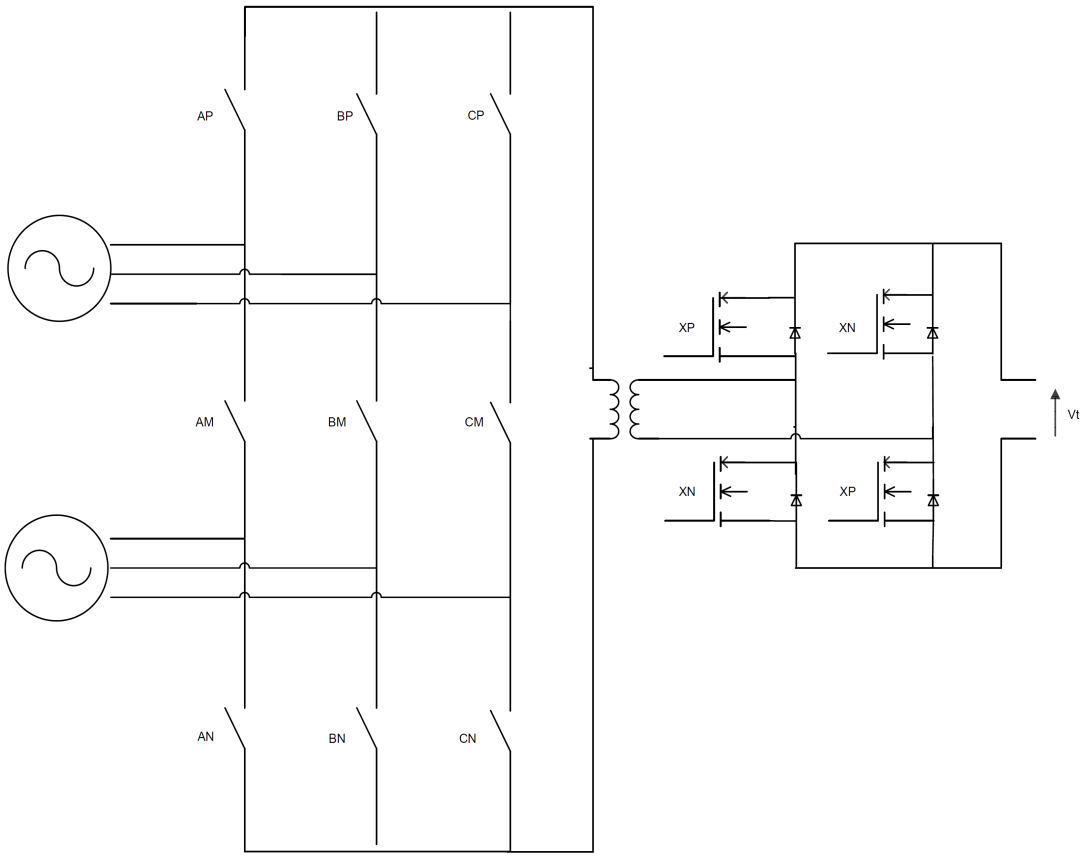

Figure 1.1: Converter Structure

Wind turbines with split drivetrains and back-to-back converters are already commercial [7] and help reduce gear size and thus weight, but still the voltage is too low for HVDC power transfer, which is the preferred offshore solution for long distances. [6] The nine-switch converter shown in figure 1.1 is suitable for split drivetrain topologies with more than one generator. The double input AC-AC nine-switch converter can convert the variable frequency AC to high-frequency square wave AC. This square wave can be fed into a transformer and converter and thus give a high voltage DC by series connection with other wind turbines and proper selection of transformation ratio. This would be a possible configuration for direct power transfer to shore. The split drivetrain configuration with multiple generators can use one nine-switch converter for each pair of generators and this is expected to reduce size and cost of the power electronics compared to conventional back-to-back converters. At the same time this will allow modularity from which reliability, maintenance and assembly will greatly benefit. The energy conversion system

is shown in figure 1.2.

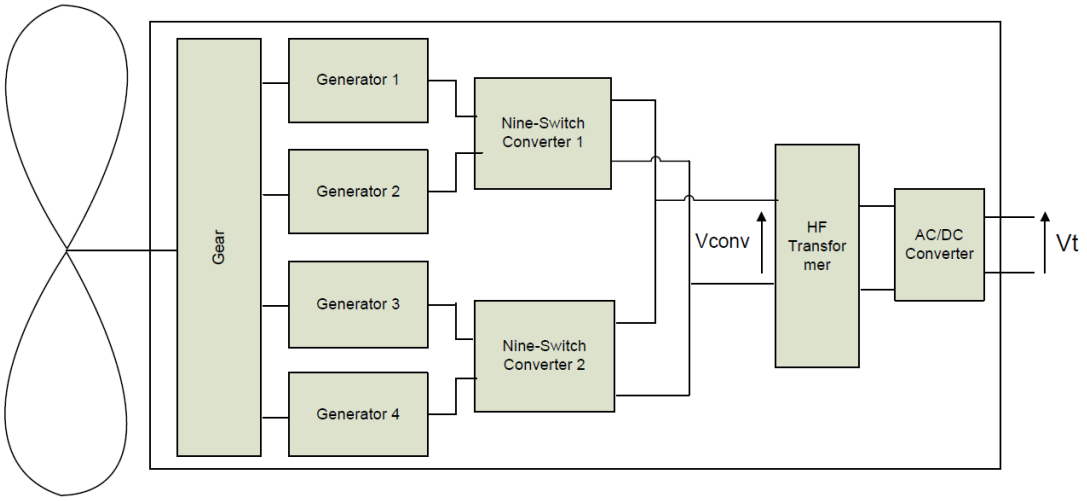

Figure 1.2: System layout of nacelle

The nine-switch converter was derived from [8] by Garcés and Molinas in [2] and modified to adapt to the specific application investigated in this thesis. The converter in [8] is a nine-switch inverter for independent control of two three-phase loads. By employing bi-directional switches instead of the IGBTs with diodes in anti-parallel, an AC square wave output can be achieved. The capacitor originally present is also eliminated, which helps reduce the weight, size and maintenance demand of the converter.

1.3 Back-to-back converter

A variable speed wind turbine with a back-to-back converter including a high-frequency isolation transformer is presented in [9] for DC series connection of wind turbines. This back-to-back converter system is used as the reference frame for the feasibility study and is depicted in figure 1.3. It is abbreviated BTB throughout the document. It has three conversion stages and therefore a high number of switches. The DC-capacitor present offers power decoupling between the generator and the grid but it is bulky and usually the component with the lowest lifetime. [10]

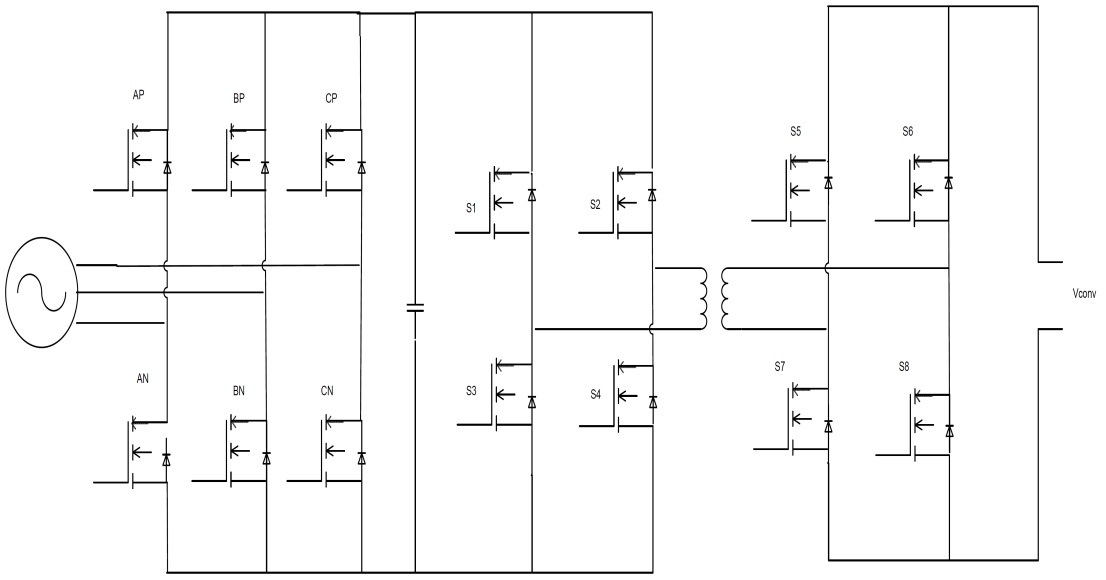

Figure 1.3: Back-to-back converter

1.4 Background

1.4.1 Previous work

A nine-switch inverter for independent control of two three-phase loads was presented in [8] and its operation and switching scheme was explained. The optimal PWM for the same converter was addressed in [11] while space vector modulation was investigated in [12]. A one-stage AC-AC converter with a quasi-DC link was investigated in [13] reducing the switch number compared to a back-to-back voltage source converter. These converters utilize IGBTs and includes a capacitor. Garcés and Molinas modified the nine-switch inverter from [8] and eliminated the DC-link capacitor in [2] by introducing reverse-blocking IGBTs for a direct AC-AC solution. With the reverse-blocking capability a direct AC-AC conversion was also obtained.

A specialization project was written as an introduction to this thesis and operation of the direct AC-AC nine-switch converter in a split-drivetrain configuration was investigated. Simulations were performed both with induction generators and a simplified synchronous generator model as input sources. The available square wave voltage was successfully shared between the two generators but with high current and voltage THDs compared to a back-to-back converter setup. The back-to-back converter setup was the same as the reference case used in this thesis. The high-voltage THD was due to the inevitable sharing of the voltage source between the two generators. The voltage in the DC-side of the converter had to be doubled in the nine-switch converter to obtain the same rated voltage at the generator terminals as in the back-to-back converter. This is visualized in figure 1.4 where the fundamental RMS voltage and the corresponding

line-to-line voltage is shown. The demanded blocking voltage in the switches was therefore doubled and this adverse property was recognized as the main disadvantage in the nine-switch converter.

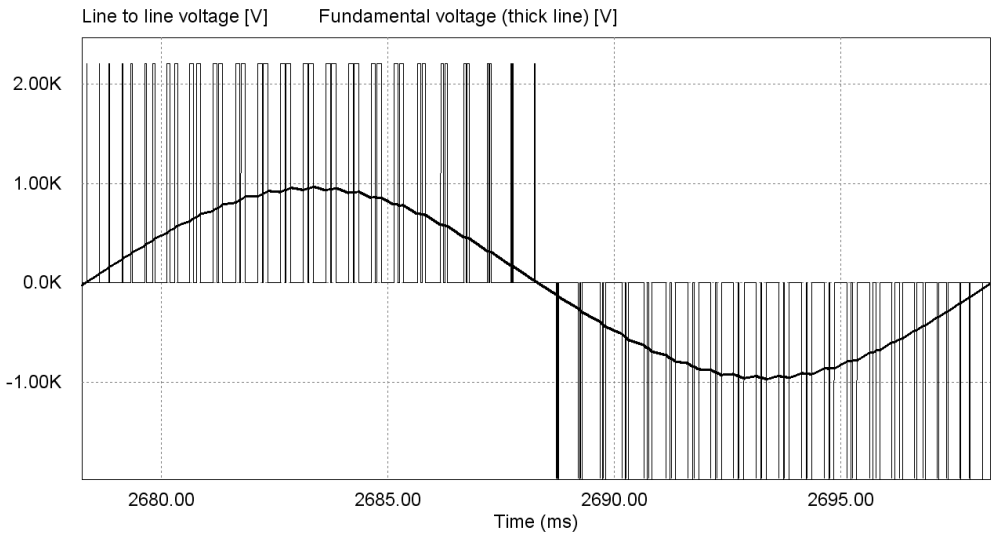

Figure 1.4: Fundamental RMS voltage and line-to-line generator voltage [1]

The number of switches in the nine-switch converter is less than for comparable converters such as the back-to-back converter which would include ten switches to obtain the high-frequency square wave but with just one input source. The DC capacitor is also eliminated which saves space, weight and cost in the nacelle. The disadvantage is the lack of power decoupling in the converter which leads to no possibility of storing the generated power during a grid fault.

Two reverse-blocking IGBTs(RB-IGBT) in anti-parallel made up the bi-directional switch. The RB-IGBT is a modified IGBT with a reverse blocking capability and this characteristic can be obtained in different ways. The production methods are time consuming and expensive and the maximum available blocking voltage today is only 1200 V compared to IGBTS that have up to 6500 V. [14] Promising production methods are mentioned in literature but mass production and high rated switches are yet to come.

1.4.2 Direct AC-AC converter solutions

Numerous solutions have been introduced by researchers to achieve low-weight, high-efficiency solutions with few components and low maintenance demands. However the number is greatly decreased if only AC-AC solutions are to be considered. Three direct AC-AC converter solutions are explained briefly to show some possible topologies for direct AC-AC conversion. A DC power transfer solution with no offshore platform for converter and transformer is set as a prerequisite so that the three-phase output has to be rectified with a transformer stage included inside the wind turbine. Garcés and Molinas

presented five different converter setups in [2] all of them including a transformer and a full converter setup in the nacelle. The nine-switch converter and the back-to-back already are already explained and are therefore omitted in this review.

The reduced matrix converter in figure 1.5 with a high-frequency converter offers a low number of switches and no DC-capacitor due to the use of bi-directional switches.

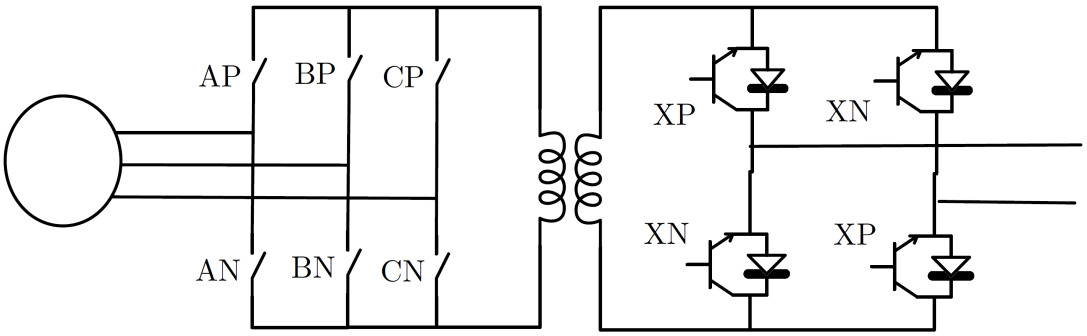

Figure 1.5: Reduced matrix converter [2]

Another reduced matrix converter with a three-winding transformer offers an even lower number of switches by having two primary windings in the transformer and only bi-directional switches. This is shown in figure 1.6.

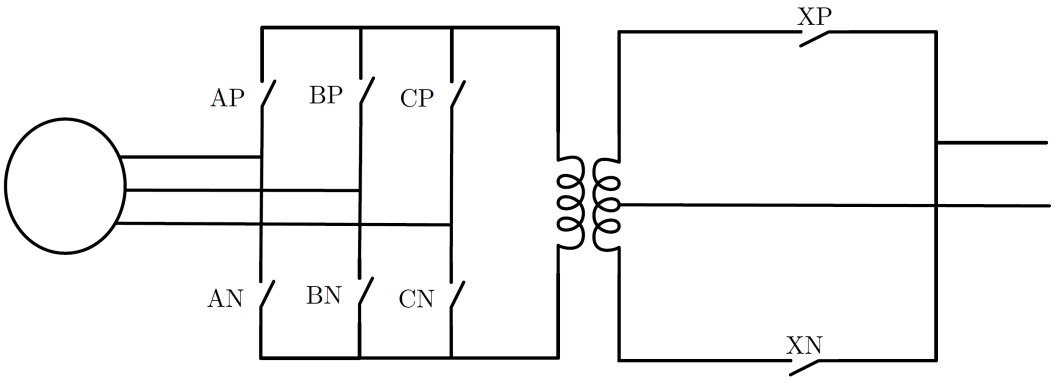

Figure 1.6: Reduced matrix converter with three-winding transformer [2]

The matrix converter in figure 1.7 has no DC-capacitor as the other AC-AC solutions but a higher number of switches is evident both due to the AC-AC stage and the three-phase output from the transformer.

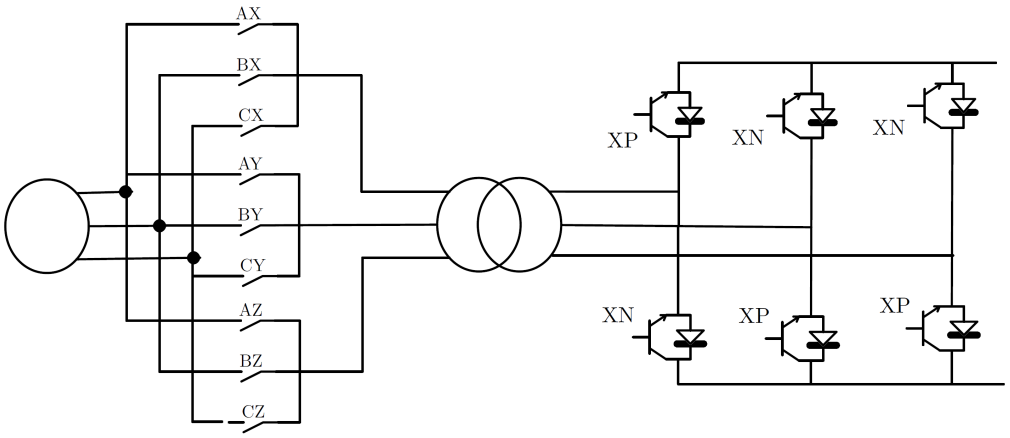

Figure 1.7: Matrix converter with three-winding transformer and full-bridge converter [2]

The different converter topologies show a variety of possibilities for implementing a high-frequency transformer and further rectification before transferring power to shore. The switch numbers and switch type differ and the capacitor is eliminated due to its maintenance demand in most of the topologies. All solutions except the nine-switch converter are based on one generator inside the turbine and then conversion and rectification after an optional gear box. When comparing different solutions several matters have to be taken into account. Efficiency, complexity, price, silicon usage, maintenance demand, size and weight are all important when determining which converter solution to be used. In this feasibility study of the nine-switch converter, efficiency, silicon usage, price and output quality is compared with the reference case.

DC series connection of wind turbines was intended in the project work and a figure of the possible layout is shown in figure 1.8. The transmission voltage is then proportional with the number of connected nacelles.

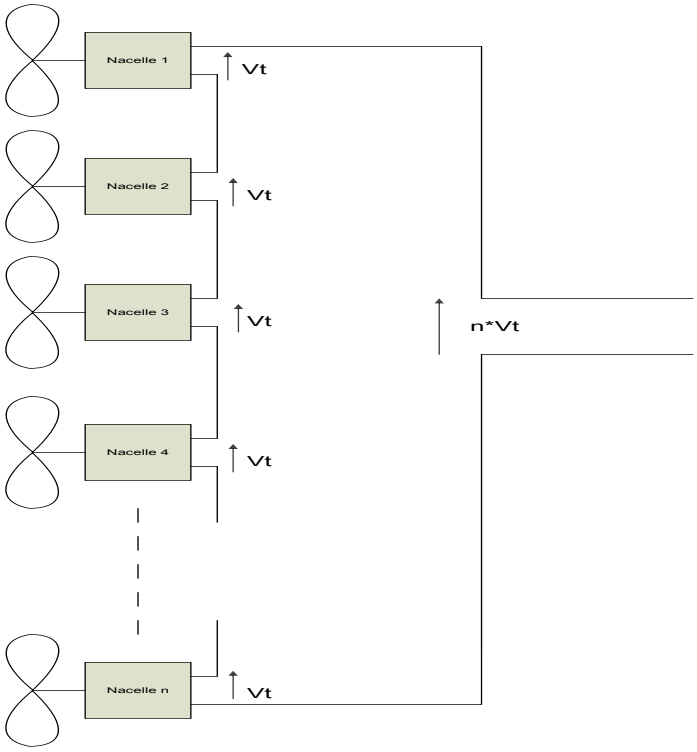

Figure 1.8: Series connection of wind turbines

1.5 Outline of the thesis

- **Section 2** includes output characteristics and special features in the converters with focus on the nine-switch converter. Results from this part is used in the further sections.
- **Section 3** presents the power losses in the semiconductors and in the DC-link capacitor. A brief explanation of the different types of losses and methods for calculating these are given. Conditions for the calculations are given and the results are presented graphically and in numbers.
- **Section 4** is included to examine the cost figures to be expected for the two different converters. Semiconductor cost per output kW is used for comparison rather than just comparing total cost for the converters as the topologies and switch number are different. Switch stresses for the given generator power is calculated to determine the necessary installed switch capacity for the given generator outputs.
- **Section 5** investigates the silicon usage in the different converter setups through a module driven method. Semiconductor losses are calculated with fixed thermal

settings for real switches to determine the maximum output power for the given switch ratings. The switch rating per output kW is then obtained and used for comparison.

- **Section 6** suggests other applications for the nine-switch converter addressing and solving some of the concerns related to its characteristics.
- **Section 7** analyze the results and methods in each part of the thesis.
- **Section 8** presents the key findings of the thesis.
- **Appendix A** contains an explanation of the special modulation technique in the nine-switch converter.
- **Appendix B** explains how the DLL-files linked with the simulation program to calculate the losses is determining what type of switching is occur
- **Appendix C** includes two conference papers with contents extracted from the research conducted in this thesis and in the specialization project.

2 Simulation study

In this section some characteristics of the converters are calculated through simulations. These characteristics are giving a background for the comparison and some values are to be used in the further sections. The simulations are performed in PSIM 9.0.1 and the transformer and semiconductors are ideal. An induction generator from the simulation program with preset parameters are used as input sources in the converters. Induction generator parameters are shown in table 2.1 and not all are given in the simulation program. The torque input to the generators are set to 60 Nm and 120 Nm for the nine-switch converter and back-to-back converter, respectively, to keep switch currents similar in the two setups.

Rated power	Not given	W
Rated voltage (line-to-line)	Not given	V
Rated frequency	Not given	Hz
Stator resistance	0.294	Ω
Stator inductance	1.39	mH
Rotor resistance	0.156	Ω
Rotor inductance	0.74	mH
Magnetization inductance	41	mΩ
Generator and rotor inertia	0.4	kgm^2
Number of poles	6	

Table 2.1: Operating data for induction generator

2.1 Phase currents and line-to-line voltages

The generator phase currents and the line-to-line voltages are given in table 2.2 for operation with DC-voltages of 400 V and 800 V. These operating voltages are chosen with background in the available switch ratings for the reverse blocking IGBTs. This is further explained in section 3.

	Fundamental RMS line-to-line voltage	RMS phase current
BTB 400 V	244.9 V	31.9 A
BTB 800 V	489.7 V	26.9 A
9SC 400 V	122.4 V	29.7 A
9SC 800 V	244.9 V	28.9 A

Table 2.2: Line-to-line voltages and phase currents in the generators

2.2 Power factor and displacement power factor

The power factor(PF) and displacement power factor(DPF) is calculated by a measuring block in the simulation program. The power factor is defined as:

$$PF = \frac{P}{S} \tag{2.1}$$

where P is the average real power and is found by filtering out the 50 Hz components from the voltage and current curves. S is the apparent power and is found from the non-filtered values. The displacement power factor is the cosine of the phase angle between the fundamental voltage and fundamental current. The PF and DPF found in the simulations are listed in the table below.

	Power factor	Displacement power factor
BTB 400 V	0.71	0.87
BTB 800 V	0.43	0.53
9SC 400 V	0.51	0.87/0.88
9SC 800 V	0.42	0.74/0.75

Table 2.3: Power factors in the converter setups

2.3 Harmonic content

The total harmonic distortion(THD) is calculated in PSIM with a THD block which uses a 2nd order filter to extract the fundamental frequency. The equation for the calculation of the THD, here with the voltage as the variable, is:

$$THD = \frac{\sqrt{V_{rms}^2 - V_1^2}}{V_1}. \tag{2.2}$$

where V_{rms} is the total RMS-value of the input voltage and V_1 is the fundamental component. The THD of the current is calculated in the same manner.

Table 2.4 shows the current and voltage harmonic distortion in the two converter setups for operating voltages of 400 and 400 V. For the nine-switch converter two numbers are given if the values are different for the two generators in the converter setup. The first number corresponds to the upper generator.

	THD_i	THD_v
BTB 400 V	4.3 %	68.6 %
BTB 800 V	19.4 %	68.6 %
9SC 400 V	8.8 %	139.4/139.3 %
9SC 800 V	27.8/27.7 %	139.4/139.3 %

Table 2.4: Harmonic content in the converter setups

2.3.1 Power oscillations

The power output from the generators in the nine-switch converter are shown in figure 2.1 and in figure 2.2 the generator power from the BTB is shown.

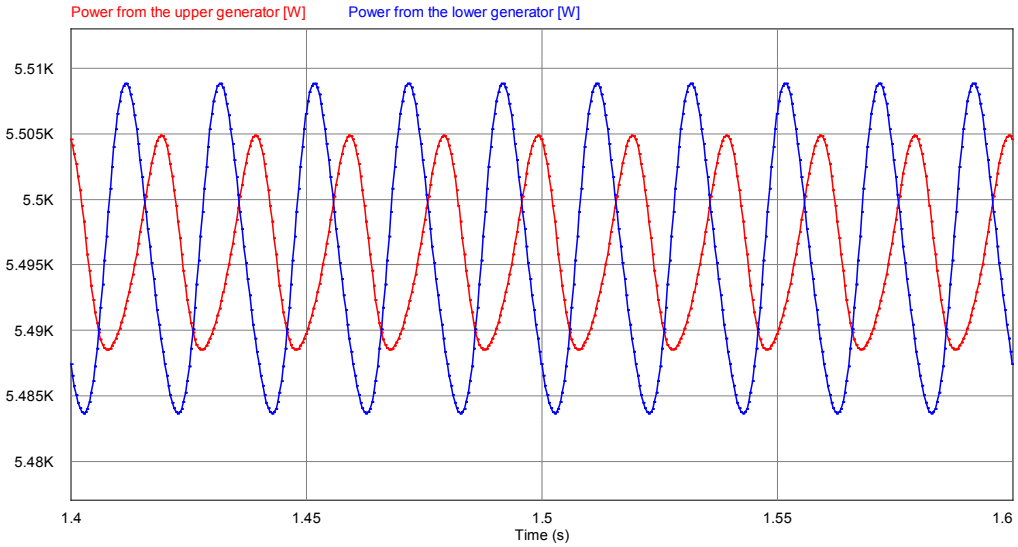

Figure 2.1: The generator output powers in the 9SC

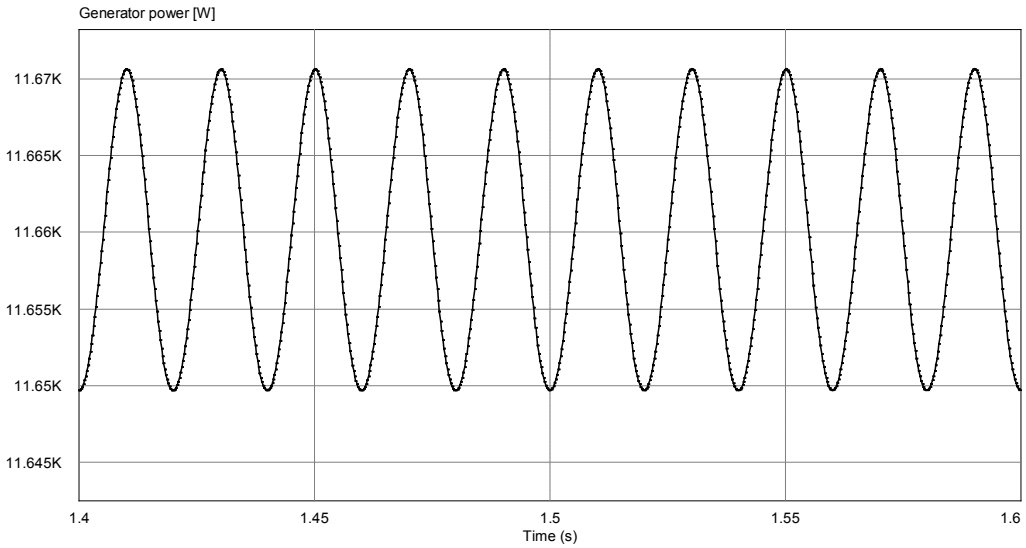

Figure 2.2: Generator output power in the BTB

Maintained oscillations with a frequency of 50 Hz is existent in all the power outputs and the amplitudes are shown in table 2.5.

	Generator 1	Generator 2
BTB 400 V	3.0 W	-
9SC 400 V	8.0 W	12.5 W

Table 2.5: Amplitude of 50 Hz power oscillations

The power output from a three phase power source is constant when the currents and voltages are both sinusoidal and each phase is shifted $\frac{2\pi}{3}$ radians from the other phases. The three-phase power can then be written as follows:

$$P_{3\phi} = \sqrt{(3)} V_{line-to-line} I \cos\phi \, [W] \tag{2.3}$$

A DC-current with amplitude I will cause a power oscillating with the same frequency as the available sinusoidal voltage with amplitude V and angular speed ω as seen in the derivation 2.4.

$$\begin{aligned} P &= IV[\sin(\omega t) + \sin(\omega t + \frac{2\pi}{3}) + \sin(\omega t \frac{-2\pi}{3})] \\ &= IV[\sin(\omega t) + \sin(\omega t)\cos(\frac{2\pi}{3}) + \cos(\omega t) sin(\frac{2\pi}{3}) \\ &+ \sin(\omega t)\cos(\frac{2\pi}{3}) - \cos(\omega t)\sin(\frac{2\pi}{3})] \\ &= VI\sin(\omega t)(1 + \cos(1 + 2\cos(\frac{2\pi}{3}))) \\ &= VI\sin(\omega t)\, [W] \end{aligned} \tag{2.4}$$

The addition theorem for sinusoidal functions given in equation 2.5 was used in the derivation.

$$\sin(\alpha + \beta) = \sin(\alpha)\cos(\beta) \pm \cos(\beta)\sin(\alpha) \tag{2.5}$$

The phase currents are plotted in figure 2.3 to investigate if a DC-current is present and thus causing the power oscillations.

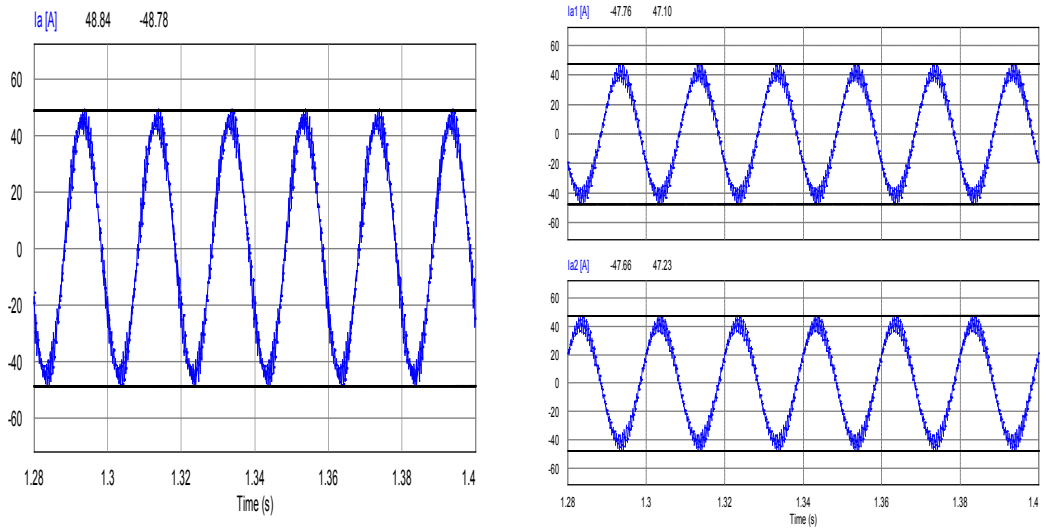

(a) Back-to-back converter

(b) Nine-switch converter

Figure 2.3: Generator phase currents in the two converters

The current in phase A in both generators are shown for the nine-switch converter and they are separated in two figures and denoted with 1 for belonging to the upper generator and 2 for the lower. In all figures a line with the curve amplitudes are included. It is evident that a small DC-offset in the current is existent and this will be the reason for the power oscillations.

2.4 Nine-switch converter

2.4.1 Generator phase shift

The switch currents in the nine-switch converter change with the phase angle between the generators. The two extremes of 0 and 180 degrees phase shift are shown in sub figures 2.4a and 2.4b.

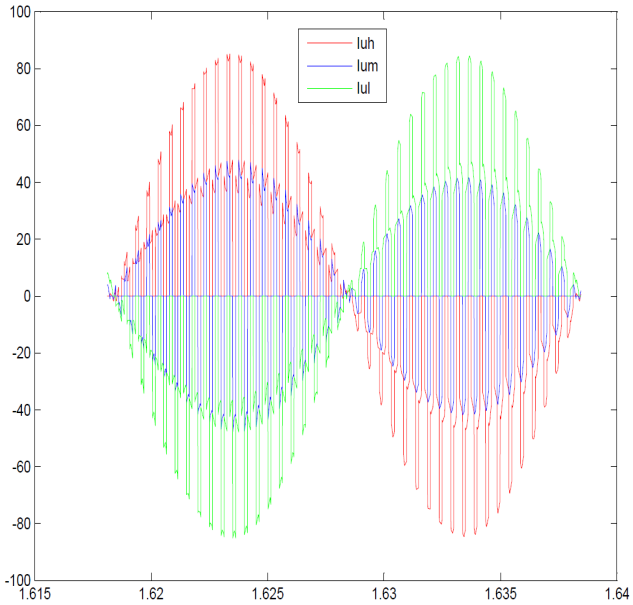

(a) 0 degrees phase shift

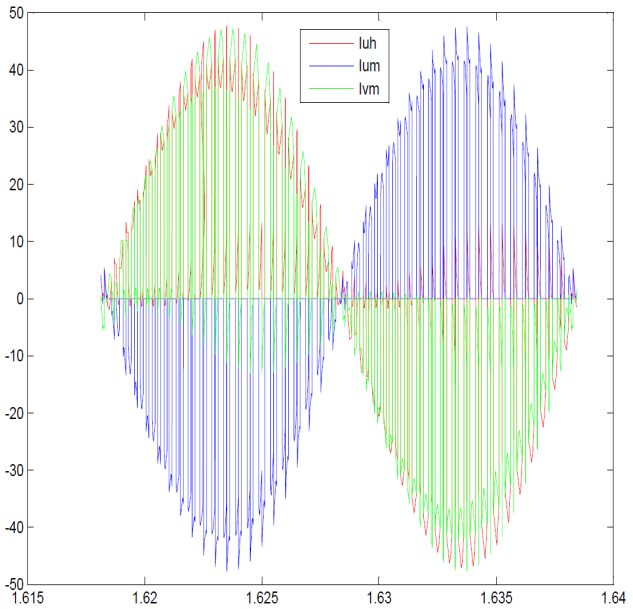

(b) 180 degrees phase shift

Figure 2.4: The switch currents in leg A with 0 and 180 degrees phase shift between the generators

The power output and generator speed are not changed with the change of phase angle and is shown in figures 2.5 and 2.6.

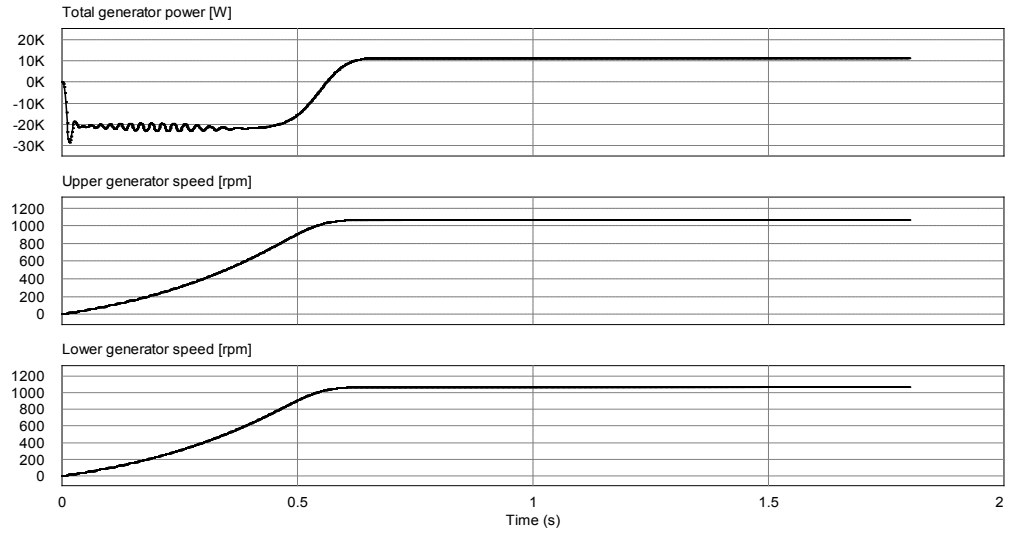

Figure 2.5: Total generator power and speed with 0 degrees phase shift between the generators

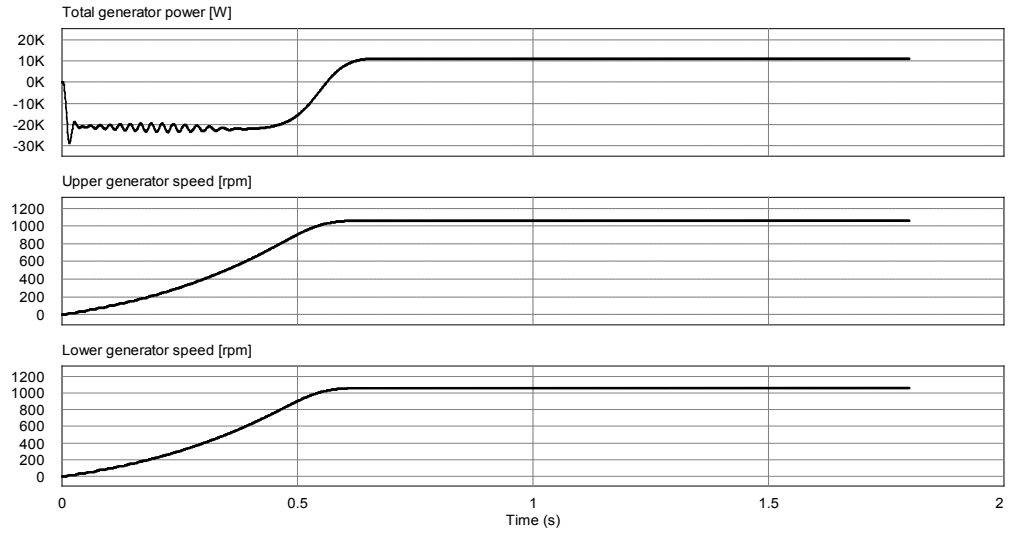

Figure 2.6: Total generator power and speed with 180 degrees phase shift between the generators

3 Efficiency investigation

Five types of losses apply in the semiconductors. Conduction, blocking, turn-on, turn-off and reverse recovery losses. The three latter ones are connected with the switching action while conduction is due to the resistance in the switch while it is conducting. The blocking losses are caused by leakage currents while the switch is blocking the voltages and are small compared to the others and thus neglected. [15]

If the switch is forward biased before turn-on, the voltage curve does not change in a step towards on-state voltage and at the same time the forward current is increasing causing a power loss. For turn-off the switch is gated off and the collector-emitter voltage starts to rise towards the blocking state value. The current does not decrease until the drain gate capacitance in the switch is fully charged. Until the current reaches zero, power losses occur.

For the reverse-blocking IGBTs the turn-on and turn-off losses are associated with the turn-on and turn-off in the IGBT part of the chip while the reverse recovery is due to the intrinsic diode in the RB-IGBT. Regular IGBTs do not have reverse-recovery but the anti-parallel diode experience reverse recovery losses. The reverse recovery loss in the RB-IGBT occur when the RB-IGBT stops conducting due to reverse-bias of the intrinsic diode, i.e. the voltage over the switch is changing polarity with the RB-IGBT still gated on. The intrinsic diode will then behave as a normal diode and exhibit reverse recovery losses.

Two different methods are used to calculate the losses in the RB-IGBTs from the two manufacturers, Fuji Electric and IXYS. No data sheets are available for the RB-IGBTs from Fuji, but a paper from Fuji Electric describing loss calculations is used. For the IXYS semiconductors, data sheets are available, and energy losses are calculated through the switching energies given in the data sheets. The two methods are described further in the next two sections.

3.1 Loss calculation for Fuji semiconductors

The losses in the RB-IGBTs are calculated by using a simplified method developed and verified by experiments in [16]. Quadratic equations describing the loss characteristics are implemented in a DLL-file connected to the simulation program. These equations are for a 600 V, 200 A RB-IGBT. The simulation program uses ideal switches and calculates the switch currents and voltages and feed the values to the DLL-file. The DLL-file classifies which switching type that is occurring and calculates the losses by using the following equations [16]:

Conduction loss, P_{cond}:

$$P_{cond} = I_C \cdot V_{CE}\,[W] \tag{3.1}$$

where I_C is from the simulation program and V_{CE} is calculated by equation 3.2.

$$V_{CE} = \frac{-b + \sqrt{b^2 - 4 \cdot a \cdot (c - I_C)}}{2a}\,[V] \tag{3.2}$$

where $a = 22.789$, $b = 28.536$, $c = -32.091$ and I_C is the collector current.

Turn-on loss, E_{on}:

$$E_{on} = k_1 \cdot {I_C}^2 + k_2 \cdot I_C \; [mJ] \tag{3.3}$$

$$k1 = 8.14 \cdot 10^{-12} \cdot V_C + 1.78 \cdot 10^{-7} \cdot V_C \tag{3.4}$$

$$k_2 = 2.78 \cdot 10^{-7} \cdot V_C^2 + 1.32 \cdot 10^{-5} \tag{3.5}$$

Turn-off loss, E_{off}

$$E_{off} = k_1 \cdot I_C^2 + k_2 \cdot I_C \; [mJ] \tag{3.6}$$

$$k1 = 4.77 \cdot 10^{-8} \cdot V_C + 4.92 \cdot 10^{-5} \cdot V_C \tag{3.7}$$

$$k_2 = -2.98 \cdot 10^{-9} \cdot V_C^2 + 2.11 \cdot 10^{-4} \tag{3.8}$$

Reverse recovery loss, E_{rr}

$$E_{rr} = k_1 \cdot I_C^2 + k_2 \cdot I_C \; [mJ] \tag{3.9}$$

$$k1 = -5.66 \cdot 10^{-11} \cdot V_C - 1.82 \cdot 10^{-7} \cdot V_C \tag{3.10}$$

$$k_2 = 3.73 \cdot 10^{-9} \cdot V_C^2 + 9.35 \cdot 10^{-5} \tag{3.11}$$

The switching losses are in mJ and are converted to instantaneous values by equation 3.12.

$$dW = \frac{E \cdot dt}{1000} \; [\mathrm{W}] \tag{3.12}$$

dW is then the instantaneous power loss found during the time step dt. The average value is found by summing up the instantaneous losses for a chosen period and then dividing by this period as shown in 3.13.

$$W_{avg} = \frac{\sum dW}{T} \; [\mathrm{W}] \tag{3.13}$$

where W_{avg} is the average power loss and T is the period for which the summation is done. The period is here set to 0.02 s and corresponds to the period of the sinusoidal voltage wave forms in the generators.

3.1.1 Special considerations for the full-bridge converters

The loss calculations for the IGBTs existing in both the full-bridge part of the nine-switch converter and in the back-to-back converter follows the same approach for calculating the conduction, turn-on and turn-off losses as for the RB-IGBT. This is because the RB-IGBTs from Fuji Electric have much the same characteristics as the IGBTs. [17] The diode conduction losses and reverse recovery of the diode are found by using values for an IGBT with anti-parallel diode with similar rating. Values for the on-state voltage as a function of the diode current has been extracted from the data sheet of the semiconductor found in [18]. The simulation program gives the diode current and a DLL-file calculates the on-state voltage and then the conduction loss for the diode. The fitted curve is shown in 3.1 and the equation describing this is included in the DLL-files in appendix B.

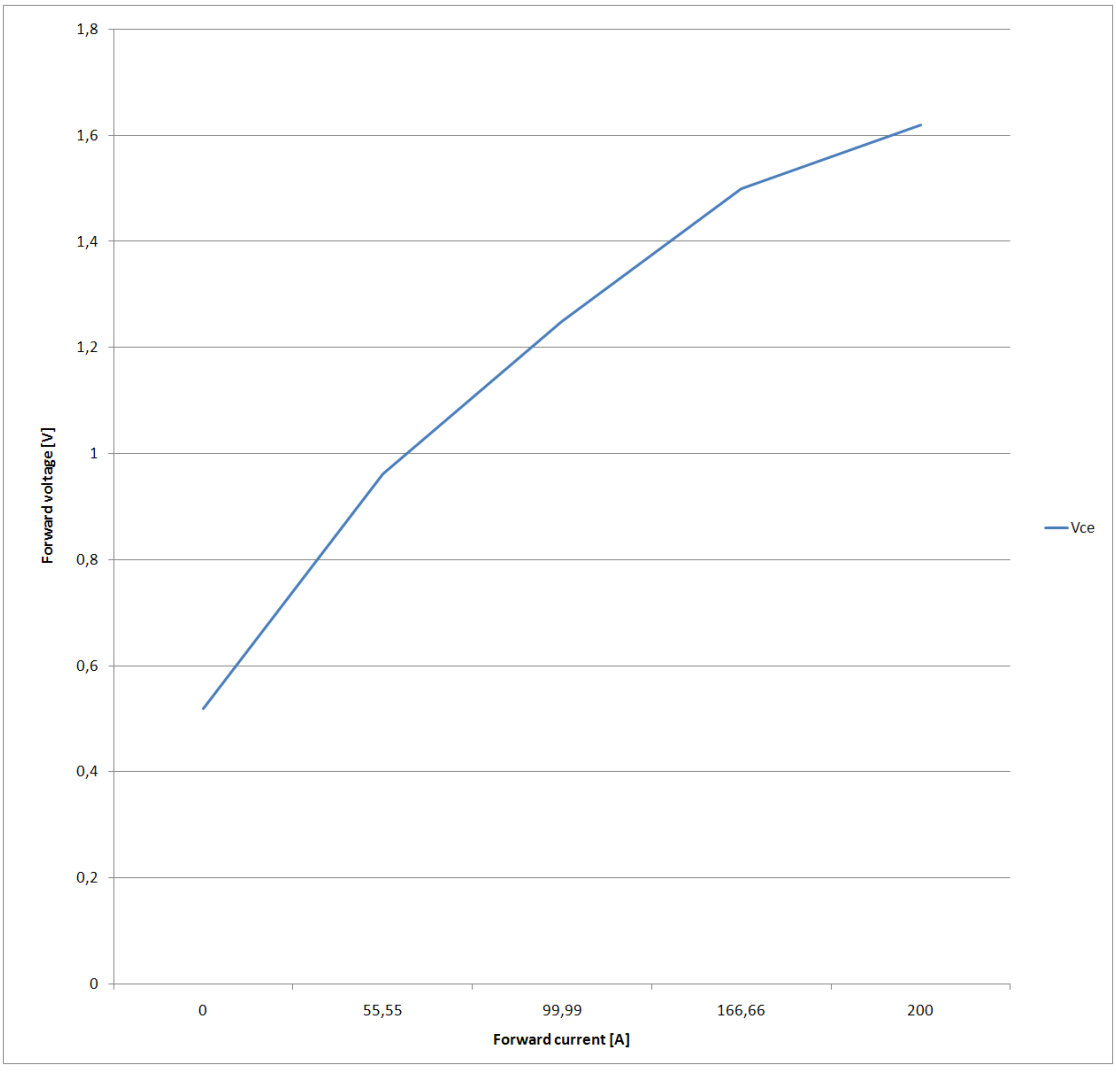

Figure 3.1: Forward voltage in the diode as a function of current

Reverse recovery losses in the diode is found by the switching energy given in the data sheets as a function of the switch current before turn-off. The voltage dependency of the losses are considered to be linear. [19] The voltage dependency is therefore added to the equations by multiplying the calculated switching energy by the ratio between the diode voltage after it stops conducting and the reference voltage at which the switch energies were given in the data sheets. Figure 3.2 shows the curve with the switching energy as a function of the current and the equations describing this is given in appendix B. The DLL-file measures current and voltage and determines if a reverse recovery is occurring in the diode. Diode turn-on losses are neglected as they are very small compared to the reverse-recovery losses. [20]

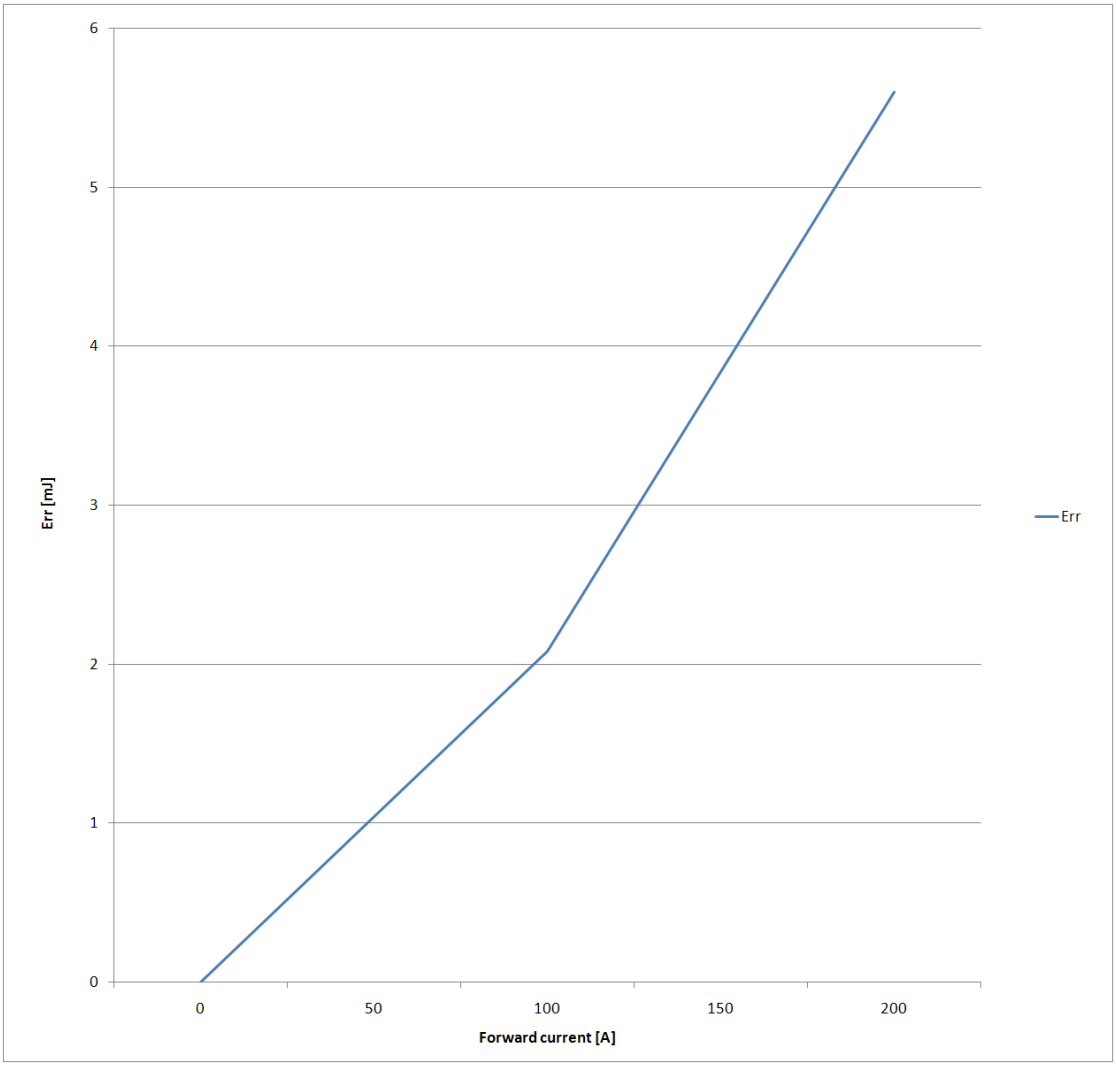

Figure 3.2: Reverse recovery in the diode as a function of current

3.2 Loss calculation for IXYS semiconductors

The switching energies from the data sheets are extracted in a piecewise linearization and the graphs showing the relation between the switching energies and forward currents are shown in figures 3.3 and 3.4. The linearized equations describing these graphs are given in the printout of the DLL-files in appendix B

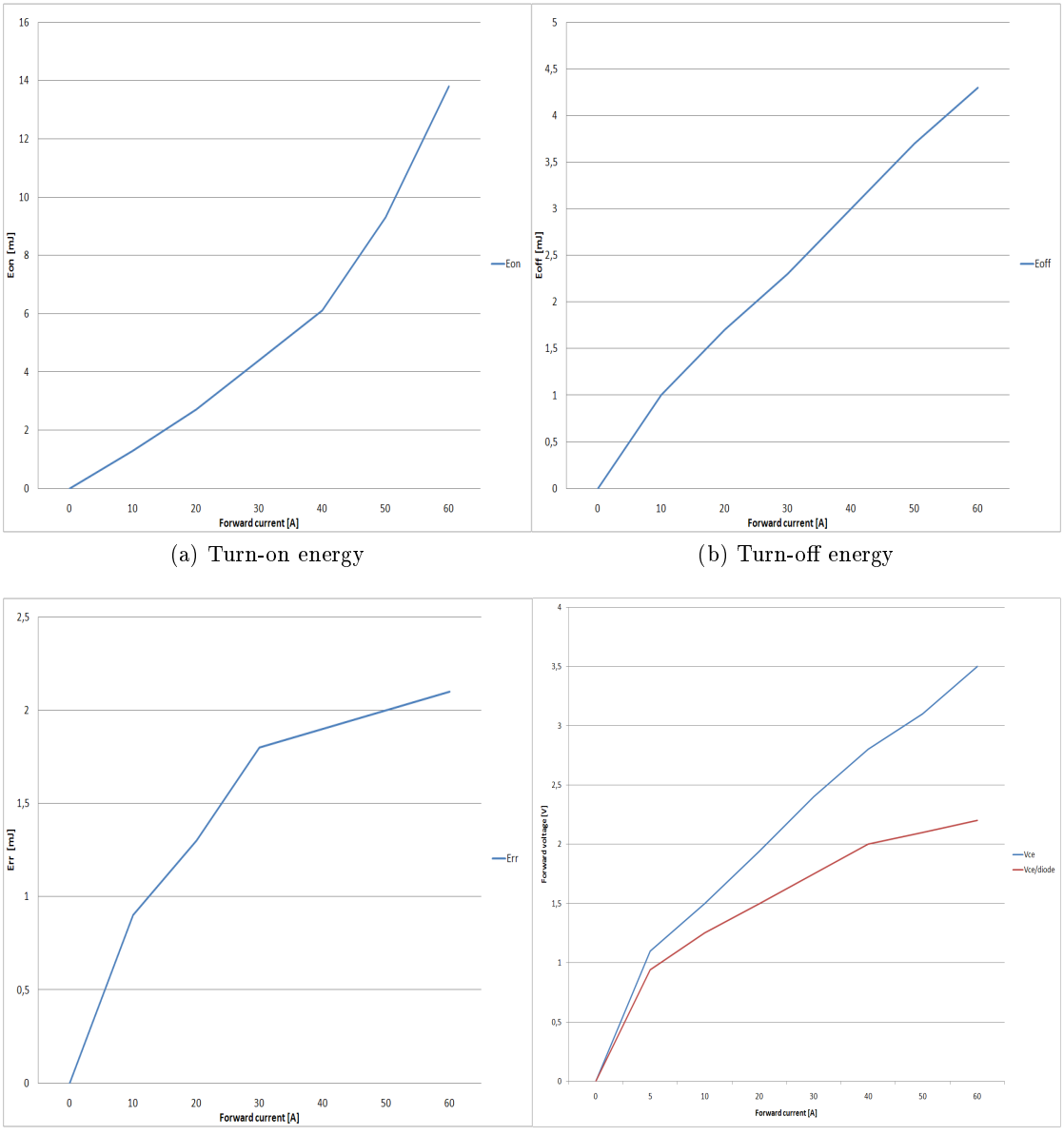

(a) Turn-on energy

(b) Turn-off energy

(c) Reverse recovery energy

(d) Forward voltages

Figure 3.3: Switching energies and forward voltages in the IGBT

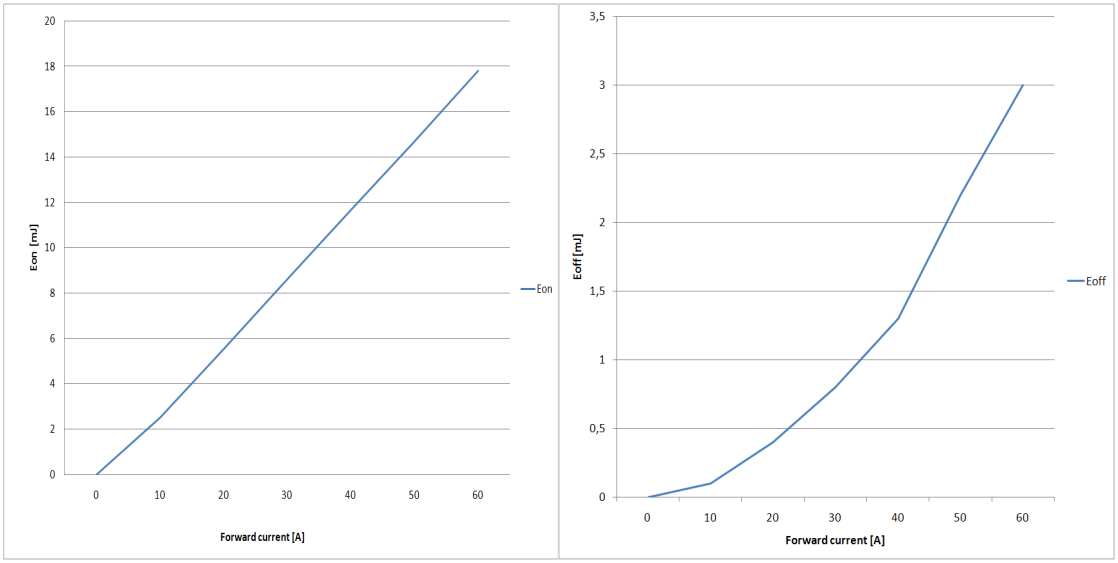

(a) Turn-on energy (b) Turn-off energy

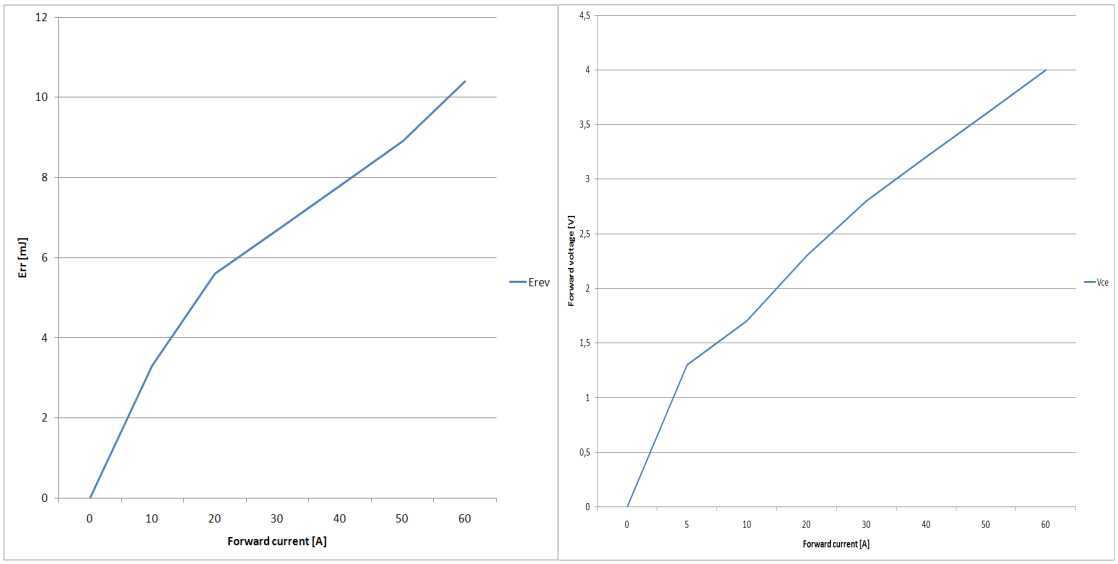

(c) Reverse recovery energy (d) Forward voltages

Figure 3.4: Switching energies and forward voltages in the RB-IGBT

3.3 Nine-switch converter

3.3.1 Results for Fuji Electric semiconductors

The loss calculations are performed with the nine-switch converter connected to two generators each running with an input torque of 60 Nm. This corresponds to a total power of 10.99 kW and the generators operate with an *RMS* line to line voltage of

122.4 V. The control signals for the converter are 180 degrees phase shifted to obtain equal current in the switches as was shown in section 2. The generator power and voltage are set in accordance with the switch ratings that the loss equations are based on. Induction generator data are given in section 2 in table 2.1.

The results are shown in table 3.1 and in figure 3.5.

	Conduction [W]	Turn-on [W]	Turn-off [W]	Reverse recovery [W]
AP	16.3	1.3	2.6	1.7
BP	16.4	1.4	2.8	1.6
CP	16.2	1.4	2.7	1.6
AM	15.5	2.6	4.8	3.4
BM	15.6	2.6	4.8	3.5
CM	15.5	2.6	4.8	3.5
AN	16.3	1.2	2.7	1.7
BN	16.4	1.4	2.7	1.6
CN	16.2	1.3	2.8	1.6
S1	11.4	0.0	0.0	0.17
S2	11.4	0.0	0.0	0.17
S3	11.4	0.0	0.0	0.17
S4	11.4	0.0	0.0	0.17
Sum	190.0	15.8	30.7	20.9

Table 3.1: Power losses in the nine-switch converter

The total switch loss and the percentage of the total losses are given in table 3.2.

	Total switch loss [W]	Percentage of total losses [%]
AP	21.9	8.5
BP	22.2	8.6
CP	21.9	8.5
AM	26.3	10.2
BM	26.5	10.3
CM	26.4	10.3
AN	21.9	8.5
BN	22.1	8.6
CN	21.9	8.5
S1	11.6	4.5
S2	11.6	4.5
S3	11.6	4.5
S4	11.6	4.5
Sum	257.5	100.0

Table 3.2: Losses per switch and percentage of total losses in the nine-switch converter

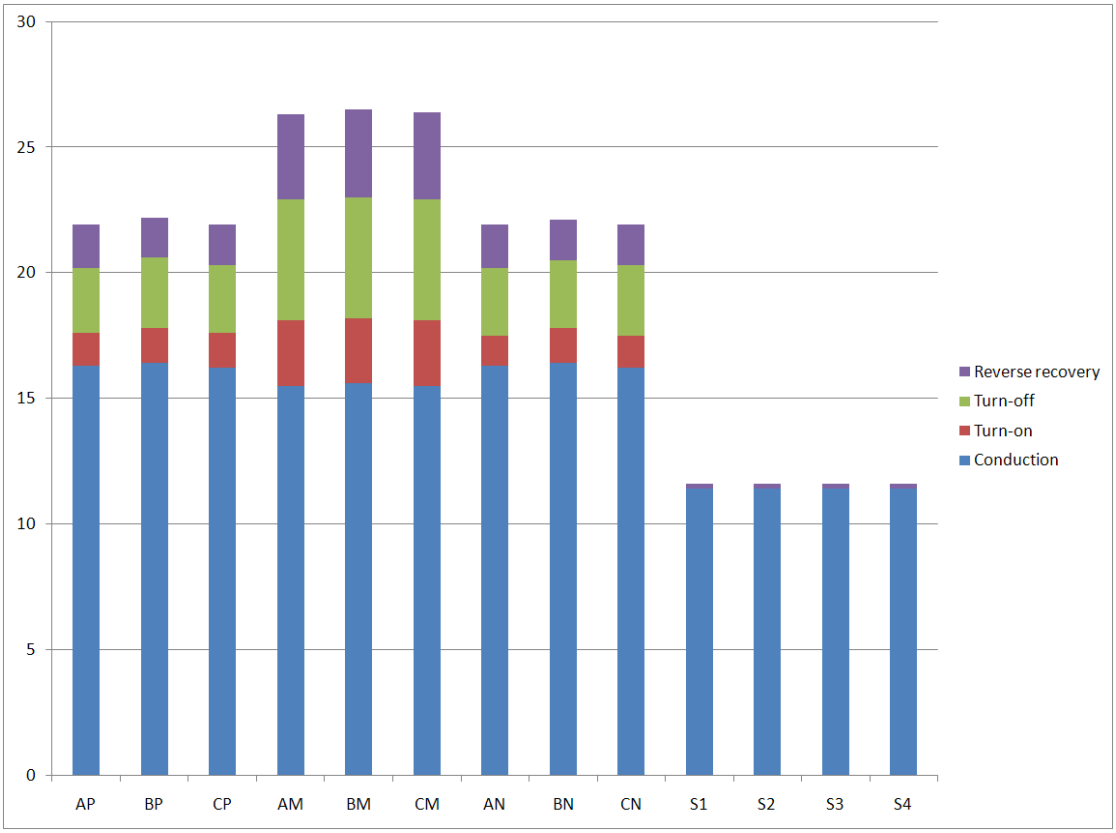

Figure 3.5: Power losses in each switch in the nine-switch converter

3.3.2 Results for IXYS semiconductors

The IXYS switches are rated at 1200 V and 55 A and 1200 V and 60 A for the RB-IGBT and the IGBT, respectively. The loss calculations for this case are done with twice the operating voltage compared to the Fuji case as the available blocking voltage is also twice. The input torques to the generators are kept at 60 Nm for each generator. The results are shown in tables 3.3 and 3.4. Figure 3.6 shows the results graphically.

	Conduction [W]	Turn-on [W]	Turn-off [W]	Reverse recovery [W]
AP	23.2	4.0	0.9	11.4
BP	23.6	4.2	0.9	11.1
CP	23.0	4.2	0.9	11.2
AM	19.7	10.4	1.2	21.3
BM	19.9	10.3	1.2	21.9
CM	19.4	10.3	1.1	21.7
AN	23.3	3.9	0.9	11.9
BN	23.5	4.2	0.9	11.3
CN	23.0	4.1	0.9	11.0
S1	11.7	0.0	0.0	0.29
S2	11.7	0.0	0.0	0.28
S3	11.7	0.0	0.0	0.28
S4	11.7	0.0	0.0	0.29
Sum	245.4	55.6	8.9	133.94

Table 3.3: Power losses in the nine-switch converter

	Total switch loss [W]	Percentage of total losses [%]
AP	39.5	8.9
BP	39.8	9.0
CP	39.3	8.9
AM	52.6	11.9
BM	53.3	12.0
CM	52.5	11.8
AN	40.0	9.0
BN	39.9	9.0
CN	39.0	8.8
S1	12.0	2.7
S2	12.0	2.7
S3	12.0	2.7
S4	12.0	2.7
Sum	443.9	100.1

Table 3.4: Losses per switch and percentage of total losses in the nine-switch converter

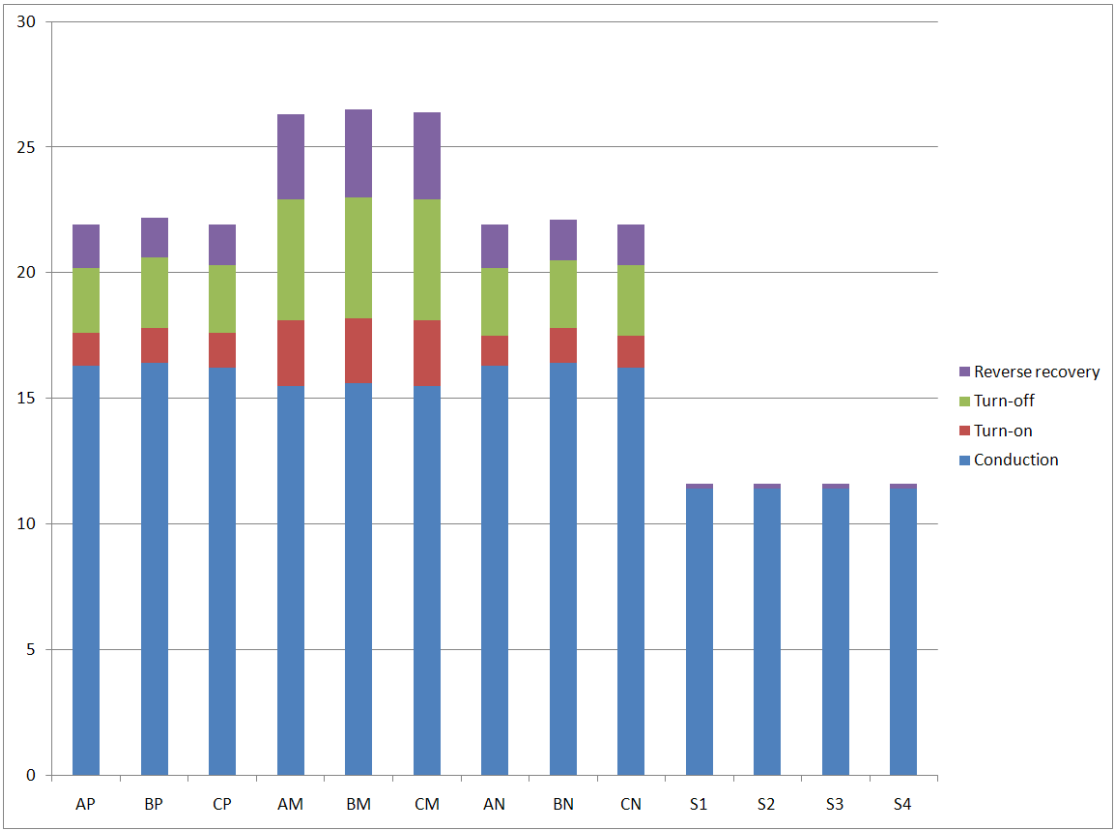

Figure 3.6: Power losses in each switch in the nine-switch converter

3.4 Back-to-back converter

The losses in the back-to-back converter are calculated for the same operating voltage as in the nine-switch converter. The line-to-line voltage in the back-to-back converter is then twice that in the nine-switch converter due to the different voltage utilization as calculated in section 5.2. The input torque to the generator is set to the sum of input torques to the nine-switch converter to keep the switch currents at similar levels in the different calculations.

3.4.1 Results for Fuji Electric semiconductors

	Conduction [W]	Turn-on [W]	Turn-off [W]	Rev. rec. [W]
AP	12.7	1.2	2.6	0.7
BP	12.7	1.2	2.6	0.7
CP	12.5	1.2	2.6	0.7
AN	12.5	1.3	2.7	0.7
BN	12.6	1.3	2.7	0.7
CN	12.6	1.2	2.6	0.7
S1	18.1	5.1	6.6	0.0
S2	18.2	5.2	6.5	0.0
S3	18.2	5.2	6.5	0.0
S4	18.1	5.1	6.6	0.0
S5	12.4	0.0	0.0	0.13
S6	12.5	0.0	0.0	0.14
S7	12.5	0.0	0.0	0.14
S8	12.4	0.0	0.0	0.13
Sum	198.0	26.6	42.0	4.7

Table 3.5: Power losses in the back-to-back converter

	Total switch loss [W]	Percentage of total losses [%]
AP	17.2	6.3
BP	17.2	6.3
CP	17.0	6.3
AN	17.2	6.3
BN	17.3	6.4
CN	17.1	6.3
S1	29.5	10.9
S2	29.5	10.9
S3	29.5	10.9
S4	29.5	10.9
S5	12.5	4.6
S6	12.6	4.7
S7	12.6	4.7
S8	12.5	4.6
Sum	271.3	100.1

Table 3.6: Losses per switch and percentage of total losses in the back-to-back converter

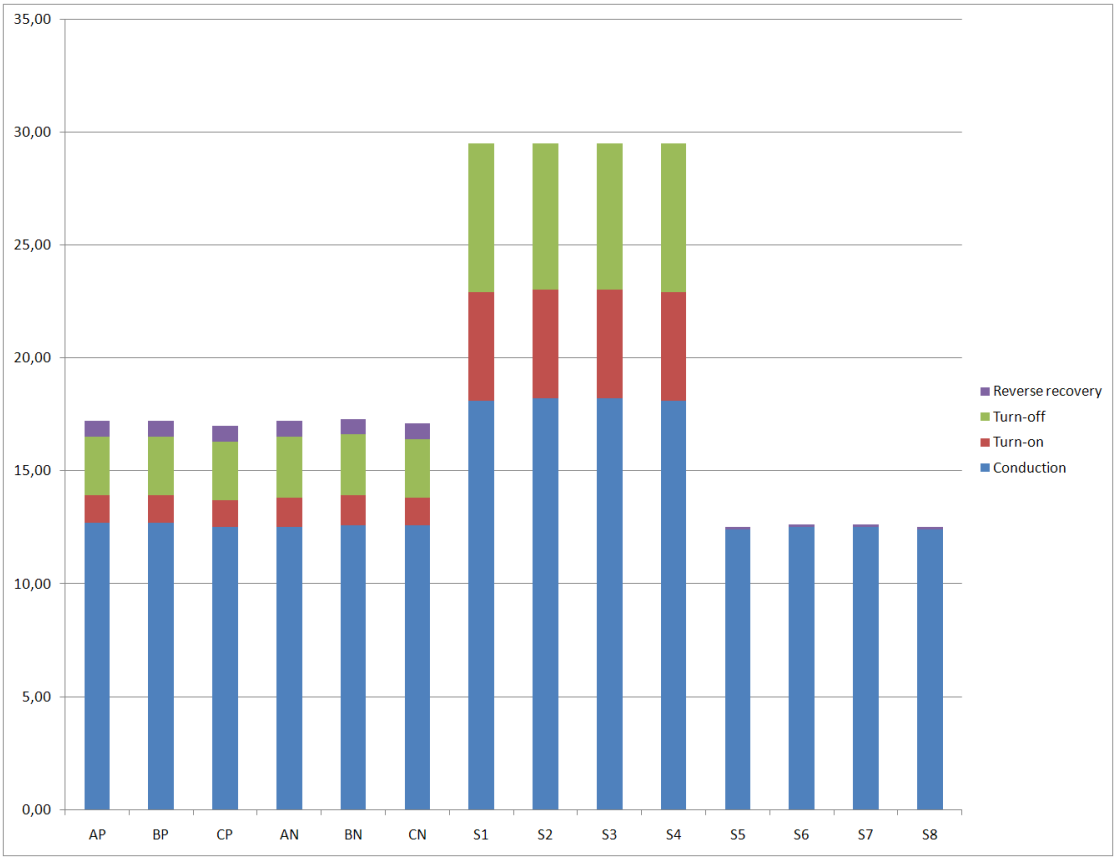

Figure 3.7: Power losses in each switch in the back-to-back converter

3.4.2 Results for IXYS semiconductors

	Conduction [W]	Turn-on [W]	Turn-off [W]	Rev. rec. [W]
AP	23.0	3.1	3.8	1.5
BP	23.1	3.2	3.8	1.5
CP	23.0	3.3	3.9	1.4
AN	22.7	3.3	3.9	1.4
BN	23.1	3.3	3.9	1.4
CN	23.3	3.1	3.8	1.5
S1	17.8	9.3	7.7	0.0
S2	17.8	9.5	7.6	0.1
S3	17.8	9.5	7.6	0.1
S4	17.8	9.3	7.7	0.0
S5	13.4	0.1	0.0	0.21
S6	13.4	0.1	0.1	0.22
S7	13.4	0.1	0.1	0.22
S8	13.4	0.1	0.0	0.21
Sum	263.0	57.3	35.1	9.8

Table 3.7: Power losses in the back-to-back converter

	Total switch loss [W]	Percentage of total losses [%]
AP	30.7	8.4
BP	30.8	8.4
CP	30.8	8.4
AN	30.5	8.4
BN	30.9	8.5
CN	30.8	8.4
S1	31.3	8.6
S2	31.5	8.6
S3	31.5	8.6
S4	31.3	8.6
S5	13.7	3.8
S6	13.8	3.8
S7	13.8	3.8
S8	13.7	3.8
Sum	365.1	100.1

Table 3.8: Losses per switch and percentage of total losses in the back-to-back converter

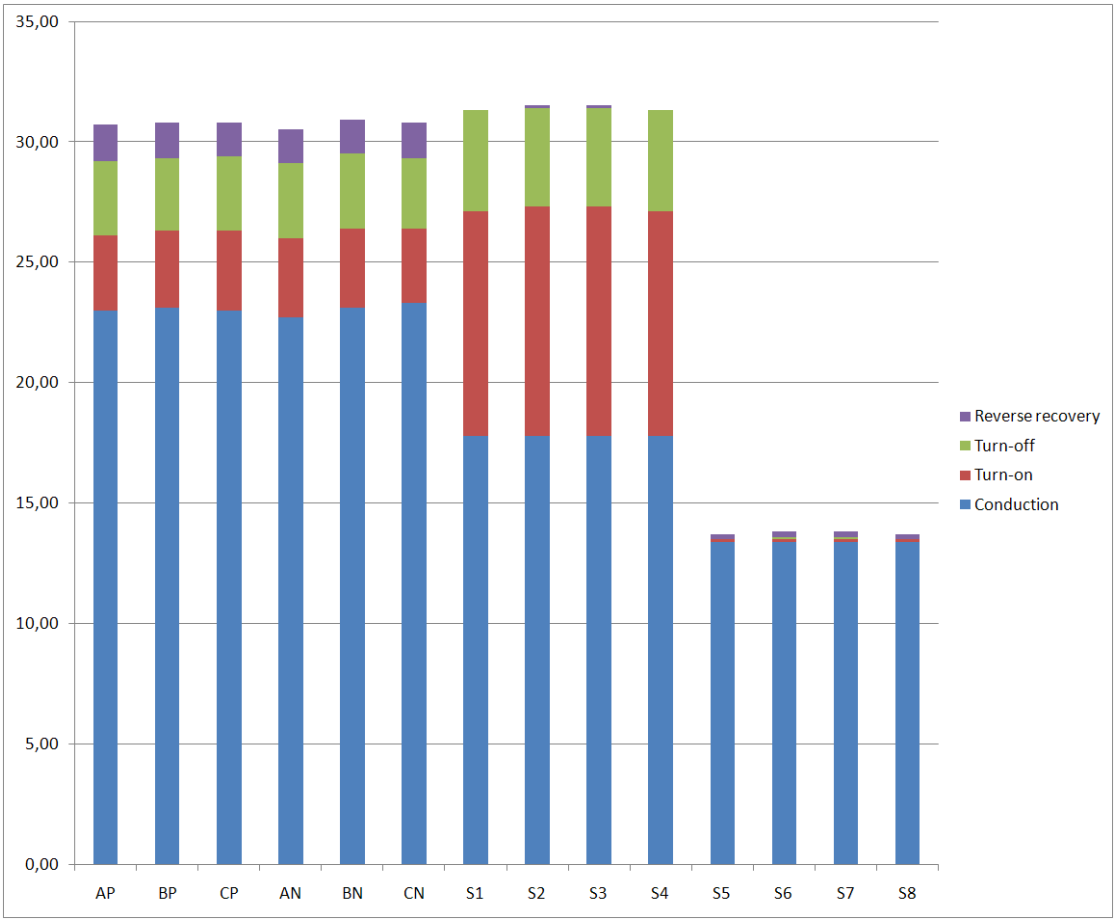

Figure 3.8: Power losses in each switch in the back-to-back converter

3.5 Capacitor losses

The DC-link capacitor in the back-to-back converter will add to the total losses due to the equivalent series resistance present in the capacitor and the leakage current. In the simulations the leakage current is neglected but the resistive losses in the series resistance is found by measuring the voltage drop in the resistance and multiplying with the capacitor current. The measured voltages and currents from the simulation program are fed to a DLL-file where the calculation is done and instantaneous loss values are obtained. The necessary capacitor rating is therefore identified and real capacitors from producers are found with the given equivalent series resistance included in the product data sheets.

The generator line-to-line voltage is governed by the switching action in the converter stage connected to the generator and has the DC-link capacitor as its voltage source. This DC-voltage is however not constant due to the high-frequency switching in the converter stages on both sides of the DC-link. The control system has to take the varying voltage into account to make sure that the generator voltage obtained is the desired one. The

voltage ripple in the capacitor can be reduced by increasing the capacitor size. The capacitor also decouples the power between the output and the input of the converter and can keep the wind turbine operating during a grid fault or such. The energy stored in a capacitor is given in the following equation.

$$E = 0.5C \cdot V^2 [\text{J}] \tag{3.14}$$

where E is the energy, C is the capacitance and V is the voltage. The energy storage capability is thus dependent on the voltage squared and on the capacitance. The capacitor operating voltage is given by the generator line-to-line voltage and the utilization of the DC-voltage for the converter found in section 5 in the voltage utilization subsection. However the voltage rating of the capacitor can be set higher than the operating voltage to allow a larger energy storage.

The lifetime and equivalent series resistance in the capacitor is also important when choosing capacitor. In an offshore environment maintenance demands should be kept at a minimum due to the fact that during winter time the possibilities for performing maintenance is small because of harsh weather conditions offshore.

In order to calculate the time the capacitor can absorb rated generated power a unit capacitance constant, (UCC), is introduced as defined by Fujita, Tominaga and Akagi in [21].

$$UCC = \frac{\frac{1}{2} \cdot C \cdot V^2}{S} \text{ [s]} \tag{3.15}$$

C is the capacitance given in Farad and V is the voltage given in volts. The available storage in the capacitor is determined by the difference between the operating voltage of the DC-link and the maximum voltage. For releasing energy the operating voltage should be used. For the back-to-back converter, the DC-link voltages are set to 400 and 800 V. The desired UCC is set to two periods of the 50 Hz rated generator frequency, equivalent to 40 ms.

The nominal power is found by using equation 3.16 where line-to-line voltages and phase currents are found in table 2.2 in section 2.

$$S = \sqrt{3} V_{line-to-line} \cdot I_{phase} \text{ [VA]} \tag{3.16}$$

The manufacturer Epcos was chosen for finding suitable capacitors and data for two capacitors are given in table 3.9. The rated voltages are 900 and 1250 V and they are to be used for DC-link operating voltages of 400 and 800 V, respectively. The capacitors are for DC-link applications and the voltage ratings were chosen well above the DC-link voltage to give a sufficient storage capacity. The capacitance is too low to obtain the desired UCC with a single capacitor, but through parallel connection this can be achieved.

Manufacturer	Epcos	Epcos
Device name	B25655M9108K	B25655A1148K000
Voltage rating	900 VRMS	1250 VRMS
Continuous current rating	200 A	135 A
Capacitance	1000 μF	4500 μF
Series resistance	0.6 mΩ	0.8 mΩ
Weight	4.5 kg	9 kg
Lifetime	80,000 h	100,000 h
Self inductance	15 nH	40 nH

Table 3.9: Capacitor data for DC-link capacitor [3]

The necessary capacitance of the two converters are then found by using equation 3.15 where the voltage is set to the difference between the operating DC-link voltage of the converter and the voltage rating of the capacitor. The results are shown in table 3.10.

	Capacitance
Back-to-back converter 400 V	4330 μF
Back-to-back converter 800 V	9014 μF

Table 3.10: Demanded capacitance for a UCC of 40 ms

Parallel connection of four and two capacitors are then necessary for operating voltages of 400 and 800 V and the corresponding UCC-values are 37.0 μF and 40 μF.

The ESR is then included in the simulations as a resistance in series with the capacitor and the calculated average losses are given in table 3.11.

	Capacitor loss [W]
Back-to-back converter 400 V	0.03
Back-to-back converter 800 V	0.04

Table 3.11: Capacitor losses

3.6 Efficiency summary

From the total switch losses and the output generator powers the efficiencies of the different converter setups are found. For the two back-to-back converter setups also the capacitor losses are included in the efficiency values. The results are presented in 3.12.

	Efficiency
9SC with Fuji switches	97.7 %
9SC with IXYS switches	96.2 %
BTB with Fuji switches	97.7 %
BTB with IXYS switches	96.9 %

Table 3.12: Converter efficiencies

4 Semiconductor cost per kW output power

The number of semiconductors and the prices associated with these is the main part of the cost in a power electronics converter. A higher number of switches and a higher rating for each switch compared to other converters will give a cost disadvantage that may leave the converter out of the question. Minimizing the number of switches and the amount of silicon used in each switch, which is connected with the switch rating, is thus a major concern when trying to obtain the best and least costly solution. To compare the cost figures for the two converters in question in this thesis the following relation found in [22]is used:

$$\begin{pmatrix} Semiconductor\ cost \\ per\ kW\ output\ power \end{pmatrix} = \frac{\begin{pmatrix} Semiconductor\ device\ cost \\ per\ rated\ KVA \end{pmatrix}}{\begin{pmatrix} Voltage \\ derating\ factor \end{pmatrix} \cdot \begin{pmatrix} Current \\ derating\ factor \end{pmatrix} \cdot \begin{pmatrix} Converter \\ switch\ utilization \end{pmatrix}} [\frac{NOK}{kW}] \tag{4.1}$$

where Semiconductor device cost per rated KVA is the cost of the semiconductor divided by its maximum rms current and maximum voltage rating multiplied. The current and voltage derating factors are safety margins that ensures operation below the current and voltage capability of the device. The goal of this work is to compare two converters and the derating factors are therefore omitted in the calculations of cost per output power. It is assumed that the derating factors will be the same and the figures found will only be a number for comparison and not real values that can be used for finding the total investment cost of the converters.

4.1 Switch utilization

Switch utilization is defined in [22] as:

$$Switch\ utilization\ =\ \frac{P_{load}}{S}\ [\text{VA}] \tag{4.2}$$

where P_{load} is the rated output power and S is the stresses imposed on the switches. S is therefore found in the following manner:

$$S\ =\ \sum_j V_j \cdot I_j\ [\text{VA}] \tag{4.3}$$

No voltage and current transients are considered in the utilization calculations and the values used for switch stresses are the amplitudes of the square wave and the DC-link in the voltage case. For the currents the RMS switch currents found through simulations are used. The bi-directional switches in the nine-switch converter is considered as a single switch in these calculations.

The simulated current and voltage stress values are shown in table 4.1 and 4.2.

	Voltage stress	Current stress
AP	400	22.4
BP	400	22.7
CP	400	22.6
AN	400	22.5
BN	400	22.5
CN	400	22.4
S1	400	23.7
S2	400	23.7
S3	400	23.7
S4	400	23.7
S5	400	23.7
S6	400	23.7
S7	400	23.7
S8	400	23.7

Table 4.1: Switch stresses in the back-to-back converter

	Voltage stress	Current stress
AP	400	21.1
BP	400	21.1
CP	400	20.9
AM	400	21.2
BM	400	21.2
CM	400	20.9
AN	400	21.1
BN	400	21.1
CN	400	20.8
S1	400	22.2
S2	400	22.2
S3	400	22.2
S4	400	22.2

Table 4.2: Switch stresses in the nine-switch converter

The total switch stress is then found from equation 4.3 and the numbers are given in table 4.3.

	Total switch stress
Back-to-back converter	129880 VA
Nine-switch converter	111280 VA

Table 4.3: Total switch stress in the converters

From tables 4.1 and 4.2 together with the power from the generators and equation 4.2 the switch utilization can be found. Table 4.4 and figure 4.1 shows the results.

	Switch utilization
Back-to-back converter 400 V	0.0898 W/VA
Nine-switch converter 400 V	0.0988 W/VA

Table 4.4: Switch utilization

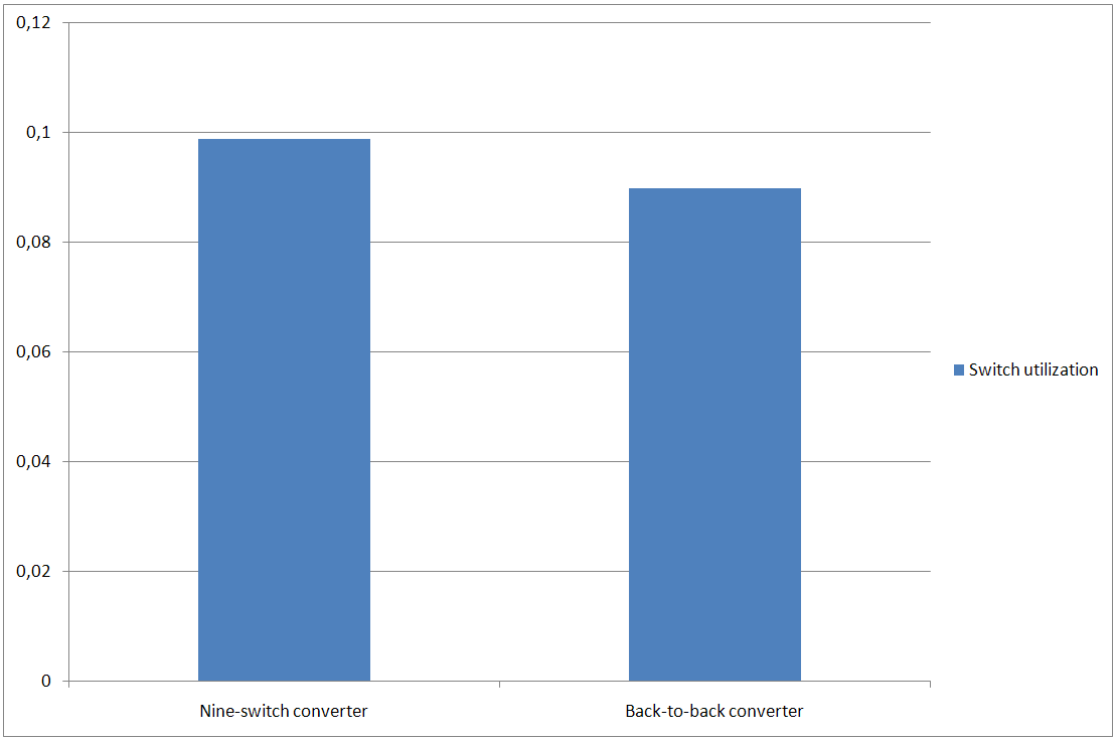

Figure 4.1: The switch utilization for the converter setups

4.2 Semiconductor cost

Information about semiconductor cost has been obtained from different producers and a summary of prices and modules are given in table 4.5.

	IGBT	IGBT
Manufacturer	Mitsubishi electric	Mitsubishi electric
Device name	CM2500DY-24S	CM1800DY-34S
Voltage rating	1200 V	1700 V
Current rating	2500 A	1800 A
Price	7579 NOK	6948 NOK
Price per kVA	2.53 NOK/VA	2.27 NOK/VA

Table 4.5: Semiconductor data for module driven comparison [4] [5]

The semiconductor cost per output power can now be calculated for the different converter setups through equation 4.1 and the data from tables 4.4 and 4.5. The available results are presented in table 4.6 but no cost figures are obtained for the RB-IGBTs.

	Semiconductor cost per kW output power
Back-to-back converter	32.9 NOK/kW
Nine-switch converter	?? NOK/kW

Table 4.6: Semiconductor cost per kW output power

5 Module driven comparison

A useful approach for comparing different converters is the module driven method presented in [23] for comparing two series compensation solutions with different topologies and number of switches. Different converter topologies may have different voltage ratings and number of switches for the same output. Operating conditions for the converters such as junction temperature and required cooling may therefore vary and thus give numbers difficult to compare. The module driven method is based on using the same semiconductor module and heat sink and define the operating temperatures. The switch current and voltage limited by these conditions can then be found and also the corresponding generator power. With this information the relative semiconductor rating, which is the total switch rating of all the converter switches divided by the output power, can be found. The silicon usage in the different converters can then be visualized and compared.

5.1 Semiconductor modules

Two semiconductor modules are chosen as basis for the comparison. One RB-IGBT and one IGBT with anti-parallel diode. Data are shown in the following table:

	IGBT	RB-IGBT
Manufacturer	IXYS	IXYS
Device name	IXEH 40N120D1	IXRH 40N120
Package	TO-247	TO-247
Voltage rating	1200 V	1200 V
Current rating	60 A	55 A
R_{jc} ((RB)IGBT)	0.42 KW^{-1}	0.42 KW^{-1}
R_{jc} (diode)	1.0 KW^{-1}	-
R_{ch}	0.25 KW^{-1}	0.25 KW^{-1}
Maximum junction temperature	150 ℃	150 ℃

Table 5.1: Semiconductor data for module driven comparison [4] [5]

5.2 Voltage utilization

When finding the line-to-line generator voltage for the module driven approach the voltage utilization has to be considered. The voltage utilization is the ratio between the line-to-line voltage obtained at the generator terminals and the available DC-voltage. The simulations used in the loss calculations showed line-to-line generator voltages of 122.4 V and 244.9 V for a DC-voltage of 400 V in the nine-switch converter setup and the back-to-back converter, respectively. The associated voltage utilization is calculated in equations 5.1 and 5.2.

$$Ideal\ voltage\ utilization\ nine-switch\ = 122.4/400 = 0.306 \tag{5.1}$$

$$Ideal\ voltage\ utilization\ six-switch\ = 244.9/400 = 0.612 \tag{5.2}$$

The voltage utilization in the back-to-back converter for unity modulation is also well known from theory and can be found from the given equation 5.3. [24]

$$V_{line-to-line} = \frac{\sqrt{(3)}}{2\sqrt{(2)}} m_a \cdot V_{dc} \approx 0.612 m_a \cdot V_{dc} \,[\mathrm{V}] \tag{5.3}$$

V_{dc} is the DC-link voltage, m_a is the modulation and $V_{line-to-line}$ is the line-to-line voltage of the three-phase input. The theoretic ratio is the same as the ratio obtained from simulations.

The available generator voltages are then given by the voltage utilization multiplied with the operating switch voltage as shown in equations 5.4 and 5.5. The operating switch voltage is set to half the available blocking voltage in the switches as a safety limit must always be included when choosing operating voltage.

$$V_{ce} = 600 -> Vgen = 600 * 0.306 = 183.6\,V\ for\ nine - switch\ converter\ setup \tag{5.4}$$

$$V_{ce} = 600 -> Vgen = 600 * 0.612 = 367.2\,V\ for\ back - to - back\ converter\ setup \tag{5.5}$$

5.3 Thermal conditions and heat transfer

Heat transfer occurs in a material with different temperatures and goes from an area with a higher temperature to an area with a lower temperature. This energy flow can be described in much the same way as an electrical system where the heat is seen as the current flowing, the temperature difference is the voltage and the thermal resistance is the electrical resistance. The energy flow in terms of watt is given by equation 5.6 found in [24] and only altered with respect to denomination.

$$Q = \frac{\lambda A \Delta T}{d} [\mathrm{W}] \tag{5.6}$$

A is the cross-sectional area of the material in m^2, ΔT is the temperature difference in K, d is the material thickness, λ is the thermal conductivity in $\mathrm{Wm^{-}1^{\circ}C^{-}1}$ and Q the heat transfer given in W. The thermal resistance is defined as follows:

$$R_\theta = \frac{\Delta T}{Q}\ [\mathrm{KW^{-}1}] \tag{5.7}$$

and by adding this to equation 5.6 the following result can be obtained:

$$R_\theta = \frac{d}{\lambda A}\ [\mathrm{KW^{-}1}] \tag{5.8}$$

The calculation of heat transfer from the semiconductor to the ambience through heat sinks can then be done with equation 5.9 by eliminating d, λ and A from equation 5.6 by inserting equation 5.8.

$$Q = \frac{\Delta T}{R_\theta} \text{ [W]} \tag{5.9}$$

5.3.1 Maximum allowable losses

The losses are not distributed equally in each switch and the anti-parallel diode in the IGBT has a higher thermal resistance than the IGBT itself. In section 3 it was seen that the maximum losses in the nine-switch converter was found in the middle switches and for the back-to-back converter in the middle converter stage. As these switches are RB-IGBTs and IGBTs with the lowest junction to case thermal resistance compared to the diodes, calculations for both the diodes and the RB-IGBTs is done to find which switch is the limiting one.

The resulting thermal system for both semiconductors is depicted in 5.1 and shows the heat source Q which is the power dissipation in the switch and the three thermal resistances, R_{jc},R_{ch} andR_{ha} which is the resistance between junction and case, case and heat sink and heat sink to ambient, respectively. The power is dissipated in the chip and gives raise to an increased junction temperature. This heat is flowing to the ambient air through the case and heat sink. The heat sink is mounted on the case with a compound designed for preventing air from getting in between the heat sink and case. As air is a poor thermal conductor this is of great importance for the least total thermal resistance. Data for the heat sink is given in table 5.2. The chosen heat sink is designed for cooling $TO-247$-packages.

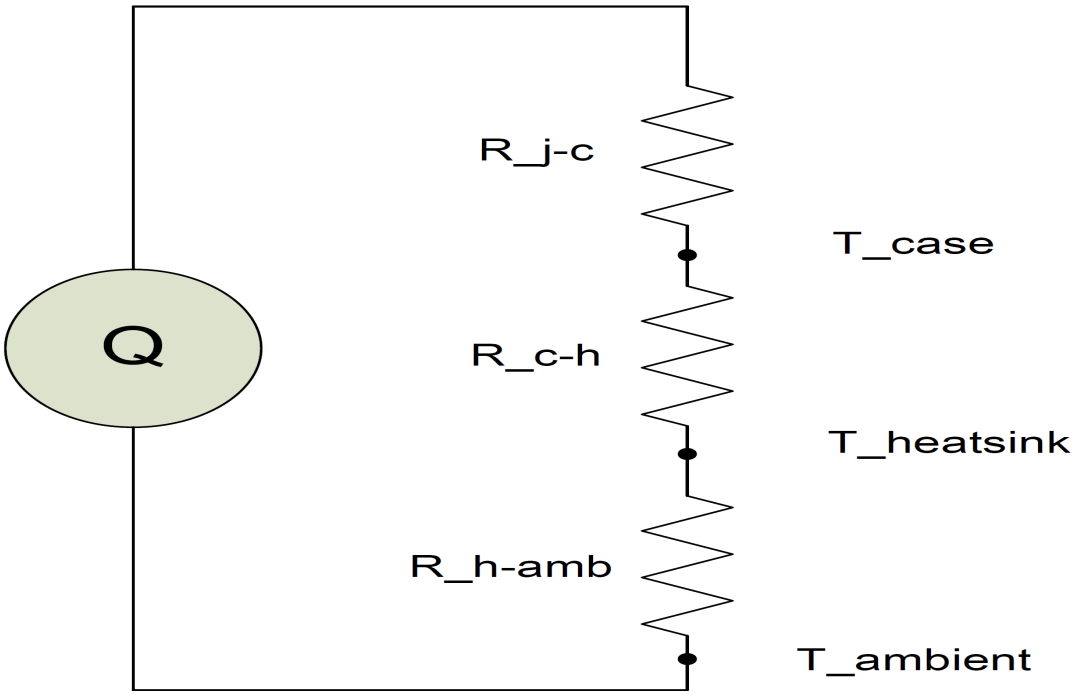

Figure 5.1: Equivalent circuit used for static calculation of heat transfer

Manufacturer	Cool innovations
Device name	2-601326RJ
R_{jc}	0.32 KW^{-1}
Air speed for given R_{jc}	3.048 ms^{-1}

Table 5.2: Heat sink data

The maximum junction temperature is 150°C for both transistors. The data sheet values for the semiconductors used in the loss calculations are given at 125°C and operating junction temperature is therefore set in accordance with this. Ambient temperature is set to 40°C so that the total temperature difference, denoted ΔT is 85°C as shown in the following equation.

$$\Delta T = T_{junction} - T_{ambient} = 125°C - 40°C = 85°C \tag{5.10}$$

The series connected thermal resistances in the heat transfer circuit in figure 5.1 can be summed up to an equivalent resistance. This is done by simply adding the resistances and is done in equation 5.11 for the IGBT-part and in equation 5.12 for the diode part. The IGBT and the RB-IGBT has the same junction to case thermal resistance so the equivalent resistance will also be the same.

$$R_{eqI} = R_{jc} + R_{ch} + R_{ha} = 0.42\text{KW}^{-}1 + 0.25\text{KW}^{-}1 + 0.32\text{KW}^{-}1 = 0.99\text{KW}^{-}1 \quad (5.11)$$

$$R_{eqD} = R_{jc} + R_{ch} + R_{ha} = 1.0\text{KW}^{-}1 + 0.25\text{KW}^{-}1 + 0.32\text{KW}^{-}1 = 1.57\text{KW}^{-}1 \quad (5.12)$$

The switch losses allowed by the thermal resistances and temperature limits are then found by equation 5.9 and given in table 5.3.

Q_{diode}	54.1 W
Q_{IGBT}	85.9 W
$Q_{\text{RB-IGBT}}$	85.9 W

Table 5.3: Loss limits due to thermal conditions

5.4 Generator power

Simulations are then run to find at which current value the switch loss limit is reached. The RMS current values are shown in table 5.4. It should be noted that the given current value for the nine-switch converter is the RMS current in the bi-directional switch. The corresponding output power with these currents are also given as the switches with the highest losses experience higher current than the phase currents in the generator. This is because there are more than one converter stage in each converter with a different number of switches in each stage. A direct calculation from switch current to phase current is therefore not possible for all switch currents. The loss calculation procedure is explained in section 3.2.

	Switch current	Generator power	Total losses	Efficiency
BTB switch S2	37.1 A	19968 W	774 W	96.1 %
9SC BM	35.4	30608 W	1579 W	94.8 %

Table 5.4: Limiting switch currents and corresponding generator power

The displacement power factor in the simulations are given in table 5.5 as they will affect the power losses.

	Displacement power factor
BTB converter	0.84
9SC converter	0.85/0.86

Table 5.5: Displacement power factors

5.5 Switch rating

The switch ratings are then the product of the switches' voltage rating, current rating and number of switches. These results are given in table 5.6.

Back-to-back converter	1008 kVA
Nine-switch converter	1476 kVA

Table 5.6: Switch ratings

5.6 Relative semiconductor rating

The relative semiconductor rating which is defined as the switch rating times the number of switches divided by the generator power can now be found by using the results from tables 5.4 and 5.6. This gives a figure of the silicon usage needed to realize the conversion stages and it is given as $\frac{\text{VA}}{\text{W}}$. The result is shown in figure 5.2

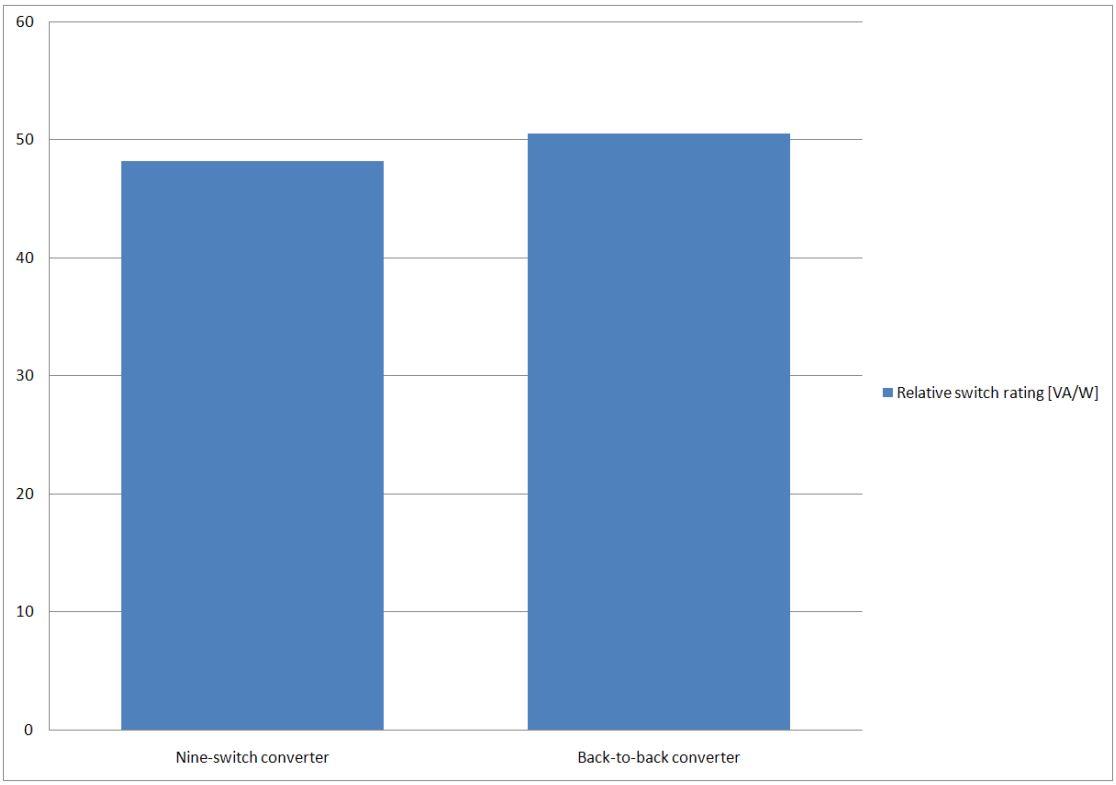

Figure 5.2: The relative switch rating found through the module driven approach

The results are also shown in numbers in table 5.7.

Back-to-back converter, IXYS 600 V	50.5 $VAW^{-}1$
Nine-switch converter, IXYS 600 V	48.2 $VAW^{-}1$

Table 5.7: Relative semiconductor ratings for the two converters

6 Other areas of application

The voltage utilization in the nine-switch converter is half that in the back-to-back converter when operating two equal generators with the same line-to-line voltage. To avoid the low voltage utilization another application is proposed. In an isolated power system with a renewable energy source such as wind, solar or tidal power the available power vary according to the available wind or time of day. Stable power output is obtained by having an auxiliary power source or energy storage that is able to compensate the varying power and also supply the total power if the renewable energy source cannot feed the total load. Diesel generators are a common choice as these are easily available and controllable. If the periods with no or little renewable energy generation are short an induction or permanent magnet synchronous generator with a large rotating mass can act as a flywheel and supply the demanded load power. Converter interfaces or energy storage systems are needed to operate the two energy sources with a stable power output. The nine-switch converter can control two generator inputs independently and only one converter with no DC-link is then needed for operating the power system. If both generators are rated for the full load power and the DC-voltage is sufficient for supplying the rated generator voltage at unity modulation the low voltage utilization can be bypassed. If the sum of the modulation indexes for the two control signals is kept equal to unity or below then the DC-voltage does not have to be rated to supply both generators with the rated voltage as the maximum output power is limited to the output power from one generator. Simulations with modulation indexes of 0.3 and 0.7 are done to verify sharing of the voltage by the same factors. The relation between the torque are kept the same as the ratio between the voltages.

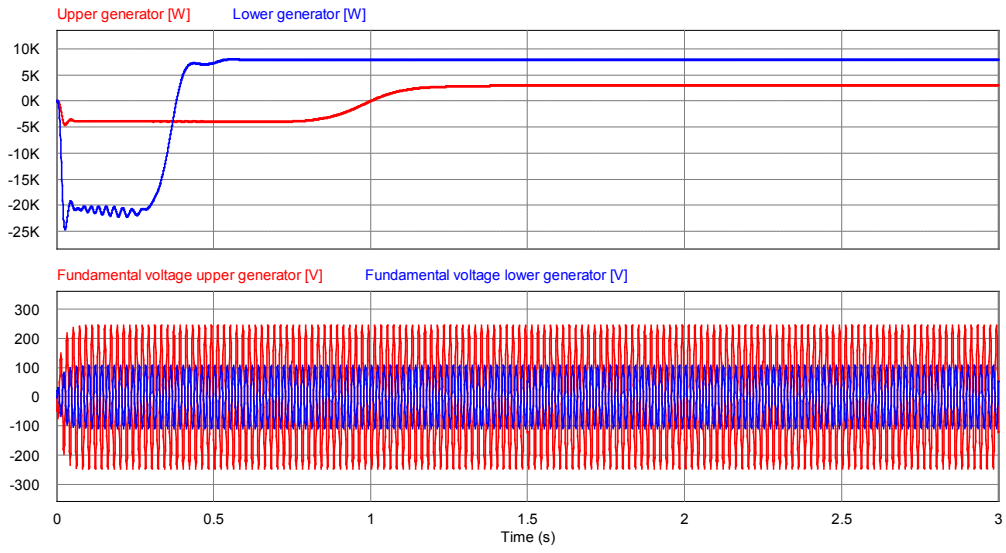

Figure 6.1: Output powers from the generators with 0.3 and 0.7 modulation index

The RMS fundamental voltages are 73 V and 171 V volts and are 30 and 70 percent of a total of 244 which is in line with the modulation of the control signals. The power outputs were 3011 W and 7965 W which corresponds to a total of 10976 and an allocation of 27 % and 73 % of the total power to the two generators.

7 Discussion

7.1 Simulation study

The harmonic contents in the phase currents and the line-to-line voltages were included to show the quality of the output from the converters and to give input on the need for filters in the converter setups. The current harmonics in the phase currents in the 9SC are 8.8 % which is twice those in the BTB in the case with 400 V operating voltage. The sharing of the available voltage between the two generators gives a doubled voltage THD and the result is a doubled current THD. The same is not seen for an operating voltage of 800 V as the power factors are different.

Power oscillations in both converters were investigated and a DC-offset was present in all the phase currents. A DC current together with the fundamental voltage will cause an oscillation at the fundamental frequency as seen in equation 2.4 and the reason for these were thus revealed. The amplitude of the oscillations in the back-to-back converter was 0.1 W per thousand while in the nine-switch converter they are 1.5 W and 2.2 W per thousand. This corresponds to 0.03 % of the output power in the back-to-back converter and 0.2 % in the nine-switch converter in the worst case.

The choice of operating the generators with a phase shift of 180 degrees between them reduced the currents in the upper and middle switches as was seen in the simulation study and this will reduce the conduction losses in the upper and lower switches.

7.2 Efficiency investigation

The efficiency investigation was conducted with switch data from two semiconductor producers. The Fuji switches were first selected for the calculations but the IXYS switches were later included as they were needed in section 5. With two different loss calculations the validity of the obtained efficiencies could be confirmed but differences in the operating conditions prevented this. A brief comparison of the two different RB-IGBTs could also be included. This was done as the RB-IGBT performance is of great importance in the investigated topology.

Data sheets are available for IXYS RB-IGBTs so a calculation based on the given switching energies could be performed. Data sheets for Fuji RB-IGBTs were not available but a method giving equations for loss calculations for a Fuji RB-IGBT is given by Fuji itself. The RB-IGBT from IXYS is rated at 1200 V and 55 A and the IGBT has the same voltage rating but the current rating is 60 A. The Fuji switches were both rated at 600 V and 200 A as is further explained in the next section.

The induction generator used in the simulations was a preset model from the simulation program. Full data were not given in the user manual with respect to rated values but examples with the induction generator from the simulation program suggest that the rated voltage is 220 V. With a different voltage utilization in the two converters a compromise had to be made regarding the line-to-line voltage in the generator. To obtain 220 V line-to-line in the generators the DC operating voltage should be 220 V divided by the voltage utilizations in the two converters. These were 0.612 and 0.306 in the BTB

and 9SC, respectively, and would have lead to DC-voltages of 359 V and 719 V, and then exceeding the switch blocking voltage in the case with the 9SC, as it has the lowest voltage utilization. As the focus in these calculations were the losses in the semiconductors the DC operating voltage were set equal to two thirds of the blocking voltage in both the two converter setups with different terminal voltages in the generators as a result.

The operating voltages in the converters were chosen to be two thirds of the switch voltage rating for the IXYS switches also. With blocking capabilities twice that of the Fuji switches, the generator voltages were also twice those in the Fuji calculations. Similar DC-voltages were not chosen as operating the switches at a very low value compared to the available is not realistic as the switch utilization would then be very low and other switches should be used instead. The generator terminal voltages could then be kept more in line with the rated voltages for the 9SC but for the BTB a generator voltage of 488.9 V was the result for the same DC-voltage. This was more than twice the rated generator voltage and operating with this over voltage caused a displacement power factor of 0.53 with correspondingly high conduction losses. If the operating voltage had been set lower the problems could have been reduced as is seen in the improved power factor in the loss calculations in the module driven method in section 5. However the operating voltage in the Fuji calculations would then have to be lowered accordingly with a very low generator voltage as a result. The forward voltage is dependent on the forward current and not the operating voltage and similar utilization of the available blocking voltage in the different rated switches was therefore important to have similar conditions for calculating the conduction losses. In the module driven method only one set of loss calculations were done and no corresponding case with lower rated switches affected the choice of operating voltage.

The simulations were done with the same input torque as in the Fuji loss calculations due to the lower current rating in the IXYS switches. The single phase equivalent circuit for the induction generator is depicted in figure 7.1 to explain the reason for the low DPF in the BTB case with 800 V operating voltage.

The impedances due to the leakage inductances in the stator and rotor are given as X_{ls} and X_{lr} and the stator copper losses are represented by R_s. The iron core losses is represented by R_fe. The power crossing the air gap between rotor and stator is represented by $\frac{R_r}{s}$ where s is the slip, which is the difference in speed between the rotating flux from the stator windings and the speed of the rotor. This power includes both the mechanical power and the rotor copper losses. The reactive current is due to the inductances present in the generator. Leakage inductances exist in both stator and rotor but the biggest inductance is the mutual inductance that magnetizes the air gap, represented by X_m. The active current is proportional with the generated power in the generator. When the line-to-line voltage is doubled the voltage over the mutual inductance will double if stator resistance and leakage inductance is neglected. The corresponding reactive power consumption will then increase. If the power level is kept the same, as was done in these simulations, the active current will decrease as a result of a doubled voltage. The DPF can be found by calculating the cosine of the ratio between the reactive and active current. The explained increase and decrease in the currents will

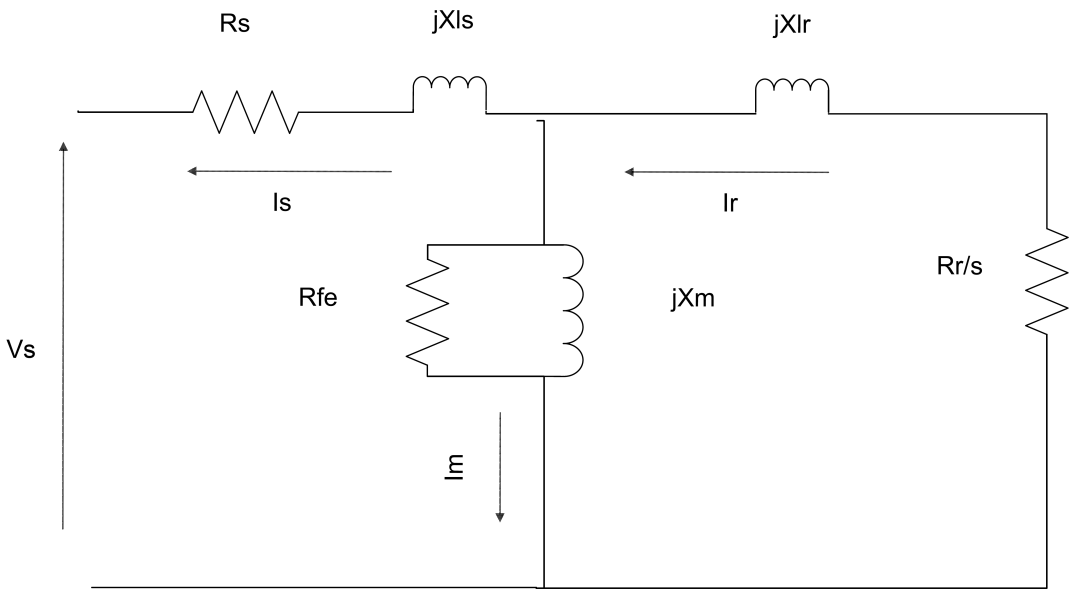

Figure 7.1: Equivalent circuit for induction generator

both lead to a reduced DPF. Other induction generators were tried for the BTB with an increased DPF as a result. However a difference in switch currents and DPF between the converters were still existing and the efficiency values were therefore different not because of switch characteristics only. The converter efficiencies found from the Fuji calculations with similar DPFs are therefore used in the conclusions. The IXYS calculations were still used in the module driven comparison with another operating voltage and for comparing the RB-IGBTs from the two different manufacturers. Input from the IXYS case is also used when discussing the loss distribution in the converters.

The back-to-back converter was run with the same input torque to the induction generator as the sum of the torque input to the two generators in the nine-switch converter setup. The switch currents were then in line with the switch currents in the nine-switch converter. For a comparison of the two converter setups in a split drivetrain configuration, the input torque to the generators should have been chosen equal and the corresponding switch ratings would then have been different from those chosen for these calculations. The voltage utilization in the converters are different and both similar switch ratings and generators could not be achieved at the same time. The torque inputs to the generators were then set different in the two converters to have as similar conditions as possible from the semiconductor point of view in the loss calculations.

7.2.1 Fuji Electric semiconductors loss calculations

The loss calculations in the reverse-blocking IGBTs were carried out by using quadratic equations for the different types of losses and including these in a DLL-file. Switch voltages and currents were measured and input to the DLL-file which determined what

type of switching action was occurring and calculated losses with the corresponding equation. The method was described in [16] and is for a RB-IGBT rated at 600 V and 200 A. The IGBT loss calculations used the same method but with no reverse recovery as the IGBT does not include an intrinsic series diode. The method was compared with an experimental setup of a matrix converter in [16] and showed good correlation. The RB-IGBT is a modified IGBT and the RB-IGBT from Fuji Electric shows much of the same characteristics as in the IGBT. [17] Therefore the same method is used for both the semiconductors.

All values were found during steady state and the switch currents and voltages were found by simulations with ideal switches. The ideal switching gives idealized currents and the inductance and resistance inevitably existent in the semiconductors would cause different switch currents in a real switch. A switching action is happening in some hundred nano seconds [4] and a simulation of the exact current and voltage waveforms would demand very low simulation steps and then time demanding simulations. The method used for the loss calculations simplifies this by describing every type of switching actions in equations dependent on voltages and currents before and after the switching occurs. The possible disparity between calculated losses and those actually occurring is attempted to be removed by comparing with experiments. The calculation method in [16] was verified with experiments but for another converter setup than the ones in this thesis. A tuning of the method in accordance with measured losses in an actual converter setup should therefore be executed to ensure the validity of this method for another setup than the original one.

The simulations were done with an operating voltage of 400 V corresponding to two thirds of the available blocking voltage in the switches. Due to the difference in voltage utilization in the converters with the 9SC having half that of the BTB the torque input to each generator in the two converters were given different values. The sum of torque to the generators in the BTB was used as input to the single generator in the BTB. This was done to keep current values in line with each other and thus have as similar conditions as possible from the semiconductor point of view.

The diode data were found from an IGBT with anti-parallel diode with similar ratings as the RB-IGBT. The use of different semiconductor data sheets for the diode and IGBT part in the IGBT with anti-parallel diode is not an ideal choice but it was done as the RB-IGBT loss calculation method were used for calculating the IGBT losses. The two different methods for calculating the losses may have different accuracy. It is therefore an uncertainty in the results obtained in the efficiency investigation. However both the converter setups use both the methods for the calculations and this may even out the potential differences in accuracy.

The diode conduction losses were found by performing a piecewise linearization of the curve describing the collector-emitter voltage as a function of the forward current. This was put in the DLL-file which calculated the collector-emitter voltage by using the switch currents obtained from the simulations. The diode reverse recovery losses were found by considering the switching energy given in the data sheets of the semiconductor and linearizing in the same manner as for the forward voltage. It was assumed linear

losses from zero current up to the first printed value in the data sheet as switching energies at very low currents were not given. This assumption and the accuracy in the linearization will affect the quality of the obtained results.

7.2.2 IXYS semiconductors loss calculation

The loss calculations for the IXYS semiconductors were done by using data sheets from IXYS and performing a piecewise linearization of the figures describing the current dependency of the switching energies. A linear voltage dependency was assumed [19], and the resulting equations were saved in a DLL-file connected to the simulation program. This file was determining which type of switching action was occur The linearization of the graphs showing the current dependency of the switching energies was done by choosing a pair of points in the graphs. A linear equation describing the line between the two points was then made. The accuracy of the method is affected by the distance between the points and the resolution of the graphs. In areas where the curves change derivative very fast the accuracy is limited.

7.2.3 Loss distribution in the nine-switch converter

The distribution of the losses are not equal in all the switches as the middle row experience higher switching losses than the upper and lower row. The upper and lower row are operated by sinusoidal pulse width modulation with an offset added to the control signals. The number of switching actions is therefore decided by the frequency of the triangular carrier. The middle switches are controlled by a $NAND$ logic which compares the upper and lower gating signals and gives the corresponding $NAND$ output.

Switches		
Upper	Lower	Middle
1	1	0
1	0	1
0	1	1
0	0	1

Table 7.1: NAND logic for gating of the middle switches

However only three of the possible switch combinations in the $NAND$-logic is passed to the switches due to the offset added to the control signal. The last combination with only one switch conducting in the switch leg is prohibited. From the $NAND$ table it can then be seen that the middle switch will change state every time the upper or lower switch is switching. The middle switches will then have an effective switching frequency two times that of the upper and lower switches and thus have higher switching losses. The nine switches are therefore exposed to the same switching losses as twelve switches with equal switching frequencies as the switch losses are proportional to the switching frequency. [24] The maximum switching frequency in the converter is then reduced and

the possibility of choosing a higher switching frequency for increasing the output quality is limited.

The conduction losses are five and eight percent lower in the middle switches for both types of semiconductors. Due to the offset and switching logic the upper and lower switch row are gated ON for half of the switching period each. A six-switch converter is then apparent consisting of the upper switch row and the middle row half of the period while lower row and the middle row constitute the six-switch converter in the other half. In the active period, the upper switch row follows the same switching action as in a regular three-phase full-bridge converter together with the middle switch row due to the PWM of the control signal for the upper switch row. The middle switch row is always a part of the two apparent six-switch converters, hence it has a duty cycle of 0.5. The upper and lower row have a duty cycle of unity while the switches are all gated ON and a duty cycle of 0.5 when the row is a part of the apparent six-switch converter. The average duty cycle is then 0.75 and a higher conduction loss may be expected in the upper and lower switches. The difference in conduction losses is however lower than the difference in duty cycle. The RMS switch currents show no significant differences between the switches and this points towards equal conduction losses. ***The difference in conduction losses may therefore be due to the difference in current shapes as the*** RMS***-value conceals these.***

The different duty cycles in the switch row and equal currents are nonetheless of great significance. The generators are active for only half a switching period each due to the gating of all switches in one row simultaneously. Gating all the switches in the upper or lower row ON means short circuiting the generator connected between this row and the middle row. The power transferred in the switches is therefore only the power from one generator at the time. The number of switches for the power to go through for each generator is therefore nine during its active period. One of the advantages with the nine-switch converter topology is the number of converter stages. The back-to-back converter has three series connected converter stages whereas the nine-switch converter has only two. Every stage has to convert the full power from the generators and thus the conduction loss was expected to be higher in the back-to-back converter. This is not the case, as can be seen in the results from the efficiency investigation for the Fuji switches with total conduction losses in line with each other. With the generators having to transfer power through nine switches in their active periods the nine-switch converter will have higher conduction losses than one of the stages in the back-to-back converter. The conduction losses for the Fuji switches from generator to transformer in the converters show that they make up 1.27 % and 1.31 % of the active power in the BTB and 9SC, respectively. The single AC/AC stage in the 9SC thus has a conduction loss in line with the two conversion stages from AC to DC and then from DC to AC in the BTB. No benefit is therefore existent in the nine-switch converter regarding the conduction losses.

The full-bridge rectifier operates as a diode rectifier during steady state and only the diode part of the IGBTs with anti-parallel diodes are conducting the current. The diode conduction losses were 11.4 W and 11.7 W in the Fuji and IXYS semiconductor,

respectively. The corresponding switch currents are 22 A and 13 A and more similar currents would be expected. However a higher blocking voltage in the IXYS switch leads to a longer drift region with correspondingly higher resistance. Similar conduction losses are therefore to be expected as long as the transferred power is the same. The diode reverse recovery losses are less than one watt per switch and do not contribute significantly to the total losses. The rectifier losses account for 0.4 % of the active power from the generator.

7.2.4 Loss distribution in the back-to-back converter

The highest losses occur in the full-bridge between the DC-link capacitor and the transformer that operates as an inverter during steady state with only the IGBTs conducting the current. The forward voltage in the IGBT is higher than in the diode and the energy loss during reverse recovery is lower than the turn-on and turn-off energies in the IGBT. This will inevitably lead to higher losses in the IGBTs than in the diodes. The cooling demand in this converter stage is therefore higher than in the other stages. With similar cooling installations this stage will greatly limit the total power output as seen in section 5.

The full-bridge converter operating as a rectifier account for 0.4 % of the active power in the BTB and is in line with the 0.4 % found in the 9SC. The reverse recovery losses are however 29.6 % higher in the 9SC. The same diode data are used for the loss calculation in the two converters and more similar results would be expected with the same operating voltage and similar power levels. From the calculated switch stress it is seen that the RMS switch currents in the rectifier part of the converters are 23.7 A and 22.2 A in the BTB and 9SC, respectively. The losses are calculated from the actual current curves and not by multiplication of the switching energies with the switching frequency. The difference has therefore to be explained from the current curves also. The current in the diodes is distorted and the loss equations for the reverse recovery uses the measured instantaneous forward current before the reverse recovery is occurring to calculate the losses. Similar switches and similar current levels are seen in the converters and the current waveforms are therefore expected to cause the difference in the results but no conclusion is drawn. The reverse recovery losses are not a significant part of the total losses and the uncertainty in these numbers are therefore not affecting highly the calculated efficiency.

The losses in the full-bridge stage with six switches is dependent on the power factor of the induction generator as this converter stage supplies the reactive power to the generator. A low displacement power factor(DPF) will give higher switch currents and higher losses than for operation with a high DPF. This is clearly seen by the fact that the DPF in the loss calculations for the IXYS switches is 0.53 and the conduction losses are correspondingly higher for this case. In the inverter and rectifier stages, no reactive power is flowing and the conduction losses in the two stages for the Fuji switches are 98 % of those with the IXYS IGBTs. The switch losses in the same stages for the Fuji switches are 82 % of those with IXYS switches. The total efficiency may therefore still be lower for the IXYS switches even with a similar power factor but it will be close to

the Fuji numbers as the conduction losses are the biggest part of the total losses in the converters. The two calculations are therefore validating each others results but not to a great extent.

The center converter stage acting as an inverter in the back-to-back converter has some diode losses during steady state when the operating voltage is set to 800 V for the IXYS loss calculations. This is not expected as the IGBTs should be the active semiconductors during inverter operation. The rectification stage is also experiencing small IGBT losses when it is expected to operate solely by the diodes. The ideal diodes in the inverter stage will nonetheless turn on when the capacitor voltage is less than the fixed DC-voltage in the grid side of the converter due to the voltage ripple. The IGBTs in the rectification stage is also gated and allows the flow of current from the grid side to the DC-link. These losses are not evident in the 400 V case as they were smaller in size than the precision in the printed results.

The capacitor losses are less than one watt and hence do not contribute much to the total converter losses.

7.2.5 Semiconductor comparison

The IXYS loss calculations for the 9SC showed an efficiency of 96.2 % compared to 97.7 % with the Fuji switches. The conduction losses in the IXYS RB-IGBTs are 37.5 % higher than in the Fuji switches. The output power in the two cases are 10992 W and 11821 W, with the highest power output for the IXYS switches. This corresponds to a difference of 7.5 % and the displacement power factor is 15 % less in the IXYS case. However these differences cannot explain the much larger difference in the losses.

The switching losses in the IXYS RB-IGBTs are three times higher in real numbers than in the RB-IGBT from Fuji Electric for the two loss calculations. Part of the difference is due to the seven percent higher power output in the IXYS case and the lower power factor but the switch loss characteristics are different in the two cases. The turn-on and reverse recovery losses are three to six times higher in the IXYS switch while turn-off losses are only half that of the Fuji switch. There is a trade-off between the turn-off losses and on-state voltages in the production of RB-IGBTs and IGBTs. [25] A high carrier density in the drift region during conduction would lead to a low on-state resistance but the time to remove the same carriers during turn-off will then increase and with it the turn-off losses. The semiconductor producers have to choose which factor to optimize and this may be the reason that the IXYS RB-IGBTs have lower turn-off losses than the Fuji switches but higher conduction losses.

In literature it is found that the reverse recovery loss can be kept low by having a thin collector layer in the RB-IGBT and also by reducing the carrier lifetime in the drift layer. [26] The actual chip structures and carrier lifetime profiles in the two types of semiconductors are not known. The higher reverse recovery in the IXYS RB-IGBT may be because of structural differences and carrier lifetimes but no evidence is present to back up this hypothesis.

In general semiconductor characteristics improve with time as new and more accurate production methods are developed. The IXYS RB-IGBTs are available in the market but

the prices are not known. To be able to sell with a reasonable price, low-cost production methods should be existent. The Fuji RB-IGBTs are just known from presented papers and thus from a research stage. Price limits with respect to a reasonable market price is not as evident in research as cost improvem

7.3 Semiconductor cost per kW output power

The switch utilization was included in the thesis to be used for calculating the total cost per kW output power. The necessary silicon area needed for designing the converter was then decided from the current and voltage stresses imposed on the switch. The switch stresses and the output power from the generators were found through simulations. The use of ideal switches in the simulations leads to a higher line-to-line voltage in the generators. This is because there is no on-state voltage drop in the ideal switches. The current is thus expected to be higher in a simulation with non-ideal switches as the input torque to the generator would stay the same. The calculated switch stress with ideal switches will therefore be lower than for a real converter. As the switch stress number is used for comparison with another converter setup the same problem will apply for the other setup. However the back-to-back converter has three conversion stages whereas the nine-switch converter has only two and consequently a lower voltage drop due to the on-state voltage in the switches.

No transients were considered during switching actions. The voltage and current stress in a real converter setup will be higher than the operating voltage and current during reverse recovery, turn-on and turn-off if no snubber circuits are included. [24] This may also be different in the converter setups as stray inductances, semiconductor switching waveforms and the modulation of the switches influence the over currents and voltages. The calculated switch stress is therefore lower than if transients had been considered.

The bi-directional switches in the nine-switch converter is considered as one switch in the calculations. A bi-directional switch is composed of two RB-IGBTs and should thus be considered as two switches. The simulations were performed with an ideal bi-directional switch so the RMS switch currents found from the simulations in the ideal bi-directional switch should be translated to equivalent RMS-currents in two RB-IGBTs. The RMS-currents can therefore be divided by the square root of two to get the RMS-current in each switch if the current is shared equally between the two switches. However the switch stress is to be used for an economical comparison. A bi-directional switch consisting of two RB-IGBTs will not have the same price as two discrete RB-IGBTs when sold in a single module, neither will it have the same price as one RB-IGBT. As no prices exist for these bi-directional switches today a compromise was made and one bi-directional switch was considered as one single switch and the current passing through it was seen as a current passing in one single switch. The price comparison has therefore a limited accuracy and should only be considered as a guideline to comparison and not as a finite number to be used for determining the total converter price.

The power output from the converters are 10992 W and 11660 W for the 9SC and BTB, respectively. Hence the power output is 6 % higher in the BTB but the switch

stress is 16.7 % higher, resulting in a lower switch utilization. The nine-switch converter shows a switch utilization of 0.0988 $\frac{\mathrm{W}}{\mathrm{VA}}$ while the back-to-back converter has 0.0898 $\frac{\mathrm{W}}{\mathrm{VA}}$. The switch utilization is thus 10 % higher in the nine-switch converter but due to the assumptions made in the calculations this is not considered significant enough to draw any conclusions regarding the switch stress.

The semiconductor cost per output kW could not be found for both the converters as data for the RB-IGBT could not be obtained in time for the deadline.

7.4 Module driven method

The module driven method was introduced in [23] to compare converter setups with different operating conditions such as number of switches, switch ratings and different cooling requirements. The aim was a fair comparison independent of topologies and it is based on choosing a semiconductor module and heat sink and setting the temperature conditions fixed. By finding the allowed voltage and current capabilities with these restrictions a generator rating could be identified. The ratio between the switch rating and the generator rating was then used as a number for comparison.

The maximum allowable loss in one switch could then be found by using the thermal resistances in the semiconductor module and heat sink and fixing the junction temperature. The power level in the generators giving the maximum allowed losses was found through simulations. The loss calculations determining the power dissipation in each switch was done by considering the switching energies given in the semiconductor data sheets. Equations for the switching energy as a function of the current was put in a DLL-file connected to the simulation program as explained for the IXYS loss calculations. The operating voltage was set to half of the available blocking voltage in the switches and thus lower than what was used in the efficiency investigation in section 3. This was done to reduce the problems with over voltages and a low DPF in the induction generators as seen in the efficiency investigation. Semiconductors from IXYS were used in the loss calculations as no thermal data was known for the Fuji switches. As seen in the efficiency investigation the losses were higher for the IXYS RB-IGBTs in the 9SC. The losses in the BTB were more similar if adjusted for the poor DPF in the induction generator. The calculated generator output in this section will be higher if the loss distribution is equal but the efficiency is higher and the results for the 9SC might therefore have been better if all necessary data could be found for the Fuji RB-IGBTs.

The limiting switch in the BTB was switch S2 which is found in the middle converter stage. The reactive power is supplied by the conversion stage closest to the generator so that only active power is flowing through switch S2. Switch BM is the limiting factor in the 9SC but in this switch also a reactive current was flowing and causing losses. The displacement power factors were found in both cases as this would affect the losses and thus which switch that was limiting the possible generator power. A difference of one and two percentage points was apparent between the generator in the BTB and the two generators in the 9SC. However as only the active power caused the losses in the BTB case, this difference in the DPFs is not significant for the results. The actual DPF value in the 9SC will on the other hand affect the conduction losses in the 9SC and a

higher power factor would have improved the results. In these simulations an induction generator was used and with it a certain DPF will be evident. Choosing a permanent magnet synchronous generator with a possibility of unity power factor could improve the results in favor of the 9SC but this was not investigated further.

The relative switch rating was found to be 48.2 $\frac{\text{VA}}{\text{W}}$ and 50.5 $\frac{\text{VA}}{\text{W}}$ in the nine-switch converter and back-to-back converter, respectively. The necessary switch capacity per output power is then 4.6 % lower in the nine-switch converter. Several factors are behind this results. The thermal resistances in the switches were equal for the IGBT parts in the semiconductors but the diode part in the IGBTs with anti-parallel diode had the highest resistance. This factor was outweighed by the fact that the diode losses were lower than in the IGBT parts and thus the limiting switches were a RB-IGBT and an IGBT.

The bi-directional switch was considered as one single switch in the switch utilization as the aim was a cost comparison and that the switch current found through simulations was the current in the bi-directional switch and not the current in each RB-IGBT. In these calculations the bi-directional switch is considered as two switches as it is the silicon usage which is to be compared and not the cost. The DLL-file could then use the polarity of the currents to calculate the losses separately in each RB-IGBT. The total switch number in the nine-switch converter is then 22, with four regular IGBTs in the full-bridge part and 18 reverse-blocking IGBTs. In comparison the back-to-back converter has fourteen switches. As the voltage utilization in the full-bridge stage with six switches in the back-to-back converter is twice that in the nine-switch converter, half the current is needed to obtain the same output power from one generator if displacement power factor and distortion is equal. This means that the 14 switches in the back-to-back setup can convert the same total power as the 22 switches in the nine-switch converter. The total switch rating is therefore high for the nine-switch converter and in numbers it is 46 % higher than in the back-to-back converter. However the losses and loss distribution are also part of determining the power level in the converter. The highest losses in the back-to-back converter is in switch $S2$ in the full-bridge stage in the middle of the converter. This switch is limiting the power output from the generator so that the power output from the back-to-back converter is lower than that in the nine-switch converter. As all the power has to go through four switches, higher losses per switch would be expected in comparison with the six-switch stage between the generator and DC-link. The total power going through only four switches is also a fact in the rectification stage in both converters but diode forward voltages and switching energies are lower in the diodes than in the IGBTs. The efficiency is better in the BTB with 96.1 % compared to 94.8 % in the 9SC with these loss calculations but still the loss distribution leaves the 9SC better out in the module driven method.

The approach in this method has similarities with the switch stress found in section 4 which is the ratio between the power output and the product of the currents and voltages the switches are exposed for. The module driven method uses the ratio between the actual switch ratings and the possible power output with these ratings. The first one therefore tries to determine the necessary switch rating from the current and voltages imposed on the switches for a given power whereas the latter calculates the possible power output

with actual switches. A generator rating or switch rating was therefore the starting point in the two methods. The switch utilization does not take into account the actual losses connected to the switch stresses and what steps that would have to be taken if the loss distribution is as shown in the efficiency investigation. The module driven method calculates a fictitious generator power and therefore does not consider if the current ratings are matching available generator ratings. Both methods were affected by the limited availability of data for RB-IGBT in a bi-directional arrangement. No thermal data for a bi-directional chip was found and prices for bi-directional switches were not obtained. The discrete RB-IGBT was therefore used in the calculations with implications for the results compared to what would have been found with a true bi-directional switch.

7.5 Other areas of application

The nine-switch converter is proposed for supplying power to an isolated power system where a varying power source needs to be complimented by an auxiliary power source. If the two generating sources are dimensioned to supply the full load power the disadvantage of the doubled DC-voltage can be eliminated. The total power output would never be higher than the rated power of one generator and the DC-voltage can therefore be dimensioned thereafter. In the wind power application both generators are suspected to supply their full power at the same time and thus a double DC-voltage is needed with a correspondingly higher switch stress. In this application the silicon usage can be reduced compared to the wind power application investigated in the other sections.

The simulations of this system verifies the voltage sharing between the generators with other modulation indexes than 0.5 for both generators. A longer time for acceleration and power levels not fully corresponding to the voltage levels are evident but these problems should be addressed in further work.

7.6 Size and reliability

In a multiple generator configuration one back-to-back converter has to be installed per generator whereas only one converter per two generators are needed for the 9SC. The converters are assumed parallel connected before the transformer stage as is done in an existing split drivetrain configuration. [27] The total switch number is then 36 and 40 for the 9SC and BTB, respectively, before the transformer and rectification stage. A lower number of installed components will reduce the maintenance need if the bi-directional switches and the IGBTs are expected to have the same reliability.

The size of the bi-directional switches compared to one single IGBT is not known as no information about this could be obtained. The connection of two RB-IGBTs in anti-parallel is however expected to be less size demanding than two stand-alone RB-IGBTs as only one heat sink is needed for mounting it. Together with the need for one capacitor per connected generator the size demand is expected to be higher for a BTB solution. The capacitors also present problems regarding maintenance. [10]

8 Conclusion

The main features of the converters withdrawn from the study is presented in a table to show the background for the comparative evaluation. The conclusion of the feasibility study and additional comments follow below. The size and reliability considerations are done for a split drivetrain configurated wind turbine with four generators.

	Nine-switch converter	Back-to-back converter
Efficiency	97.7 %	97.7 %
Silicon usage	48.2 $VAW^{-}1$	50.5 $VAW^{-}1$
Cost per output kW	Not available	32.9 NOK/kW
Size	36 switches	40 switches and four DC-capacitors
Reliability	No specific issues	DC-capacitors with high maintenance demand [10]
Switching frequency limit	The middle switch row has an effective switching frequency twice that in the upper and lower row and this limits the maximum switching frequency	No specific issues
Loss distribution	The middle switch row experiences the highest losses in the converter due to the doubled switching frequency	The inverter stage in the converter has the highest losses
THD_v	139.4/139.3 %	68.6 %
THD_i	8.8 %	4.3 %
Voltage utilization	0.306	0.612
Power oscillations at 50 Hz	0.2 % of output power	0.03 % of output power
Switch availability	RB-IGBTs of today have low ratings and this complicates the production of a converter with a high power rating	High IGBT ratings easily available

Table 8.1: Key results from the feasibility study

- With these characteristics the nine-switch converter is concluded to be a feasible converter solution for a split drivetrain configuration.
- Conduction losses in the single AC-AC stage in the nine-switch converter were in line with those in the two AC-DC-AC stages in the back-to-back converter. Expected benefits from a lower number of converter stages were therefore not existent regarding the conduction losses.

- The price comparison has a limited accuracy due to the assumptions that had to be made because of lacking data for the bi-directional switches. It should therefore only be considered as a guideline to comparison and not as a finite number to be used for determining the total converter price. Semiconductor cost per output kW could however not be found for the nine-switch converter due to lacking price data for the RB-IGBT. This part of the feasibility study therefore did not lead to any conclusions.
- Another application is proposed for taking advantage of the characteristics of the nine-switch converter and at the same time avoiding the low voltage utilization. In an isolated power system where a varying power generation needs to be complimented with an auxiliary power generation two generators can each be rated to supply the total load power. The DC-voltage can then be rated to only be able to give rated voltage in one generator at the time and the switch ratings are also correspondingly lower.

9 Suggestions for further work

- A laboratory experiment should be performed to verify the loss calculations and the operation of the nine-switch converter.
- Further investigation of the proposed application with two different generating sources should be done to examine the load sharing and the ability of the converter to maintain a stable output power under all conditions.

References

[1] K. P. Astad, "Double Input AC/AC Nine-Switch Converter for Wind Power Applications," tech. rep., 2009.

[2] A. Garcés and M. Molinas, "Cluster interconnection of offshore wind farms using direct AC high frequency links," *8th International Workshop on Large-Scale Integration of Wind Power into Power Systems as well as on Transmission Networks for Offshore Wind Farms, Bremen, Germany*, 2009.

[3] Epcos, "Film capacitors Ű power electronic capacitors." `http://www.epcos.com/inf/20/50/ds/B3236X.pdf`, 2010.

[4] IXYS, "Ixeh 40n120d1." `http://www.ixys.com/Product_portfolio/power_devices.asp`, 2010.

[5] IXYS, "Ixrh 40n120." `http://www.ixys.com/Product_portfolio/power_devices.asp`, 2010.

[6] P. Bresesti, W. Kling, R. Hendriks, and R. Vailati, "HVDC connection of offshore wind farms to the transmission system," *Energy Conversion, IEEE Transactions on*, vol. 22, pp. 37 –43, march 2007.

[7] C. W. Plc., "The Liberty 2.5 MW wind turbine." `http://www.clipperwind.com/pdf/Liberty_Brochure_2009_LR.pdf`, 2006.

[8] T. Kominami and Y. Fujimoto, "A novel nine-switch inverter for independent control of two three-phase loads," in *Industry Applications Conference, 2007. 42nd IAS Annual Meeting. Conference Record of the 2007 IEEE*, pp. 2346–2350, Sept. 2007.

[9] S. Lundberg, "Wind farm configuration and energy efficiency studies - series DC versus AC layouts," Master's thesis, Chalmers University of Technology, 2006.

[10] J. Kim and S. Sul, "New control scheme for AC-DC-AC converter without DC link electrolytic capacitor," in *Power Electronics Specialists Conference, 1993. PESC '93 Record., 24th Annual IEEE*, pp. 300 –306, 20-24 1993.

[11] F. Gao, L. Zhang, D. Li, P. C. Loh, Y. Tang, and H. Gao, "Optimal pulse-width modulation of nine-switch converter," *Power Electronics, IEEE Transactions on*, vol. PP, no. 99, pp. 1 –1, 2010.

[12] S. M. Dehghan, M. Mohamadian, A. Yazdian, and F. Ashrafzadeh, "Space vectors modulation for nine-switch converters," *Power Electronics, IEEE Transactions on*, vol. PP, no. 99, pp. 1 –1, 2009.

[13] C. Liu, B. Wu, N. Zargari, and D. Xu, "A novel three-phase three-leg AC/AC converter using nine IGBTs," in *Power Electronics Specialists Conference, 2007. PESC 2007. IEEE*, pp. 2685 –2690, 17-21 2007.

[14] "Infineon." http://www.infineon.com/cms/en/product/channel.html.

[15] S. Kharitonov, M. Petrov, D. Korobkov, M. Maslov, and T. Zhoraev, "A principle of calculation dynamic and static power losses with hard-switching IGBT," pp. 147 – 149, july 2005.

[16] A. Odaka, J. Itoh, I. Sato, H. Ohguchi, H. Kodachi, N. Eguchi, and H. Umida, "Analysis of loss and junction temperature in power semiconductors of the matrix converter using simple simulation methods," vol. 2, pp. 850 – 855 vol.2, Oct. 2004.

[17] T. Naito, M. Takei, M. Nemoto, T. Hayashi, and K. Ueno, "1200v reverse blocking IGBT with low loss for matrix converter," in *Power Semiconductor Devices and ICs, 2004. Proceedings. ISPSD '04. The 16th International Symposium on*, pp. 125 – 128, 24-27 2004.

[18] Semikron, "Semikron skm195gb066d igbt with anti-parallel diode." http://www.semikron.com.au/internet/gecont/pdf/1614.pdf, 2010.

[19] M. Bierhoff and F. Fuchs, "Semiconductor losses in voltage source and current source IGBT converters based on analytical derivation," in *Power Electronics Specialists Conference, 2004. PESC 04. 2004 IEEE 35th Annual*, vol. 4, pp. 2836 – 2842 Vol.4, 2004.

[20] M. Chinthavali, L. Tolbert, and B. Ozpineci, "4h-SiC GTO thyristor and p-n diode loss models for HVDC converter," in *Industry Applications Conference, 2004. 39th IAS Annual Meeting. Conference Record of the 2004 IEEE*, vol. 2, pp. 1238 – 1243 vol.2, 3-7 2004.

[21] H. Fujita, S. Tominaga, and H. Akagi, "Analysis and design of a DC voltage-controlled static VAr compensator using quad-series voltage-source inverters," *Industry Applications, IEEE Transactions on*, vol. 32, pp. 970 –978, jul/aug 1996.

[22] R. W. Erickson and D. Maksimovic, *Fundamentals of power electronics.* Kluwer Academic Publishers, 2001.

[23] J. Wiik, A. Kulka, T. Isobe, K. Usuki, M. Molinas, T. Takaku, T. Undeland, and R. Shimada, "Loss and rating considerations of a wind energy conversion system with reactive compensation by Magnetic Energy Recovery Switch (MERS)," in *Wind Power to the Grid - EPE Wind Energy Chapter 1st Seminar, 2008. EPE-WECS 2008*, pp. 1 –6, march 2008.

[24] N. Mohan, T. M. Undeland, and W. P. Robbins, *Power Electronics - Converters, applications and design.* John Wiley and Sons Inc, 2003.

[25] M. Takei, Y. Harada, and K. Ueno, "600 V-IGBT with reverse blocking capability," in *Power Semiconductor Devices and ICs, 2001. ISPSD '01. Proceedings of the 13th International Symposium on*, pp. 413–416, 2001.

[26] M. Takei, T. Naito, and K. Ueno, "The reverse blocking IGBT for matrix converter with ultra-thin wafer technology," in *Power Semiconductor Devices and ICs, 2003. Proceedings. ISPSD '03. 2003 IEEE 15th International Symposium on*, pp. 156–159, April 2003.

[27] L. E. Teschler, "Green technology: Inside an advanced wind turbine." `http://machinedesign.com/article/green-technology-inside-an-advanced-wind-turbine-0605`, 2008.

[28] A. Garcés, "Conversations and discussions at the University of Science and Technology(NTNU),Trondheim," Spring 2010.

A Modulation technique for the nine-switch converter

This section is a part of the specialization study that this work is a continuation of. The full project work can be found in [1] and this chapter is included here as it is necessary to understand the characteristics of the nine-switch converter.

The modulation technique for the nine-switch converter is a modified pulse width modulation(PWM) technique found in [8]. A control signal for each phase of the upper input is compared with a triangular carrier and when the control signal is higher than the carrier wave the upper switch is gated ON. Switch AP is thus gated by the reference signal for phase A of the upper input, BP is controlled by the reference for phase B, upper input, and so on. The control signals for the lower switches follows the opposite logic and the switches are gated OFF when the control signals are higher than the carrier. The gating signals from the upper and lower switches are fed into a NAND logic and the output is used as gating signals for the middle switches. The NAND logic is shown in table A.1. An offset of 0.5 is added to the upper control signals and -0.5 is added to the lower control signals before they are compared with the triangular carrier. The switching logic for the middle switches and the offset ensures the sharing of the square wave voltage.

The switchings are visualized in A.1 together with the reference signals and the carrier. The colors of the reference signals are the same as for the switches they are controlling. The figure shows two switching periods with a switching frequency of 2.0 kHz which is the frequency used in the simulations. It can be seen that the upper and lower row have all their switches gated ON simultaneously for approximately half the period each with an overlap when they shift. This corresponds with Mode 1 and Mode 2 in the figure where the former means all the lower switches ON and the latter that all the upper switches are ON. When all the switches in one row is gated ON, one of the generators is shorted and the six other switches can be seen as a regular six-switch converter. If the lower row is gated ON, a six-switch converter is existent consisting of the upper and middle switches. Due to the NAND logic the upper switch will never be gated ON at the same time as its lower switch is ON as can be seen from table A.1. This is recognized as the normal switching pattern in a regular six-switch converter to ensure that DC-side is never shorted. In the nine-switch converter this means that one phase of the generator is not connected with the same phase in the other generator through the transformer. This would however happen if both upper and lower inputs are OFF at the same time, then the middle switch would follow the NAND logic and be gated ON. With the modulation technique described this is nevertheless avoided. The upper and lower row gated OFF would mean the control signal for the upper switch lower than the carrier at the same time as the control signal for the lower row is higher than the carrier. For this to happen the lower control signal should be higher than the upper. With the offset added to the control signals this will not happen independent of the phase angles between the upper and lower generator as long as the modulation rates are not higher than 0.5. Modulation with no offset added would not leave all the switches in one row gated ON simultaneously for approximately half a period each and the middle switches will stay gated ON. This

is shown in figure A.2. With a phase angle between the two generators the shorting of one phase through the middle switch with the upper and lower switch OFF would also happen. This is because the phase angle allows the control signal for the lower switches to be higher than the upper control signal. These differences seem to be important for the operation of the nine-switch converter. However it is not yet fully understood why it has to be like this.

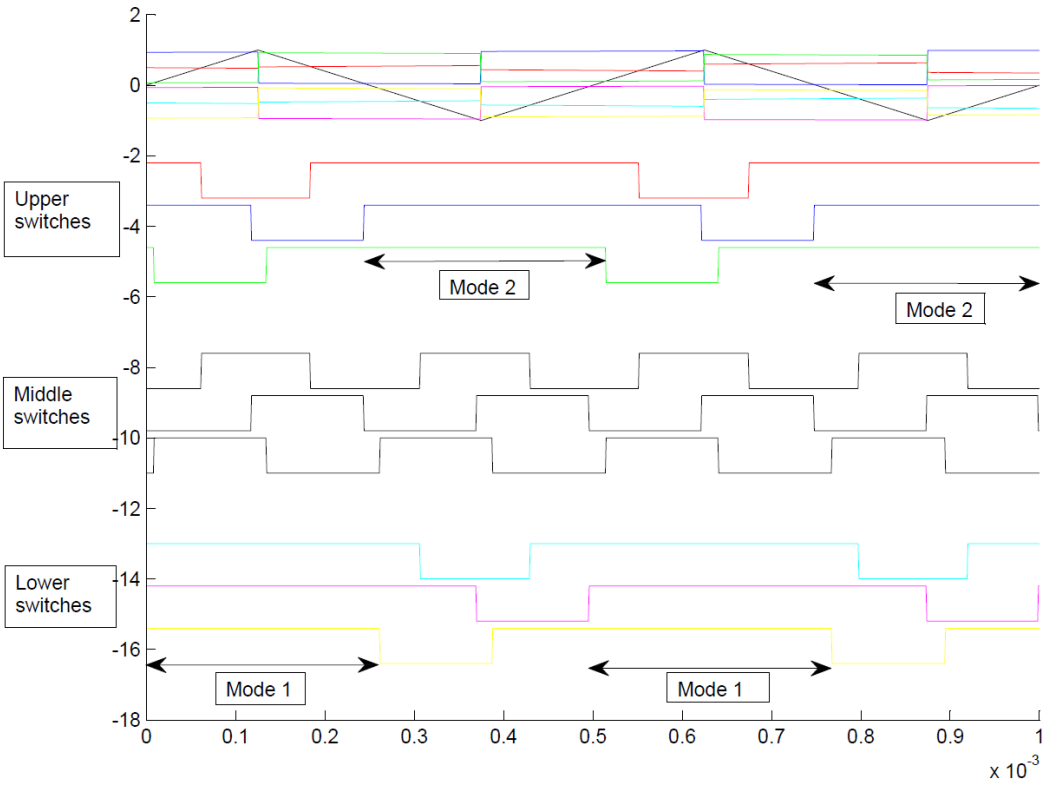

Figure A.1: Switching sequences with offset of 0.5 and -0.5 added to the control signals

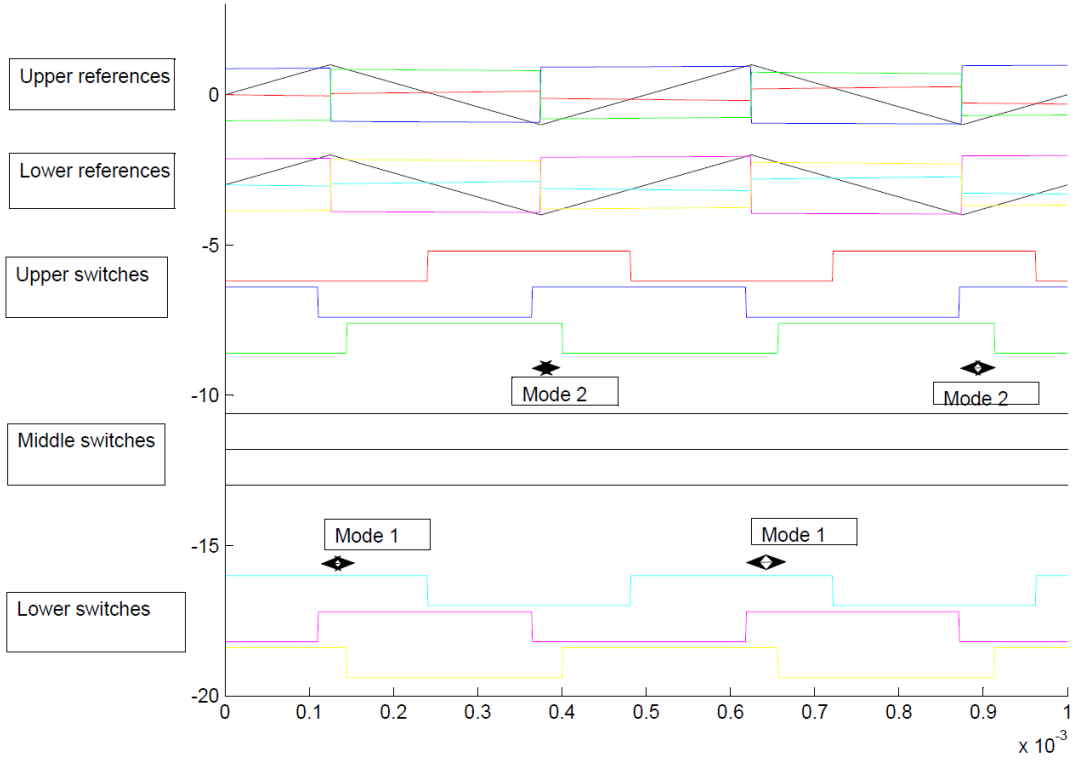

Figure A.2: Switching sequences with no offset added to the control signals

Switches		
Upper	Lower	Middle
1	1	0
1	0	1
0	1	1
0	0	1

Table A.1: NAND logic for gating of the middle switches

To achieve a square wave output the control signals are inverted with the frequency desired for the square wave. The equations for the reference signals are as follows:

$$V_1ref = A_1sin(2\pi f_1 + \phi_1)(2sx - 1) \tag{A.1}$$

$$V_2ref = A_2sin(2\pi f_2 + \phi_2)(2sx - 1) \tag{A.2}$$

where A is the desired amplitude, ϕ is the phase angle for the three different phases and f_1 and f_2 are the input frequencies. The factor sx has the function of inverting the

switching signal. It is produced by comparing a sinusoidal signal with frequency equal to the desired square wave frequency with zero. When it is higher than zero sx is set to one else it is zero. A value sy is set to the logic opposite of sx. These two signals can then control the full-bridge converter.

A general modulation rate without any offset is given by equation A.3 [8].

$$m = \frac{\widehat{V}_{ref}}{\frac{\widehat{V}_{dc}}{2}} \tag{A.3}$$

With the offset described previously the final modulation rates become as shown in equation A.4 and A.5.

$$m_1 = \frac{\widehat{V}_{1ref}}{\frac{\widehat{V}_{dc}}{2}} + 0.5 \tag{A.4}$$

$$m_2 = \frac{\widehat{V}_{2ref}}{\frac{\widehat{V}_{dc}}{2}} - 0.5 \tag{A.5}$$

The DLL-files containing the implementation of this modulation and the pulse width modulation for the back-to-back converter is attached in the pages below and was made with help from [28].

D:\home\kristast\Master\Masteroppgåve\HFLinkDoblePrinte.c 1

```
//*/
//  Switching for the nine-switch converter
//*/

#include <math.h>

//triangular: between -1 y 1: f(0) = 0 y df(0)>0
double portadora(double t, double f,double carAngle)
{
    double y ;
    y =  1-0.636619772367581*acos(sin(6.28318531*f*t-carAngle));
    return y;
}

// a useful function: get the max between three double values
double maximo(double A, double B, double C)
{
    double y;
    if (A>B)
        y = A;
    else
        y = B;
    if (C>y)
        y = C;
    return y;
}
double nand(double A, double B)  // NAND logic
{
    double y;
    y = 0;
    if (A == 0)
        y = 1;
    if (B == 0)
        y = 1;
    return y;
}

// Switching
__declspec(dllexport) void simuser (t, dt, in, out)
double t, dt;
double *in, *out;
{
    const double ph = 2.094395102393195;  // 120 degres
    const double pi = 3.141592653589793;  // pi
    double fp;                // frecuenciy of the carrier
    double w1;                // frecuenciy of signal 1 (50 Hz)
    double w2;                // frecuenciy of signal 2 (50 Hz) but could be diferent
    double wt;                // frecuenciy in the transformer
    // Control signal variables
    double VA;
    double VB;
    double VC;
    double Va;
    double Vb;
    double Vc;
    double y;   //Carrier variable
    //Variables for calculating the offset
    double r1;
    double r2;
    double a1;   //offset in the upper generator
    double a2;   //offset in the lower generator
    double m1;      // = Vref1/(Vdc/2)
    double m2;      // = Vref2/(Vdc/2)
    //gate signal variables
    double uh;
    double vh;
    double wh;
    double ul;
    double vl;
    double wl;
    double hg;
    //inverting signal variables
    double sx;
    double sy;
```

D:\home\kristast\Master\Masteroppgåve\HFLinkDoblePrinte.c 2

```
    // variables for calculating the offset
    double r11;
    double r22;
    //variables for angle in the carrier and inverting signal
    double carAngle;
    double invertering;


    fp = in[0];
    w1 = 2*pi*in[1];
    w2 = 2*pi*in[2];
    m1 = in[3];       //modulation upper generator
    m2 = in[4];       //modulation lower
    hg  = pi*in[5]/180;     //Phase shift between the generators
    wt = 2*pi*in[6];        //Angular frequency of the inverting signal
    carAngle=2*pi*in[7];  //Angle of the carrier signal
    invertering=2*pi*in[8];  // Angle of the inverting signal

    // Switching for the full bridge

y = cos(wt*t-invertering);
if (y>0)
{
    sx = 0;
    sy = 1;
}
else
{
    sx = 1;
    sy = 0;
}
//// Control signals for the nine-switch converter
//

VA = m1*sin(w1*t    )*(2*sx-1);
VB = m1*sin(w1*t-ph )*(2*sx-1);
VC = m1*sin(w1*t+ph )*(2*sx-1);

Va = m2*sin(w2*t    + hg)*(2*sx-1);
Vb = m2*sin(w2*t-ph + hg)*(2*sx-1);
Vc = m2*sin(w2*t+ph + hg)*(2*sx-1);

r1 = maximo(VA,VB,VC);
r2 = maximo(Va,Vb,Vc);
a2 =r1/(r1+r2);
a1 =r2/(r1+r2);

VA = VA + a1;     //Upper generator references
VB = VB + a1;
VC = VC + a1;

Va = Va - a2;     //Lower generator references
Vb = Vb - a2;
Vc = Vc - a2;

y = portadora(t,fp,carAngle);


//Nine-switch converter output signals
//UH

    if (VA>y)
        uh = 1;
    else
        uh = 0;
//VH
    if (VB>y)
        vh = 1;
    else
        vh = 0;
//WH
    if (VC>y)
        wh = 1;
    else
```

```
D:\home\kristast\Master\Masteroppgåve\HFLinkDoblePrinte.c                    3
        wh = 0;
//UL
    if (Va<y)
        ul = 1;
    else
        ul = 0;
//VL
    if (Vb<y)
        vl = 1;
    else
        vl = 0;
//WL
    if (Vc<y)
        wl = 1;
    else
        wl = 0;

//Back-to-back converter output signals(no offset and no inverting of control signal)
//UH
//if (VA>y){
//      uh = 1;
//      ul = 0;}
//else{
//      uh = 0;
//      ul = 1;}
////VH
//if (VB>y){
//      vh = 1;
//      vl = 0;}
//else{
//      vh = 0;
//      vl = 1;}
////WH
//if (VC>y){
//      wh = 1;
//      wl = 0;}
//else{
//      wh = 0;
//      wl = 1;}



    out[0] = uh;
    out[1] = vh;
    out[2] = wh;
    out[3] = nand(uh,ul);
    out[4] = nand(vh,vl);
    out[5] = nand(wh,wl);
    out[6] = ul;
    out[7] = vl;
    out[8] = wl;
    out[9] = sx;
    out[10]= sy;
    out[11]= y;
    out[12]=VA;
    out[13]=VB;
    out[14]=VC;
    out[15]=Va;
    out[16]=Vb;
    out[17]=Vc;
    out[18]=a1; //Prev[0];
    out[19]=a2;//testesvitsjingar;
    }
```

B DLL-files for loss calculations

The DLL-files linked with the simulation program receive switch current and voltage values from the ideal switching and calculates the losses with these values. To determine what type of switching is occurring values from three time steps are stored and compared. Figure B.1 visualizes the three measured values for both current and voltage during a turn-on and turn-off transition. Point zero is the measurement first in time while point two is the measurement last in time. For every time step the points advance in time. Point zero is then the former point one and point one is the former point two while the new measurement is stored in point two.

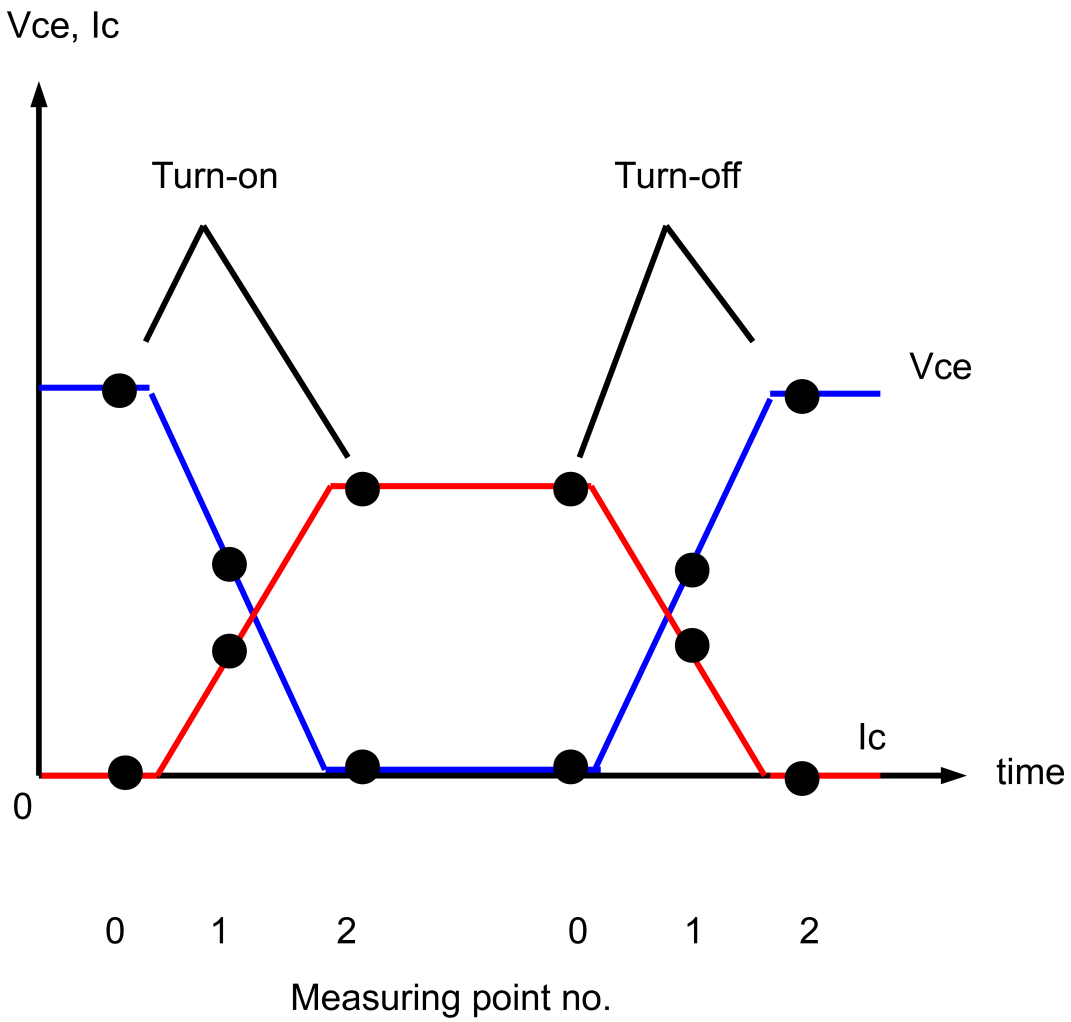

Figure B.1: Visualization of DLL-script measurements during switching transitions

Three stored values are used as a safety measure even though only two are needed.

For turn-on and turn-off the method is the same for both RB-IGBTs and regular IGBTs as the ideal switchings in the simulation program are not affected by the semiconductor type. In the DLL-files there is however a difference as the switching transitions are determined simultaneously for both RB-IGBTs in the bi-directional switch.

To first identify if a switching is occurring, regardless of what type, the amplitude of the absolute value of the point zero and point two currents are compared. If the absolute value is higher than 0.01 A and then goes lower than this in point two a turn-on switching or reverse recovery is evident. If it goes from below 0.01 A and higher a turn-off or reverse recovery is happening. A value higher than zero is used to prevent noise in the measurements to count as switchings. With ideal measurement tools in the simulation program no noise should be evident but noise due to numerical problems may exist. The limit is set very low to prevent any effect on the number of switchings found. The reason for the reverse recovery being part in both transitions of the absolute value of the current is that it is done for both the anti-parallel RB-IGBTs at the same time. The turn-on or turn-off determined by comparing the absolute value of the currents is actually the turn-on or turn-off of the bi-directional switch. Separating the turn-on and the turn-off in each discrete RB-IGBT therefore needs another step before they are found. The counterpart of a turn-on or turn-off in the bi-directional switch is therefore the reverse recovery which can happen in both the RB-IGBTs.

Distinguishing the turn-on from the reverse recovery is done by comparing the first and last measurement in time. When the voltage measured at point one is positive and the current at point two is also positive a turn-on is evident. As there is no on-state voltage in the ideal switches the voltage during conduction is zero and the voltage will only be positive in the blocking state of the switch. The explanation here is for the RB-IGBT with its forward current being positive with the same reference frame as the measured current. The forward current in the other RB-IGBT would correspond to a negative measured current and the switchings can be decided in the same way just by changing the polarities of voltages and currents in the explained method. Turn-on in the other switch is found by changing the polarities of the voltage and currents in the explained method.

The determination of the turn-off uses the current measured in point one and the voltage measured in point two, that is the opposite of the turn-on method. If they are positive and negative, respectively, a turn-off is occurring. As for turn-on the turn-off in the other anti-parallel RB-IGBT is found by changing the polarities of the voltage and currents.

The reverse recovery in the diode is determined in the same way as the turn-off in the IGBTs as the ideal switching of a diode is similar with the ideal switching in an IGBT. The RB-IGBT experiences reverse recovery when the switch is turned off by a reverse voltage rather than being gated off. The RB-IGBT reverse recovery is nevertheless included in the general switching action in the bi-directional switch determined by the absolute value of the current going below or higher than 0.01 A. A simple else command in the script therefore separates the reverse recovery from the regular turn-on or turn-off. If the switching was not caused by a regular turn-on or turn-off the reverse recovery is

evident in one of the RB-IGBTs.

The DLL-files for the nine-switch converter and back-to-back converter are attached in the pages below and they were made with help from [28].

D:\home\kristast\Master\Masteroppgåve\printeperdidas.c 1

```c
#include <math.h>
#include <stdio.h>

// Equations for Fuji Electric semiconductors
// Conduction losses
double conduccion(double Ica)
{
    const double a =  22.789;
    const double b =  28.536;
    const double c = -32.091;
    double Vce;
    double Pc;
    double Ic;
    Ic = fabs(Ica);
        Vce = (-b+sqrt(b*b-4*a*(c-Ic)))/(2*a);
    Pc = Ic*Vce;
    return Pc;
}
double conducciondiode(double Ica)
{
    double Pc;
    double Ic;
    double Vc;
    Ic=fabs(Ica);
    if(Ic>=0 && Ic<55.55){
    Vc=-0.000037*Ic*Ic+0.01*Ic+0.52;
    }
    else if(Ic>=55.55 && Ic<100){
    Vc=1+(Ic-55.55)*0.0056;
    }
    else if (Ic>=100 && Ic<166.66){
    Vc=1.25+(Ic-100)*0.00375;
    }
    else{
    Vc=1.5+(Ic-166.66)*0.0036;
    }

    Pc = Ic*Vc;
    return Pc;
}
// Turn-on losses
double EpOn(double Ic,double Vc)
// Vc is mesured before the switching and Ic after
{
    double Icc;
    double Vcc;
    double k1;
    double k2;
    double Eon;
    Vcc = fabs(Vc);
    Icc = fabs(Ic);
    k1 = (8.14e-12)*Vcc*Vcc + (1.78e-7)*Vcc;
    k2 = (2.78e-7 )*Vcc*Vcc + (1.32e-5)*Vcc;
    Eon = k1*Icc*Icc + k2*Icc;
    return Eon;
}


// Turn-off losses
double EpOff(double Ic,double Vc)
{
    double Icc;
    double Vcc;
    double k1;
    double k2;
    double Eoff;
    Icc = fabs(Ic);
    Vcc = fabs(Vc);
    k1 = ( 4.77e-8)*Vcc + (4.92e-5);
    k2 = (-2.98e-9 )*Vcc*Vcc + (2.11e-4)*Vcc;
    Eoff = k1*Icc*Icc + k2*Icc;
    return Eoff;
}
// Reverse recovery losses in the RB-IGBT
```

D:\home\kristast\Master\Masteroppgåve\printeperdidas.c 2

```
double EpRR(double Ic,double Vc)
{
    double Vcc;
    double Icc;
    double k1;
    double k2;
    double Err;
    Vcc = fabs(Vc);
    Icc = fabs(Ic);
    k1 = (-5.66e-11)*Vcc*Vcc + (-1.82e-7)*Vcc;
    k2 = ( 3.73e-9 )*Vcc*Vcc + ( 9.35e-5)*Vcc;
    Err = k1*Icc*Icc + k2*Icc;
    return Err;
}
//Reverse recovery losses for the diode
double EpRRdiode(double Ic,double Vc)
{
    double Icc;
    double Err;
    double Vrr;
    double Vref=300;
    double Iref=100;
    Vrr=fabs(Vc);
    Icc=fabs(Ic);
    if(Icc<100){
    Err=2.08*Icc/Iref;  //2,08mJ
    }
    else if(Icc>=100 && Icc<200){
    Err =(2.08+((5.6-2.08)/100)*(Icc-100));
    }
    else{
    Err=5.6; //5.6mJ
    }
    //Changing the value due to different Err as a function of voltage
    Err=Err*Vrr/Vref;
    return Err;
}

//Equations for IXYS semiconductors
//Conduction losses
double conduccion(double Ica)
{
    double Vce;
    double Pc;
    double Icc;
    Icc = fabs(Ica);
    if(Icc>=0 && Icc<5){
        Vce =1.3*Icc/5;}
    else if(Icc>=5 && Icc<10){
    Vce=1.3+(Icc-5)*0.4/5;
    }
    else if(Icc>=10 && Icc<20){
    Vce=1.7+(Icc-10)*0.6/10;
    }
    else if(Icc>=20 && Icc<30){
    Vce=2.3+(Icc-20)*0.5/10;
    }
    else if(Icc>=30 && Icc<40){
        Vce=2.8+(Icc-30)*0.4/10;}
    else if(Icc>=40 && Icc<50){
    Vce=3.2+(Icc-40)*0.4/10;
    }
    else if(Icc>=50){
    Vce=3.6+(Icc-50)*0.4/10;
    }

    Pc = Icc*Vce;
    return Pc;
}
double conducciondiode(double Ica)
{
    double Vce;
    double Pc;
    double Icc;
```

D:\home\kristast\Master\Masteroppgåve\printeperdidas.c 3

```
    Icc = fabs(Ica);
    if(Icc>=0 && Icc<5){
        Vce =0.94*Icc/5;}
    else if(Icc>=5 && Icc<10){
    Vce=0.94+(Icc-5)*0.31/5;
    }
    else if(Icc>=10 && Icc<20){
    Vce=1.25+(Icc-10)*0.25/10;
    }
    else if(Icc>=20 && Icc<30){
    Vce=1.5+(Icc-20)*0.25/10;
    }
    else if(Icc>=30 && Icc<40){
        Vce=1.75+(Icc-30)*0.25/10;}
    else if(Icc>=40 && Icc<50){
    Vce=2+(Icc-40)*0.1/10;
    }
    else if(Icc>=50){
    Vce=2.1+(Icc-50)*0.1/10;
    }

    Pc = Icc*Vce;
    return Pc;
}
// On losses
double EpOn(double Ica,double Vc)
// Vc is mesured before the switching and Ic after
{
    double Vce;
    double Eon;
    double Icc;
    double Vref=600;
    Icc = fabs(Ica);
    Vce=fabs(Vc);
    if(Icc>=0 && Icc<10){
    Eon=Icc*2.5/10;
    }
    else if(Icc>=10 && Icc<20){
    Eon=2.5+(Icc-10)*3.05/10;
    }
    else if(Icc>=20 && Icc<30){
    Eon=5.55+(Icc-20)*3.05/10;
    }
    else if(Icc>=30 && Icc<40){
    Eon=8.6+(Icc-30)*3.05/10;}

    else if(Icc>=40 && Icc<50){
    Eon=11.65+(Icc-40)*3.05/10;
    }
    else if(Icc>=50){
    Eon=14.7+(Icc-50)*3.1/10;
    }
    Eon=Eon*Vce/Vref;
    return Eon;
}
// Off losses
double EpOff(double Ica,double Vc)
{
    double Vce;
    double Eoff;
    double Icc;
    double Vref=600;
    Icc = fabs(Ica);
    Vce=fabs(Vc);
    if(Icc>=0 && Icc<10){
    Eoff=Icc*0.1/10;
    }
    else if(Icc>=10 && Icc<20){
    Eoff=0.1+(Icc-10)*0.3/10;
    }
    else if(Icc>=20 && Icc<30){
    Eoff=0.4+(Icc-20)*0.4/10;
    }
    else if(Icc>=30 && Icc<40){
```

D:\home\kristast\Master\Masteroppgåve\printeperdidas.c 4

```
    Eoff=0.8+(Icc-30)*0.5/10;}

    else if(Icc>=40 && Icc<50){
    Eoff=1.3+(Icc-40)*0.9/10;
    }
    else if(Icc>=50){
    Eoff=2.2+(Icc-50)*0.8/10;
    }
    Eoff=Eoff*Vce/Vref;
    return Eoff;
}

// Reverse recovery
double EpRR(double Ica,double Vc)
{
    double Vce;
    double Err;
    double Icc;
    double Vref=600;
    Icc = fabs(Ica);
    Vce=fabs(Vc);
    if(Icc>=0 && Icc<10){
    Err=Icc*3.3/10;
    }
    else if(Icc>=10 && Icc<20){
    Err=3.3+(Icc-10)*2.3/10;
    }
    else if(Icc>=20 && Icc<30){
    Err=5.6+(Icc-20)*1.1/10;
    }
    else if(Icc>=30 && Icc<40){
    Err=6.7+(Icc-30)*1.1/10;}

    else if(Icc>=40 && Icc<50){
    Err=7.8+(Icc-40)*1.1/10;
    }
    else if(Icc>=50){
    Err=8.9+(Icc-50)*1.5/10;
    }
    Err=Err*Vce/Vref;
    return Err;
}
double EpRRdiode(double Ica,double Vc)
{
double Vce;
    double Err;
    double Icc;
    double Vref=600;
    Icc = fabs(Ica);
    Vce=fabs(Vc);
    if(Icc>=0 && Icc<10){
    Err=Icc*0.9/10;
    }
    else if(Icc>=10 && Icc<20){
    Err=0.9+(Icc-10)*0.4/10;
    }
    else if(Icc>=20 && Icc<30){
    Err=1.3+(Icc-20)*0.5/10;
    }
    else if(Icc>=30 && Icc<40){
    Err=1.8+(Icc-30)*0.1/10;}

    else if(Icc>=40 && Icc<50){
    Err=1.9+(Icc-40)*0.1/10;
    }
    else if(Icc>=50){
    Err=2+(Icc-50)*0.1/10;
    }
    Err=Err*Vce/Vref;
    return Err;
}

// Main function
__declspec(dllexport) void simuser (t, dt, in, out)
```

D:\home\kristast\Master\Masteroppgåve\printeperdidas.c 5

```
double t, dt;
double *in, *out;
{
    /*  Input
      in 0-12       Switch currents
      in 13-25      Voltage collector emitter

   */
// Static vectors for storing data from the last time step
   static double Pcond[13] =  { 0, 0, 0, 0, 0, 0, 0, 0, 0, 0, 0, 0, 0 };
   static double Pcondv[13] =  { 0, 0, 0, 0, 0, 0, 0, 0, 0, 0, 0, 0, 0 };
   static double Pconddiode[13]={ 0, 0, 0, 0, 0, 0, 0, 0, 0, 0, 0, 0, 0 };
   static double PcondvDiode[13]={ 0, 0, 0, 0, 0, 0, 0, 0, 0, 0, 0, 0, 0 };
   static double Son[13] =  { 0, 0, 0, 0, 0, 0, 0, 0, 0, 0, 0, 0, 0 };
   static double Sondiode[13]={ 0, 0, 0, 0, 0, 0, 0, 0, 0, 0, 0, 0, 0 };
   static double Soff[13] =  { 0, 0, 0, 0, 0, 0, 0, 0, 0, 0, 0, 0, 0 };
   static double Srev[13] =  { 0, 0, 0, 0, 0, 0, 0, 0, 0, 0, 0, 0, 0 };
   static double Pon[13] =  { 0, 0, 0, 0, 0, 0, 0, 0, 0, 0, 0, 0, 0 };
   static double Poff[13] =  { 0, 0, 0, 0, 0, 0, 0, 0, 0, 0, 0, 0, 0 };
   static double Prev[13] =  { 0, 0, 0, 0, 0, 0, 0, 0, 0, 0, 0, 0, 0 };
   static double Iaa0[13];
   static double Iaa1[13];
   static double Iaa2[13];
   static double Vaa0[13];
   static double Vaa1[13];
   static double Vaa2[13];
   static double Tp = 0;
   int k;
   double Ic[13];
   double Vc[13];
   double Pcc;



// to take to input data
   for (k = 0; k<13; k++)
   {
      Ic[k] = in[k];
      Vc[k] = in[k+13];
   }

// Initialization:

   if(t<2*dt)
   {
     for (k = 0; k<13; k++)
     {
        Iaa0[k]  = 0;
        Iaa1[k]  = 0;
        Iaa2[k]  = 0;
        Vaa0[k]  = 0;
        Vaa1[k]  = 0;
        Vaa2[k]  = 0;

     }
   }
for (k =0; k<13; k++)
{
// Conduction losses
    if(k<9){                //RB-IGBT
    Pcc = conduccion(Ic[k]);
   Pcond[k] = Pcond[k] + Pcc;}
    else{
        if(Ic[k]<0){                    //IGBT with anti-parallel diode
            Pcc= conducciondiode(Ic[k]);
            Pconddiode[k]=Pconddiode[k]+Pcc;}
        else {
            Pcc = conduccion(Ic[k]);
            Pcond[k] = Pcond[k] + Pcc;}

    }
```

D:\home\kristast\Master\Masteroppgåve\printeperdidas.c 6

```
// Switching losses
   Iaa0[k] = Iaa1[k];
   Iaa1[k] = Iaa2[k];
   Iaa2[k] = Ic[k];

   Vaa0[k] = Vaa1[k];
   Vaa1[k] = Vaa2[k];
   Vaa2[k] = Vc[k];
   if(k<9){                                    //  Switch losses in the bi-directional
    switches
if((fabs(Iaa0[k])<0.01)&&(fabs(Iaa2[k])>0.01))  // Determining turn-on in the bi-
    directional switch
{
    if(((Iaa2[k]>0)&&(Vaa0[k]>0))|((Iaa2[k]<0)&&(Vaa0[k]<0)))  // Determining turn-on in
    the RB-IGBTs
    {
        Son[k] = Son[k] + EpOn(Iaa2[k],Vaa0[k]);

    }
    else                            // Determining reverse-recovery in the RB-IGBTs
    {
        Srev[k] = Srev[k] + EpRR(Iaa2[k],Vaa0[k]);
        reverse++;
    }
}
if((fabs(Iaa0[k])>0.01)&&(fabs(Iaa2[k])<0.01))  // Determining turn-off in the bi-
    directional switch
{
        if(((Iaa0[k]>0)&&(Vaa2[k]>0))|((Iaa0[k]<0)&&(Vaa2[k]<0)))  // Determining turn-off
    in the RB-IGBTs
        {
            Soff[k] = Soff[k] + EpOff(Iaa0[k],Vaa2[k]);
        }
        else                                            //Determining reverse-recovery in
    the RB-IGBTs
        {
        Srev[k] = Srev[k] + EpRR(Iaa0[k],Vaa2[k]);
        }
}
   }
   // Switch losses in the full-bridge converter
   else{
   if((fabs(Iaa0[k])<0.01)&&(fabs(Iaa2[k])>0.01))  // Determining turn-on in the IGBT with
    anti-parallel diode
   {
    if(((Iaa2[k]>0)&&(Vaa0[k]>0)))   // Determining turn-on in the IGBT part
    {
        Son[k] = Son[k] + EpOn(Iaa2[k],Vaa0[k]);

    }
    else if (((Iaa2[k]<0)&&(Vaa0[k]<0)))  // Determining turn-on in the diode
    {Sondiode[k] = 0;}             //Turn-on losses in diode neglected
    else
    {}
   }


if((fabs(Iaa0[k])>0.01)&&(fabs(Iaa2[k])<0.01))  // Determining turn-off in the IGBT with
    anti-parallel diode. 0.01 is used
                        //as a limit to prevent influence from simulation noise
{
    if(((Iaa0[k]>0)&&(Vaa2[k]>0)))  // Determining turn-off in the IGBT part
    {
        Soff[k] = Soff[k] + EpOff(Iaa0[k],Vaa2[k]);
    }
    else if((Iaa0[k]<0)&&(Vaa2[k]>=0)) {     //Determining reverse recovery in the diode
        Srev[k]=Srev[k]+EpRRdiode(Iaa0[k],Vaa2[k]);
    }
    else
    {}
}

   }
}
```

D:\home\kristast\Master\Masteroppgåve\printeperdidas.c 7

```
// The switching losses are in mJ, therefore it is necessary to calculate it in W:  = 1/T* integral(E(t)*dt)
Tp = Tp + dt;

if(Tp>0.02)                          //Averaging switch losses for a 50 hz period
{   for(k=0; k<13; k++){
    Pcondv[k] = Pcond[k]*dt/Tp;
    PcondvDiode[k]= Pconddiode[k]*dt/Tp;
    Pon[k]  =  Son[k]/Tp*0.001;
    Poff[k] = Soff[k]/Tp*0.001;
    Prev[k] = Srev[k]/Tp*0.001;
//Deleting old values
    Pcond[k] = 0;
    Pconddiode[k]=0;
    Son[k]   = 0;
    //
    Son2[k]  = 0;
    //
    Soff[k]  = 0;
    Srev[k]  = 0;
}
    Tp = 0;
}
// putting the output, switch losses are divided by two as they are calculated twice
// because of the three storage vectors

       out[1]=Pcondv[0];
       out[2]=Pon[0]/2;
       out[3]=Poff[0]/2;
       out[4]=Prev[0]/2;
       out[5]=Pcondv[1];
       out[6]=Pon[1]/2;
       out[7]=Poff[1]/2;
       out[8]=Prev[1]/2;

       out[9]=Pcondv[2];
       out[10]=Pon[2]/2;
       out[11]=Poff[2]/2;
       out[12]=Prev[2]/2;

       out[13]=Pcondv[3];
       out[14]=Pon[3]/2;
       out[15]=Poff[3]/2;
       out[16]=Prev[3]/2;

       out[17]=Pcondv[4];
       out[18]=Pon[4]/2;
       out[19]=Poff[4]/2;
       out[20]=Prev[4]/2;

       out[21]=Pcondv[5];
       out[22]=Pon[5]/2;
       out[23]=Poff[5]/2;
       out[24]=Prev[5]/2;

       out[25]=Pcondv[6];
       out[26]=Pon[6]/2;
       out[27]=Poff[6]/2;
       out[28]=Prev[6]/2;

       out[29]=Pcondv[7];
       out[30]=Pon[7]/2;
       out[31]=Poff[7]/2;
       out[32]=Prev[7]/2;

       out[33]=Pcondv[8];
       out[34]=Pon[8]/2;
       out[35]=Poff[8]/2;
       out[36]=Prev[8]/2;

       out[46]=PcondvDiode[9];
       out[47]=PcondvDiode[10];
       out[48]=PcondvDiode[11];
```

```
D:\home\kristast\Master\Masteroppgåve\printeperdidas.c                                                8
       out[49]=PcondvDiode[12];

       out[50]=Prev[9]/2;
       out[51]=Prev[10]/2;
       out[52]=Prev[11]/2;
       out[53]=Prev[12]/2;
}
```

D:\home\kristast\Master\Masteroppgåve\perdidasIGBT.c 1

```c
#include <math.h>
#include <stdio.h>
//Equations for Fuji Electric semiconductors
// Conduction losses
double conduccion(double Ica)
{
    const double a =  22.789;
    const double b =  28.536;
    const double c = -32.091;
    double Vce;
    double Pc;
    double Ic;
    Ic = fabs(Ica);
    Vce = (-b+sqrt(b*b-4*a*(c-Ic)))/(2*a);
    Pc = Ic*Vce;
    return Pc;
}
double conducciondiode(double Ica)
{
    double Pc;
    double Ic;
    double Vc;
    Ic=fabs(Ica);
    if(Ic>=0 && Ic<55.55){
    Vc=-0.000037*Ic*Ic+0.01*Ic+0.52;
    }
    else if(Ic>=55.55 && Ic<100){
    Vc=1+(Ic-55.55)*0.0056;
    }
    else if (Ic>=100 && Ic<166.66){
    Vc=1.25+(Ic-100)*0.00375;
    }
    else{
    Vc=1.5+(Ic-166.66)*0.0036;
    }

    Pc = Ic*Vc;
    return Pc;
}
// Turn-on losses
double EpOn(double Ic,double Vc)
// Vc is mesured before the switching and Ic after
{
    double Icc;
    double Vcc;
    double k1;
    double k2;
    double Eon;
    Vcc = fabs(Vc);
    Icc = fabs(Ic);
    k1 = (8.14e-12)*Vcc*Vcc + (1.78e-7)*Vcc;
    k2 = (2.78e-7 )*Vcc*Vcc + (1.32e-5)*Vcc;
    Eon = k1*Icc*Icc + k2*Icc;
    return Eon;
}
// Turn-off losses
double EpOff(double Ic,double Vc)
{
    double Icc;
    double Vcc;
    double k1;
    double k2;
    double Eoff;
    Icc = fabs(Ic);
    Vcc = fabs(Vc);
    k1 = ( 4.77e-8)*Vcc + (4.92e-5);
    k2 = (-2.98e-9 )*Vcc*Vcc + (2.11e-4)*Vcc;
    Eoff = k1*Icc*Icc + k2*Icc;
    return Eoff;
}

// Reverse recovery losses
double EpRR(double Ic,double Vc)
{
```

```
    double Vcc;
    double Icc;
    double k1;
    double k2;
    double Err;
    Vcc = fabs(Vc);
    Icc = fabs(Ic);
    k1 = (-5.66e-11)*Vcc*Vcc + (-1.82e-7)*Vcc;
    k2 = ( 3.73e-9 )*Vcc*Vcc + ( 9.35e-5)*Vcc;
    Err = k1*Icc*Icc + k2*Icc;
    return Err;
}


double EpRRdiode(double Ic,double Vc)
{
    double Icc;
    double Err;
    double Vrr;
    double Vref=300;
    double Iref=100;
    Vrr=fabs(Vc);
    Icc=fabs(Ic);
    if(Icc<100){
    Err=2.08*Icc/Iref;  //2,08mJ
    }
    else if(Icc>=100 && Icc<200){
    Err =(2.08+((5.6-2.08)/100)*(Icc-100));
    }
    else{
    Err=5.6; //5.6mJ
    }
    //Changing the value due to different Err as a function of voltage
    Err=Err*Vrr/Vref;
    return Err;
}

//Equations for IXYS semiconductors
//Conduction losses
double conduccion(double Ica)
{
    double Vce;
    double Pc;
    double Icc;
    Icc = fabs(Ica);
    if(Icc>=0 && Icc<5){
        Vce =1.1*Icc/5;}
    else if(Icc>=5 && Icc<10){
    Vce=1.1+(Icc-5)*0.4/5;
    }
    else if(Icc>=10 && Icc<20){
    Vce=1.5+(Icc-10)*0.44/10;
    }
    else if(Icc>=20 && Icc<30){
    Vce=1.94+(Icc-20)*0.46/10;
    }
    else if(Icc>=30 && Icc<40){
        Vce=2.4+(Icc-30)*0.4/10;}
    else if(Icc>=40 && Icc<50){
    Vce=2.8+(Icc-40)*0.3/10;
    }
    else if(Icc>=50){
    Vce=3.1+(Icc-50)*0.4/10;
    }
    Pc = Icc*Vce;
    return Pc;
}
//Conduction losses in the diode
double conducciondiode(double Ica)
{
    double Vce;
    double Pc;
    double Icc;
    Icc = fabs(Ica);
```

D:\home\kristast\Master\Masteroppgåve\perdidasIGBT.c 3

```
    if(Icc>=0 && Icc<5){
        Vce =0.94*Icc/5;}
    else if(Icc>=5 && Icc<10){
    Vce=0.94+(Icc-5)*0.31/5;
    }
    else if(Icc>=10 && Icc<20){
    Vce=1.25+(Icc-10)*0.25/10;
    }
    else if(Icc>=20 && Icc<30){
    Vce=1.5+(Icc-20)*0.25/10;
    }
    else if(Icc>=30 && Icc<40){
        Vce=1.75+(Icc-30)*0.25/10;}
    else if(Icc>=40 && Icc<50){
    Vce=2+(Icc-40)*0.1/10;
    }
    else if(Icc>=50){
    Vce=2.1+(Icc-50)*0.1/10;
    }
    Pc = Icc*Vce;
    return Pc;
}
// Turn-on losses
double EpOn(double Ica,double Vc)
// Vc is mesured before the switching and Ic after
{
    double Vce;
    double Eon;
    double Icc;
    double Vref=600;
    Icc = fabs(Ica);
    Vce=fabs(Vc);
    if(Icc>=0 && Icc<10){
    Eon=Icc*1.3/10;
    }
    else if(Icc>=10 && Icc<20){
    Eon=1.3+(Icc-10)*1.4/10;
    }
    else if(Icc>=20 && Icc<30){
    Eon=2.7+(Icc-20)*1.7/10;
    }
    else if(Icc>=30 && Icc<40){
    Eon=4.4+(Icc-30)*1.7/10;}

    else if(Icc>=40 && Icc<50){
    Eon=6.1+(Icc-40)*3.2/10;
    }
    else if(Icc>=50){
    Eon=9.3+(Icc-50)*4.5/10;
    }
    Eon=Eon*Vce/Vref;
    return Eon;
}
// Turn-off losses
double EpOff(double Ica,double Vc)
{
    double Vce;
    double Eoff;
    double Icc;
    double Vref=600;
    Icc = fabs(Ica);
    Vce=fabs(Vc);
    if(Icc>=0 && Icc<10){
    Eoff=Icc*1/10;
    }
    else if(Icc>=10 && Icc<20){
    Eoff=1+(Icc-10)*0.7/10;
    }
    else if(Icc>=20 && Icc<30){
    Eoff=1.7+(Icc-20)*0.6/10;
    }
    else if(Icc>=30 && Icc<40){
    Eoff=2.3+(Icc-30)*0.7/10;}
```

D:\home\kristast\Master\Masteroppgåve\perdidasIGBT.c 4

```
    else if(Icc>=40 && Icc<50){
    Eoff=3+(Icc-40)*0.7/10;
    }
    else if(Icc>=50){
    Eoff=3.7+(Icc-50)*0.6/10;
    }
    Eoff=Eoff*Vce/Vref;
    return Eoff;
}
// Reverse recovery
double EpRRdiode(double Ica,double Vc)
{
    double Vce;
    double Err;
    double Icc;
    double Vref=600;
    Icc = fabs(Ica);
    Vce=fabs(Vc);
    if(Icc>=0 && Icc<10){
    Err=Icc*0.9/10;
    }
    else if(Icc>=10 && Icc<20){
    Err=0.9+(Icc-10)*0.4/10;
    }
    else if(Icc>=20 && Icc<30){
    Err=1.3+(Icc-20)*0.5/10;
    }
    else if(Icc>=30 && Icc<40){
    Err=1.8+(Icc-30)*0.1/10;}
    else if(Icc>=40 && Icc<50){
    Err=1.9+(Icc-40)*0.1/10;
    }
    else if(Icc>=50){
    Err=2+(Icc-50)*0.1/10;
    }
    Err=Err*Vce/Vref;
    return Err;
}

// Main function
__declspec(dllexport) void simuser (t, dt, in, out)
double t, dt;
double *in, *out;
{
    /*  Input
      in 0-13       Current in the bidirectional switch
      in 14-27      Voltage collector emitter
        Output

   */

   static double Pcond[14] =  { 0, 0, 0, 0, 0, 0, 0, 0, 0, 0, 0 ,0 ,0 ,0 };          //    ↙
    Vectors for storing loss values in watt
   static double Pconddiode[14] =  { 0, 0, 0, 0, 0, 0, 0, 0, 0, 0, 0 ,0 ,0 ,0 };
   static double Pcondv[14] =  { 0, 0, 0, 0, 0, 0, 0, 0, 0, 0, 0 ,0 ,0 ,0 };
   static double PcondvDiode[14] =  { 0, 0, 0, 0, 0, 0, 0, 0, 0, 0, 0, 0 ,0 ,0 ,0 };
   static double Son[14] =  { 0, 0, 0, 0, 0, 0, 0, 0, 0, 0, 0 ,0 ,0 ,0 };             //    ↙
    Vectors for storing loss values in joule
   static double Sondiode[14]= { 0, 0, 0, 0, 0, 0, 0, 0, 0, 0, 0 ,0 ,0 ,0 };
   static double Soff[14] =  { 0, 0, 0, 0, 0, 0, 0, 0, 0, 0, 0 ,0 ,0 ,0 };
   static double Srev[14] =  { 0, 0, 0, 0, 0, 0, 0, 0, 0, 0, 0 ,0 ,0 ,0 };
   static double Pon[14] =  { 0, 0, 0, 0, 0, 0, 0, 0, 0, 0, 0 ,0 ,0 ,0 };
   static double Poff[14] =  { 0, 0, 0, 0, 0, 0, 0, 0, 0, 0, 0 ,0 ,0 ,0 };
   static double Prev[14] =  { 0, 0, 0, 0, 0, 0, 0, 0, 0, 0, 0 ,0 ,0 ,0 };
    static double Iaa0[14];                                                          //    ↙
    Vectors for storing measured currents
   static double Iaa1[14];
   static double Iaa2[14];
   static double Vaa0[14];                                                           //    ↙
    Vectors for storing measured voltages
   static double Vaa1[14];
   static double Vaa2[14];
   static double Tp = 0;   //Time
   double Vkap;            //Capacitor voltage
```

D:\home\kristast\Master\Masteroppgåve\perdidasIGBT.c 5

```
   double Ikap;            //Capacitor current
   double Pkap;            //Capacitor losses
   int k;                  //counter
   double Ic[14];          //Measured current
   double Vc[14];          //Measured voltage
   double Pcc;              //For storing conduction loss temporarily
   double teste=0;                          //Testing variables
   static double testesvitsjingar[14];
   double Vceteste;
    double Icteste;
    double a =  22.789;                       //Data values for loss calculations
    double b =  28.536;
    double c = -32.091;


// to take to input data
   for (k = 0; k<14; k++)
   {
      Ic[k] = in[k];
      Vc[k] = in[k+14];
   }
// Inicialization: is not necesary.
   if(t<2*dt)
   {
     for (k = 0; k<14; k++)
     {
        Iaa0[k]  = 0;
        Iaa1[k]  = 0;
        Iaa2[k]  = 0;
        Vaa0[k]  = 0;
        Vaa1[k]  = 0;
        Vaa2[k]  = 0;
        testesvitsjingar[k]=0;
     }
   }
   // capacitor conduction losses
   Vkap=in[28];
   Ikap=in[29];
   Pkap=Vkap*Ikap;

for (k =0; k<14; k++)
{
// conduction losses in the IGBTs
    if(Ic[k]<0){
    Pcc=conducciondiode(Ic[k]);
    Pconddiode[k]=Pconddiode[k]+Pcc;

    }
    else{        // conduction losses in the diodes

    Pcc = conduccion(Ic[k]);
        Pcond[k] = Pcond[k] + Pcc;
    }

// Switching losses
   Iaa0[k] = Iaa1[k];
   Iaa1[k] = Iaa2[k];
   Iaa2[k] = Ic[k];

   Vaa0[k] = Vaa1[k];
   Vaa1[k] = Vaa2[k];
   Vaa2[k] = Vc[k];
if((fabs(Iaa0[k])<0.01)&&(fabs(Iaa2[k])>0.01))  // Determining turn-on in the IGBT
                                                //  with anti-parallel diode
{
    if(((Iaa2[k]>0)&&(Vaa0[k]>0)))   // ON IGBT
    {
        Son[k] = Son[k] + EpOn(Iaa2[k],Vaa0[k]);

    }
    else if (((Iaa2[k]<0)&&(Vaa0[k]<0)))  // Determining Turn-on in diode
    {Sondiode[k] = 0;}
    else
    {
```

D:\home\kristast\Master\Masteroppgåve\perdidasIGBT.c 6

```
        //Srev[k] = 0; //Srev[k] + EpRR(Iaa2[k],Vaa0[k]);

    }
}
if((fabs(Iaa0[k])>0.01)&&(fabs(Iaa2[k])<0.01))  // OFF
{
    if(((Iaa0[k]>0)&&(Vaa2[k]>0)))  // IGBT OFF
    {
        Soff[k] = Soff[k] + EpOff(Iaa0[k],Vaa2[k]);
    }
    else if((Iaa0[k]<0)&&(Vaa2[k]>=0)) {     // Har skifta til Vaa2 istadenfor Iaa2
        Srev[k]=Srev[k]+EpRRdiode(Iaa0[k],Vaa2[k]);      //Srev[k]=Srev[k]+EpRR(Iaa0[k],
    Vaa2[k]);
    testesvitsjingar[k]=testesvitsjingar[k]+1;}
    else
    {}
}


//if((fabs(Iaa0[k])>0.01)&&(fabs(Iaa2[k])<0.01))  // Determining Turn-off in IGBT
//{
//  if(((Iaa0[k]>0)&&(Vaa2[k]>0)))  // IGBT OFF
//  {
//      Soff[k] = Soff[k] + EpOff(Iaa0[k],Vaa2[k]);
//  }
//  else if((Iaa0[k]<0)&&(Iaa2[k]>=0)) {     // Determining Turn-off in diode=rev.rec.
//  Srev[k]=Srev[k]+EpRRdiode(Iaa0[k],Vaa2[k]);
//  testesvitsjingar[k]=testesvitsjingar[k]+1;
//  }
//
//  else
//  {
//      teste++;     //Test variable
//  }
//}

}


// The switching losses are in mJ, therefore it is necesary to calculate it in W:  = 1/T*
    integral(E(t)*dt)
Tp = Tp + dt;

if(Tp>0.02)
{   for(k=0; k<14; k++){
    Pcondv[k] = Pcond[k]*dt/Tp;
    PcondvDiode[k]=Pconddiode[k]*dt/Tp;
    Pon[k]  =  Son[k]/Tp*0.001;

    Poff[k] = Soff[k]/Tp*0.001;
    Prev[k] = Srev[k]/Tp*0.001;

    Pcond[k] = 0;
    Pconddiode[k]=0;
    Son[k]   = 0;

    Soff[k]  = 0;
    Srev[k]  = 0;
    }
    Tp = 0;
}
// put the output
       out[0]=Pcondv[0];
       out[1]=Pon[0]/2;
       out[2]=Poff[0]/2;
       out[3]=Prev[0]/2;


       out[4]=Pcondv[1];
       out[5]=Pon[1]/2;
       out[6]=Poff[1]/2;
       out[7]=Prev[1]/2;
```

D:\home\kristast\Master\Masteroppgåve\perdidasIGBT.c 7

```
       out[8]=Pcondv[2];
       out[9]=Pon[2]/2;
       out[10]=Poff[2]/2;
       out[11]=Prev[2]/2;

       out[12]=Pcondv[3];
       out[13]=Pon[3]/2;
       out[14]=Poff[3]/2;
       out[15]=Prev[3]/2;

       out[16]=Pcondv[4];
       out[17]=Pon[4]/2;
       out[18]=Poff[4]/2;
       out[19]=Prev[4]/2;

       out[20]=Pcondv[5];
       out[21]=Pon[5]/2;
       out[22]=Poff[5]/2;
       out[23]=Prev[5]/2;

       out[24]=Pcondv[6];
       out[25]=Pon[6]/2;
       out[26]=Poff[6]/2;
       out[27]=Prev[6]/2;

       out[28]=Pcondv[7];
       out[29]=Pon[7]/2;
       out[30]=Poff[7]/2;
       out[31]=Prev[7]/2;

       out[32]=Pcondv[8];
       out[33]=Pon[8]/2;
       out[34]=Poff[8]/2;
       out[35]=Prev[8]/2;

       out[36]=Pcondv[9];
       out[37]=Pon[9]/2;
       out[38]=Poff[9]/2;
       out[39]=Prev[9]/2;

       out[40]=Pcondv[10];
       out[41]=Pon[10]/2;
       out[42]=Poff[10]/2;
       out[43]=Prev[10]/2;

       out[44]=Pcondv[11];
       out[45]=Pon[11]/2;
       out[46]=Poff[11]/2;
       out[47]=Prev[11]/2;

       out[48]=Pcondv[12];
       out[49]=Pon[12]/2;
       out[50]=Poff[12]/2;
       out[51]=Prev[12]/2;

       out[52]=Pcondv[13];
       out[53]=Pon[13]/2;
       out[54]=Poff[13]/2;
       out[55]=Prev[13]/2;

       out[56]=PcondvDiode[0]+PcondvDiode[1]+PcondvDiode[2]+PcondvDiode[3];
       out[57]=PcondvDiode[4]+PcondvDiode[5]+PcondvDiode[6]+PcondvDiode[7];
       out[58]=PcondvDiode[8]+PcondvDiode[9]+PcondvDiode[10]+PcondvDiode[11]+PcondvDiode
   [12]+PcondvDiode[13];

       out[59]=Pcondv[0]+Pcondv[1]+Pcondv[2]+Pcondv[3];
       out[60]=Pcondv[4]+Pcondv[5]+Pcondv[6]+Pcondv[7];
       out[61]=Pcondv[8]+Pcondv[9]+Pcondv[10]+Pcondv[11]+Pcondv[12]+Pcondv[13];
       out[62]=(Pon[0]+Pon[1]+Pon[2]+Pon[3]+Poff[0]+Poff[1]+Poff[2]+Poff[3])/2;
       out[63]=(Pon[4]+Pon[5]+Pon[6]+Pon[7]+Poff[4]+Poff[5]+Poff[6]+Poff[7])/2;
       out[64]=(Pon[8]+Pon[9]+Pon[10]+Pon[11]+Pon[12]+Pon[13]+Poff[8]+Poff[9]+Poff[10]+Poff
   [11]+Poff[12]+Poff[13])/2;
       out[65]=testesvitsjingar[0];    //(Prev[0]+Prev[1]+Prev[2]+Prev[3])/2;
       out[66]=(Prev[4]+Prev[5]+Prev[6]+Prev[7])/2;
```

D:\home\kristast\Master\Masteroppgåve\perdidasIGBT.c 8

```
       out[67]=(Prev[8]+Prev[9]+Prev[10]+Prev[11]+Prev[12]+Prev[13])/2;
       out[68]=PcondvDiode[8];
       out[69]=PcondvDiode[9];
       out[70]=PcondvDiode[10];
       out[71]=PcondvDiode[11];
       out[72]=PcondvDiode[12];
       out[73]=PcondvDiode[13];
       out[74]=PcondvDiode[0];
       out[75]=PcondvDiode[1];
       out[76]=PcondvDiode[2];
       out[77]=PcondvDiode[3];
       out[78]=Pkap; //Vceteste; //testesvitsjingar[3];


}
```

C Conference papers

Results from the specialization project and the master's thesis have been extracted and are presented in two papers. The paper with title "Direct AC/AC power converter for wind power application" was published in the 15th IEEE Mediterranean Electrotechnical Conference (MELECON 2010). The conference was held in Valletta, Malta the 25-28 April.

The paper with title "Double Input AC/AC Nine-Switch Converter for Multiple-Generator Drivetrain Configuration in Wind Turbines" has been accepted for the IEEE International Symposium on Industrial Electronics (ISIE 2010). The symposium is taking place in Bari, Italy in July 2010 and the findings are to be presented orally there. Both papers are included in the next pages.

Direct AC/AC power converter for wind power application

Kristian Prestrud Astad, Marta Molinas
Norwegian University of Science and Technology
Department of Electric Power Engineering
Trondheim, Norway
E-mail: kristast@stud.ntnu.no

***Abstract*—Split drivetrain configurations with multiple generators are one of the solutions for increasing the reliability and reducing the cost of wind turbines. The split drivetrain technology gives the ability to introduce multiple generators and by that reduces the gear size and facilitates variable-speed operation. This paper proposes a double input AC/AC nine-switch converter for direct conversion of low-frequency AC from the generators to high-frequency AC square wave for input to a high frequency transformer used for isolation purposes. The high frequency transformer in connection with a diode rectifier will give a high voltage DC output. With the nine-switch topology a pair of generators can then share one converter and thus reduce the cost of the power electronics. Performance and operation are explained and illustrated in this paper through simulations.**

I. Introduction

Wind power has been and is a major contributor to the generation of renewable energy. The size and rating of the turbines are increasing and research is being done to overcome problems with weight, cost and reliability. For offshore applications the need for large transformer before transferring power to shore is also a challenge. Wind turbines with split drivetrains and back-to-back converters are already commercial [1] and help reduce gear size and thus weight, but still the voltage is too low for HVDC power transfer, which is the preferred offshore solution for long distances. The double input AC/AC nine-switch converter proposed in this paper can convert the variable frequency AC to high-frequency square wave AC. This square wave can be fed into a transformer and rectifier and thus give a high voltage DC by series connection with other wind turbines and proper selection of transformation ratio. This would be a possible configuration for direct power transfer to shore. The split drivetrain configuration with multiple generators can use one nine-switch converter for each pair of generators and reduce the total numbers of switches compared to those needed in a conventional back-to-back converter setup. Both size and cost of the power electronics is then expected to decrease. At the same time the conversion system will allow modularity from which reliability, maintenance and assembly will greatly benefit.

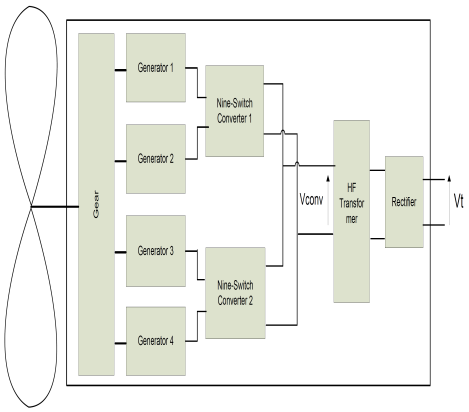

Fig. 1. System layout of nacelle in a split drivetrain turbine with the proposed nine-switch converter

II. Energy Conversion System layout

The proposed converter can be used in a multiple-generator drivetrain as shown in figure 1. The number of generators is here set to four but a higher number is possible. A multiple-generator drivetrain with four permanent magnet generators already exists. [1] The layout consists of a propeller and shaft connected to a gear which distributes the power to four equal sized generators. These can be both induction generators or permanent magnet synchronous generators. A pair of generators share the proposed nine-switch converter and outputs a square wave voltage. The two nine-switch converters are then parallel connected before the voltage is transformed in the high-frequency transformer and then rectified. The output from the wind turbine is now a high voltage DC, and through series connection with n wind turbines as seen in figure 2, a voltage level, $n * V_t$, sufficient for direct power transfer to shore will be achieved.

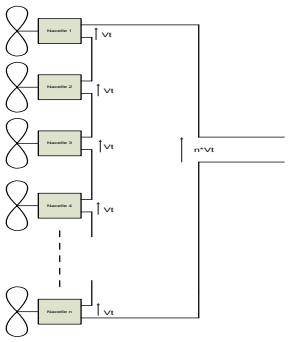

Fig. 2. Series connection of wind turbines in a park with the suggested converter

III. Converter Structure

A. Topology

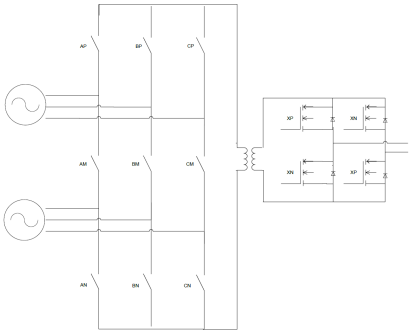

Fig. 3. Nine-switch AC/AC converter structure, high-frequency transformer and full bridge converter

The double input converter is shown in figure 3 and consists of nine bi-directional switches. The switches are bi-directional so as to make possible an AC square wave output. The chosen switches will consist of two reverse-blocking IGBTs (RB-IGBT) in anti-parallel. This choice is due to the possibility of minimizing the losses in the bi-directional switches. Other setups include IGBTs with series connected diodes, however these setups include more components for the current to go through during on-state and thus higher on-state losses. [2] The RB-IGBTs have higher switching losses but a comparison between two anti-paralleled RB-IGBTs and two anti-paralleled sets of an IGBT in series with a diode showed a 1.8 points increase in overall efficiency for the RB-IGBT setup. [3] [4]

The nine-switch converter proposed in this paper is inspired by the one presented in [5] and modified by Garcés and Molinas in [6] to adapt to the specific application investigated here. The topology in [5] is for independent control of to three-phase loads and is an inverter consisting of IGBTs with anti-parallel diodes. The proposed topology here is a converter setup with the power flow in the opposite direction and employs bi-directional switches to enable a square wave output. The three switches in the middle are common for each input. The upper switches are called AP, BP and CP, the lower switches are AN, BN and CN and the middle switches are AM, BM and CM. The upper and lower switches are controlled by using sinusoidal pulse width modulation (PWM), while the switches in the middle get their gating signals by using a logic calculation. [5] The input frequency does not need to be the same but in a split drivetrain configuration with equal gear ratios and generators the frequency of the generators will stay the same. Figure 3 includes a rectifier with switches XP and XN to rectify the square wave after transforming it to a high voltage DC. The structure of this rectifier is dependent on what type of generator at the input. A permanent magnet synchronous machine does not need power transfer in both directions and can thus use a diode rectifier. An induction generator can use an arrangement as shown in figure 3 with standard IGBTs.

B. Modulation Technique

The two control signals are compared against a carrier signal by using PWM modulation. When the control signal for one of the upper switches is higher than the carrier signal the switch will turn ON. For a value lower than the carrier the switch is OFF. The lower switches follow an opposite logic. When the control signals for the lower switches are higher than the carrier the switches are OFF. The gating signals from the upper and lower switches are fed into a NAND logic and the output is used as gating signals for the middle switches. To achieve a square wave output the control signals are inverted with the frequency desired for the square wave. The equations for the control signals are as follows:

$$V_1ref = m_1 sin(2\pi f_1 + \phi_1) \tag{1}$$

$$V_2ref = m_2 sin(2\pi f_2 + \phi_2) \tag{2}$$

where m is the modulation, ϕ is the phase angle for the three different phases, f_1 and f_2 are the input frequencies.

Equation 3 gives a general modulation rate.

$$m = \frac{V_{ref}}{\frac{V_{dc}}{2}} \tag{3}$$

In [5] an offset is used to ensure the sharing of the DC-source between the two generators. These offsets are calculated through the following equations:

$$Offset_1 = 1 - \alpha \tag{4}$$

and

$$Offset_2 = \alpha \tag{5}$$

where α is given in the following equation:

$$\alpha = \frac{|r1|}{|r1| + |r2|}. \quad (6)$$

$|r1|$ and $|r2|$ is the maximum value of the phase voltages for the upper and lower input respectively.

The switchings are visualized in 4 together with the reference signals and the carrier. The colors of the reference signals are the same as for the switches they are controlling. The figure shows two switching periods with a switching frequency of 2.0 kHz which is the frequency used in the simulations. It can be seen that the upper and lower row have all their switches gated ON simultaneously for approximately half the period each with an overlap when they shift. This corresponds with Mode 1 and Mode 2 in the figure where the former means all the lower switches ON and the latter that all the upper switches are ON. When all the switches in one row is gated ON, one of the generators is shorted and the six other switches can be seen as a regular six-switch converter. If the lower row is gated ON, a six-switch converter is existent consisting of the upper and middle switches. Due to the NAND logic the upper switch will never be gated ON at the same time as its lower switch is ON as can be seen from table I. This is recognized as the normal switching pattern in a regular six-switch converter to ensure that DC-side is never shorted. In the nine-switch converter this means that one phase of the generator is not connected with the same phase in the other generator through the transformer. This would however happen if both upper and lower inputs are OFF at the same time, then the middle switch would follow the NAND logic and be gated ON. With the modulation technique described this is nevertheless avoided. The upper and lower row gated OFF would mean the control signal for the upper switch lower than the carrier at the same time as the control signal for the lower row is higher than the carrier. For this to happen the lower control signal should be higher than the upper. With the offset added to the control signals this will not happen independent of the phase angles between the upper and lower generator as long as the modulation rates are not higher than 0.5. Modulation with no offset added would not leave all the switches in one row gated ON simultaneously for approximately half a period each and the middle switches will stay gated ON. The sharing of the square wave is then absent.

Switches		
Upper	Lower	Middle
1	1	0
1	0	1
0	1	1
0	0	1

TABLE I
NAND LOGIC FOR GATING OF THE MIDDLE SWITCHES

IV. SIMULATION STUDY

The simulations are performed in PSIM and in this paper connection of two induction generators to the converter is investigated. Two equal induction generators with rated output of 2 MW each are used as input sources and a DC source of 2.2 kV models the connection to the DC cable. The data of the induction generator are shown in table II. The rectifier is built up with four IGBTs with anti-parallel diodes and there is an ideal transformer between the converter and the rectifier. All the switches in the simulations are ideal as the perspective of these simulations is to examine and verify the functionality of the converter without considering losses at this stage. Two wattmeters are used for measuring output and input power to make sure that the two input sources do not feed the other instead of supplying power to the output. The simulations are performed in PSIM and both modulation and offset is set to 0.5. The switching frequency is set to 2.0 kHz and the inverting frequency of the control signal is set to the same. The input power to the generators is set to 2 MW for each and is ramped up from zero to full power.

Rated power	2	MW
Rated voltage	690	V
Rated frequency	50	Hz
Stator resistance	0.0022	Ω
Stator reactance	0.0376	Ω
Rotor resistance	0.0018	Ω
Rotor reactance	0.0155	Ω
Magnetization reactance	0.9209	Ω
Generator and rotor inertia	5.33	kgm^2
Number of poles	4	

TABLE II
CHARACTERISTIC DATA FOR INDUCTION GENERATOR [7]

The plot in figure 5 shows the obtained square wave and it can be seen that the amplitude of this coincides with the amplitude of the DC-source. The period of the square wave is seen to be 0.5 ms from figure 5. This gives a frequency of 2.0 kHz and thus is the same as the inverting frequency.

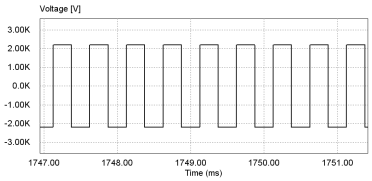

Fig. 5. The square wave input to the transformer

The currents from the input sources are slightly distorted sine waves as can be seen in figure 6 and 7. These shows the respective phase A currents of both inputs of the converter. The amplitudes are the same for the two currents and indicate shared load between the inputs.

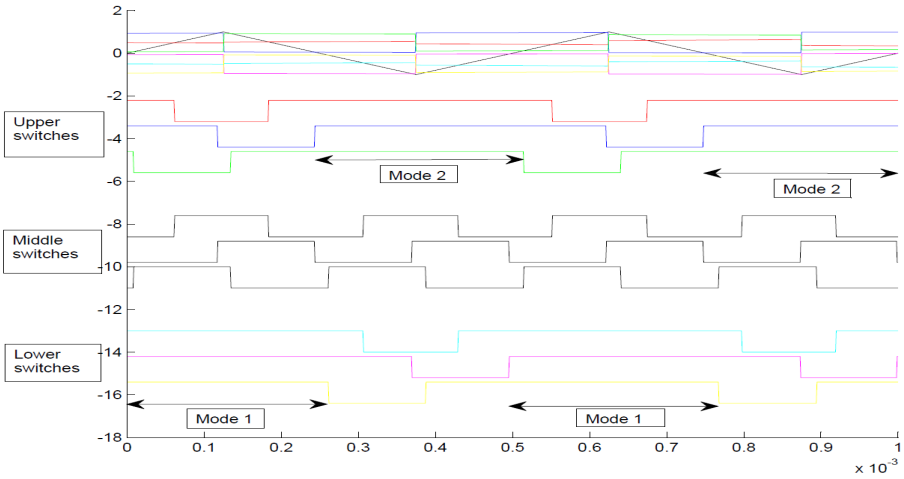

Fig. 4. Switching sequences with carrier and reference signals as shown

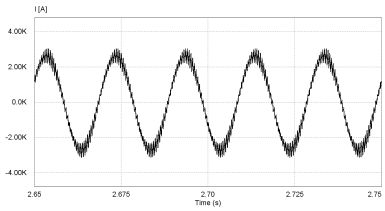

Fig. 6. Phase current of phase A in the upper input

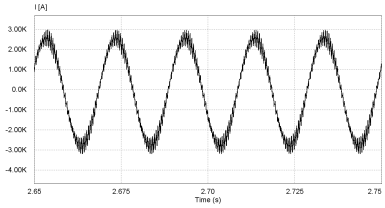

Fig. 7. Phase current of phase A in the lower input

Figure 8 shows that the power oscillates during start up and that the magnetizing current draws a substantial power. A power balance is established after 2 s and it can be seen that the total power is 3.9 Mwatt for both the DC power and for the sum of the two generators.

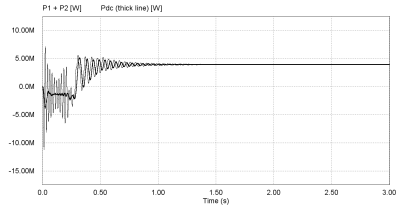

Fig. 8. The input power from the generators and the power consumed in the DC voltage source output

The current input to the transformer is shown in figure 10 and in figure 9 the square wave voltage and the current are shown together. The switchings are clearly visible and there are some disturbances in the current. When the current is positive some notches of negative current occur and vice versa. Evidently this will cause power losses but in this paper a loss model is not included.

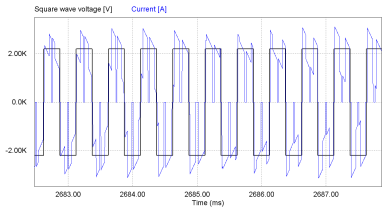

Fig. 9. Square wave voltage and associated current

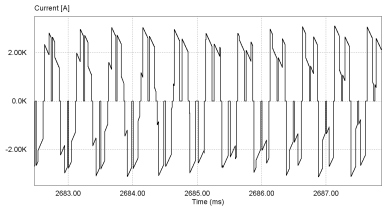

Fig. 10. The current input to the transformer

The harmonic spectrum is shown for the line to line voltage and the phase A current of the upper input in figures 11 to 12. It can be seen that the voltage has harmonic components in a sub bands around the switching frequency and the inverting frequency.

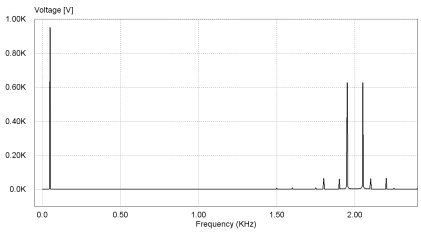

Fig. 11. The harmonic spectrum of the line to line voltage in the upper input with fundamental and switching frequency visible

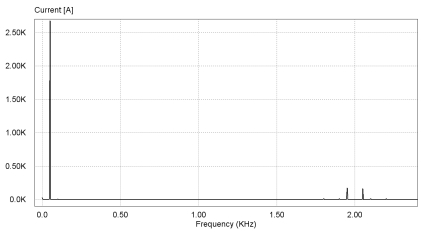

Fig. 12. The harmonic spectrum of the phase A voltage in the upper input with fundamental and switching frequency visible

The total harmonic distortion(THD) is calculated in PSIM with a THD block which uses a 2nd order filter to extract the fundamental frequency. The equation for the calculation of the THD, here with the voltage as the variable, is:

$$THD = \frac{\sqrt{V_{rms}^2 - V_1^2}}{V_1}. \tag{7}$$

where V_{rms} is the total RMS-value of the input voltage and V_1 is the fundamental component. The THD of the current is calculated in the same manner. The THDs of the input line to line voltage and phase A current is seen in 13. The THD of the current is 9.6% while for the voltage the value is 139%.

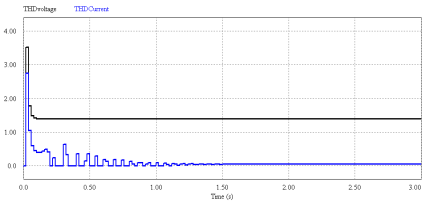

Fig. 13. The total harmonic distortion of the phase A current and the line to line voltage of the upper input

The converter shares the square wave voltage between the two generators. In a back-to-back converter the DC source voltage needed to give 690 V line to line voltage on a generator is 1127 V as this is $\frac{2\sqrt{2}}{\sqrt{3}}$ times the rated line to line voltage of the generator. This relation is for regular PWM and is found in [8]. The nine-switch converter uses a DC source of 2.2 kV to obtain the same rated voltage. This is 1.95 times higher than DC source in a back-to-back converter. Figure 14 shows the relation between the line to line voltage on the generator and the fundamental voltage with two different modulation techniques. The difference between the RMS of the line to line voltage and the RMS of the fundamental voltage constitutes the harmonics in the signal. A DC-voltage with twice the amplitude applied for half the time would give a higher RMS value as the RMS includes squaring the voltage but integrating

over time. The THD in a back-to-back converter is therefore lower than for the THD in the nine-switch converter. As can be seen from the figure it is possible to increase the fundamental voltage by applying another modulation technique. Injection of a third harmonic makes it possible to increase the modulation without the control signal going higher than the carrier and thus avoiding overmodulation. [9]

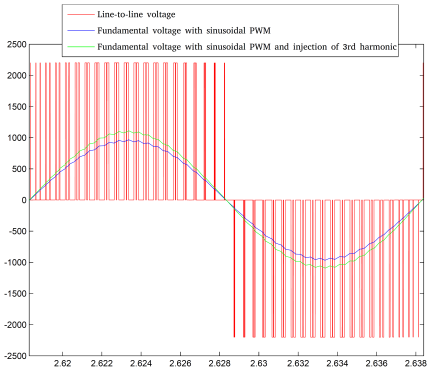

Fig. 14. The fundamental RMS voltage and line to line voltage in the nine-switch converter with and without injection of 3rd harmonic

V. Discussion

This paper has presented a new converter topology for a double-input system to be used for multiple-generator wind turbines. By using this converter in a multiple-generator wind turbine, the total number of switches can be reduced compared to a conventional back-to-back converter. No DC capacitor is present and together with the high frequency transformer, size and and weight of the nacelle can be reduced. Simulations verify that a square wave is obtained by the switching scheme utilized. There are some notches in the current input to the transformer, which will cause power losses. The frequency of the square wave has the same frequency as the inverting frequency of the control signal. The voltage capability of the switches has to be twice that of the back-to-back converter as the two generators share the same voltage source. This higher DC voltage compared to a back-to-back converter gives high THD values and measures should be taken to reduce this. Different modulation techniques such as injecting a third harmonic is one way to reduce the voltage THD. Further work will include investigation of the current notches, implementation of a loss model and examination of the total efficiency of the system. The parallel connection of two converters as proposed in the nacelle layout will be investigated and a control strategy for the converter and rating of the converter will also be performed.

References

[1] Clipper Windpower Plc, *T*he Liberty 2.5 MW Wind Turbine, http://www.clipperwind.com/pdf/Liberty_Brochure_2009_LR.pdf, 2006.
[2] C. Klumpner and F. Blaabjerg, *U*sing reverse-blocking IGBTs in power converters for adjustable-speed drives, IEEE Transactions on Industry Applications, 2006.
[3] M. J. Bland, P. W. Wheeler, J. C. Clare, L. Empringham, *C*omparison of Bi-directional Switch Components for Direct AC/AC Converters, Annual IEEE Power Electronics Conference, 2004.
[4] Taltronics, *A*pplication technologies of reverse-blocking IGBT, http://www.eepublishers.co.za/images/upload/Taltronics\%20267.pdf, 2007.
[5] T. Kominami and Y. Fujimoto, *A* Novel Nine-Switch Inverter for Independent Control of Two Three-phase Loads, IEEE, 2007.
[6] A. Garcés and M. Molinas, *C*luster Interconnection of Offshore Wind Farms Using Direct AC High Frequency Links, IEEE, 2007. J. Cotrell,*A* Preliminary Evaluation Of a Multiple-Generator Drivetrain Configuration for Wind Turbines, National Renewable Energy Laboratory, 2002.
[7] Anders Elvebakk, *M*odelling of a wind farm with induction generator in PSCAD, static and dynamic reactive power compensation, Mastersthesis, NTNU, 2004.
[8] N. Mohan, T. M. Undeland, W. P. Robbins, *P*ower Electronics - Converters, applications and design, John Wiley and Sons Inc, 2003.
[9] J. A. Houldsworth and D. A. Grant, *T*he Use of Harmonic Distortion to Increase the Output Voltage of a Three-Phase PWM Inverter, IEEE Transactions on Industry Applications, 1984.

Fig. 15. Marta Molinas received the diploma of Electromechanical engineer from the National University of Asunción, Paraguay in 1992; MSc from Ryukyu University, Japan, in 1997, and Doctor of Engineering from Tokyo Institute of Technology, Japan, in 2000. She is now Professor at the Norwegian University of Science and Technology engaged in the research of renewable energy systems. Her focus is in FACTS and power electronics for harvesting renewable energy.

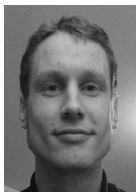

Fig. 16. Kristian Prestrud Astad is currently finishing his Master's Thesis in Electric Power Engineering at the Norwegian University of Science and Technology under the supervision of Prof. Marta Molinas. In his thesis he is working with a feasibility study about an AC/AC converter for wind power applications. His other fields of interest include motor drives and electric machines.

Double Input AC/AC Nine-Switch Converter for Multiple-Generator Drivetrain Configuration in Wind Turbines

Kristian Prestrud Astad, Marta Molinas
Norwegian University of Science and Technology
Department of Electric Power Engineering
Trondheim, Norway
E-mail: kristast@stud.ntnu.no

***Abstract*—Split drivetrain configurations with multiple generators are one of the solutions for increasing the reliability and reducing the cost of wind turbines. The split drivetrain technology gives the ability to introduce multiple generators and by that reduces the gear size and facilitate variable-speed operation. This paper proposes a double input AC/AC nine-switch converter for direct conversion of low-frequency AC from the generators to high-frequency AC square wave for input to a high frequency transformer used for isolation purposes. The high frequency transformer in connection with a diode rectifier will give a high voltage DC output. With the nine-switch topology a pair of generators can then share one converter and thus reduce the cost of the power electronics. Performance and operation are explained and illustrated in this paper through simulations.**

I. Introduction

Wind power has been and is a major contributor to the generation of renewable energy. The size and rating of the turbines are increasing and research is being done to overcome problems with weight, cost and reliability. For offshore applications the need for large transformer before transferring power to shore is also a challenge. Wind turbines with split drivetrains and back-to-back converters are already commercial [1] and help reduce gear size and thus weight, but still the voltage is too low for HVDC power transfer, which is the preferred offshore solution for long distances. The double input AC/AC nine-switch converter proposed in this paper can convert the variable frequency AC to high-frequency square wave AC. This square wave can be fed into a transformer and rectifier and thus give a high voltage DC by series connection with other wind turbines and proper selection of transformation ratio. This would be a possible configuration for direct power transfer to shore. The split drivetrain configuration with multiple generators can use one nine-switch converter for each pair of generators and thus reduce size and cost of the power electronics compared to conventional back-to-back converters. At the same time this will allow modularity from which reliability, maintenance and assembly will greatly benefit.

II. Energy Conversion System layout

The proposed converter can be used in a multiple-generator drivetrain as shown in figure 1. The number of generators is here set to four but a higher number is possible. A multiple-generator drivetrain with four generators already exists. [1] The layout consists of a propeller and shaft connected to a gear which distributes the power to four equal sized generators. These can be both induction generators or permanent magnet synchronous generators. A pair of generators share the proposed nine-switch converter and outputs a square wave voltage. The two nine-switch converters are then parallel connected before the voltage is transformed in the high-frequency transformer and then rectified. The output from the wind turbine is now a high voltage DC, and through series connection with n wind turbines as seen in figure 2, a voltage level, $n * V_t$, sufficient for direct power transfer to shore will be achieved.

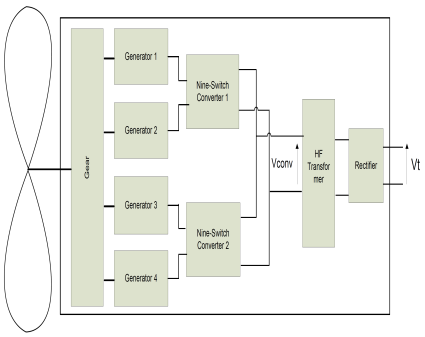

Fig. 1: System layout of nacelle in a split drivetrain turbine with the proposed nine-switch converter

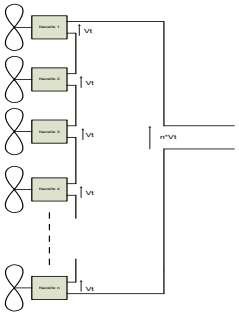

Fig. 2: Series connection of wind turbines in a park with the suggested converter

III. Converter Structure

A. Topology

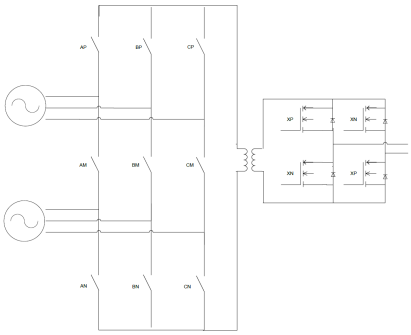

Fig. 3: Nine switch AC/AC converter structure, high-frequency transformer and full bridge converter

The double input converter is shown in figure 3 and consists of nine bi-directional switches. The switches are bi-directional so as to make possible an AC square wave output. The chosen switches will consist of two reverse-blocking IGBTs (RB-IGBT) in anti-parallel. This choice is due to the possibility of minimizing the losses in the bi-directional switches. Other setups include IGBTs with series connected diodes, however these setups include more components for the current to go through during on-state and thus higher on-state losses. [7] A comparison between two anti-paralleled RB-IGBTs and two anti-paralleled sets of an IGBT in series with a diode showed a 1.8 points increase in overall efficiency for the RB-IGBT setup. [8] [6]

The nine-switch converter proposed in this paper is inspired by the one presented in [3] and modified to adapt to the specific application investigated here. The topology in [3] is for independent control of to three-phase loads and is an inverter consisting of IGBTs with anti-parallel diodes. The proposed topology here is a converter setup with the power flow in the opposite direction and employs bi-directional switches to enable a square wave output. The three switches in the middle are common for each input. The upper switches are called AP, BP and CP, the lower switches are AN, BN and CN and the middle switches are AM, BM and CM. The upper and lower switches are controlled by using pulse width modulation (PWM) with a sine wave control signal while the switches in the middle get their gating signals by using a logic calculation. [3] The input frequency does not need to be the same but in a split drivetrain configuration with equal gear ratios and generators the frequency of the generators will stay the same. Figure 3 includes a rectifier with switches XP and XN to rectify the square wave after transforming it to a high voltage DC.

B. Modulation Technique

The two control signals are compared against a carrier signal by using PWM modulation. When the control signal for one of the upper switches is higher than the carrier signal the switch will turn ON. For a value lower than the carrier the switch is OFF. The lower switches follow an opposite logic. When the control signals for the lower switches are higher than the carrier the switches are OFF. The gating signals from the upper and lower switches are fed into a NAND logic and the output is used as gating signals for the middle switches. This logic is shown in table I.

Switches		
Upper	Lower	Middle
1	1	0
1	0	1
0	1	1
0	0	1

TABLE I: NAND logic for gating of the middle switches

To achieve a square wave output the control signals are inverted with the frequency desired for the square wave. The equations for the control signals are as follows:

$$V_1ref = m_1 sin(2\pi f_1 + \phi_1) \tag{1}$$

$$V_2ref = m_2 sin(2\pi f_2 + \phi_2) \tag{2}$$

where m is the modulation, ϕ is the phase angle for the three different phases and f_1 and f_2 are the input frequencies.

Equation 3 shows a general modulation rate.

$$m = \frac{V_{ref}}{\frac{V_{dc}}{2}} \tag{3}$$

In the simulations an offset is added to ensure the sharing of the square wave voltage between the two generators. The modulation rate then becomes:

$$m = \frac{V_{ref}}{\frac{V_{dc}}{2}} + Offset \tag{4}$$

In the following simulations the offset is set to 0.5 and -0.5 for the upper and lower inputs and the modulation is then limited to 0.5 to avoid square wave modulation. Together with the NAND logic this offset leaves all upper switches gated ON simultaneously for half a period and the lower switches gated ON for the other half and thus ensuring a sharing of the available voltage. When this occurs a regular six-switch converter is evident serving only one of the generators. The NAND logic makes it possible to gate only the middle switch ON and thus deviate from this manner. However this will never occur as this action would demand the upper control signal to be lower than the triangular signal at the same time as the lower control signal is higher than the triangular signal. When an offset of 0.5 is added to and subtracted from the control signals this cannot happen for modulation ratios lower than 0.5.

IV. Simulation Study

The simulation model is set up in PSIM and consists of two permanent magnet generators from the PSIM library. These are run with a constant torque of $5\,\mathrm{Nm}$. On the DC side, a DC source of $500\,\mathrm{V}$ models the connection to the DC cable. The rectifier is built up with four IGBTs with anti-parallel diodes and there is an ideal transformer between the converter and the rectifier. All the switches in the simulations are ideal as the perspective of these simulations is to examine and verify the functionality of the converter without considering losses at this stage. Two wattmeters are used for measuring output and input power to make sure that the two input sources do not feed the other instead of supplying power to the output.

The simulations are performed in PSIM and both modulation and offset is set to 0.5. The switching frequency is set to $2.0\,\mathrm{kHz}$ and the inverting frequency of the control signal is set to $2.0\,\mathrm{kHz}$. A dq-control is implemented to control the generator speed and currents. The block diagram of the converters is depicted in figure 4 and shows the dq-control for each generator and the logic for the modulation.

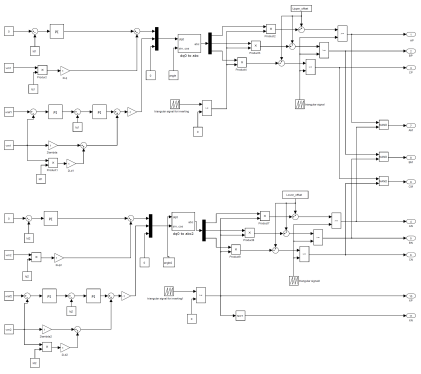

Fig. 4: Control system

The plot in figure 5 shows the obtained square wave which is coinciding with the amplitude of the DC-source. The period of the square wave is seen to be $0.5\,\mathrm{ms}$ from figure 5. This gives a frequency of $2.0\,\mathrm{kHz}$ and thus is the same as the inverting frequency.

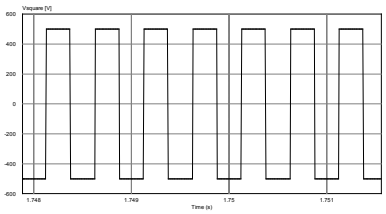

Fig. 5: The square wave input to the transformer

The currents from the input sources are slightly distorted sine waves as can be seen in figure 6 and 7. These shows the respective phase A currents of both inputs of the converter. The amplitudes are the same for the two currents and indicate shared load between the inputs.

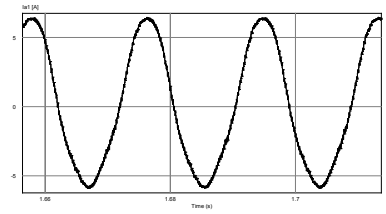

Fig. 6: Phase current of phase A in the upper input

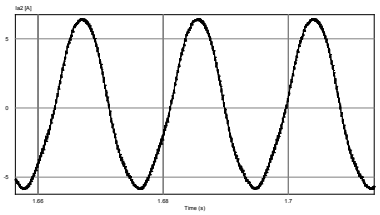

Fig. 7: Phase current of phase A in the lower input

Figure 8 shows that the generator powers are oscillating and not reaching a stable performance. The same is seen for the power to the DC-source in figure 9. The difference between the DC-source power and the power from the generators is seen in figure 10 and is not zero. As the switches and transformer are ideal no difference should be apparent but may be due to the low and high pass filters used in the wattmeters. The wattmeter on the DC-side uses a low pass filter with cut-off frequency of 20 Hz while the AC-side wattmeter uses a high pass filter with cut-off at 30 Hz.

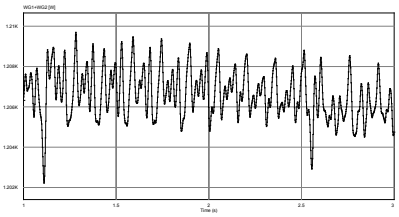

Fig. 8: The input power from the generators

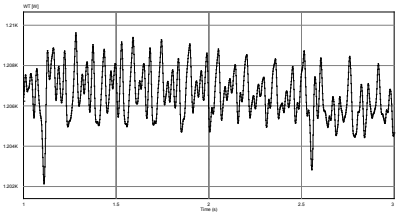

Fig. 9: The power consumed in the DC voltage source output

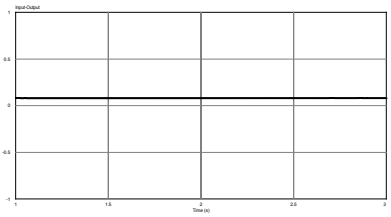

Fig. 10: The power difference between the DC-source power and the power from the generators

The current input to the transformer is shown in figure 12 and the switchings are clearly visible. There are some disturbances in the current. When the current is positive some notches of negative current occur and vice versa. Evidently this will cause power losses but in this paper a loss model is not included. In figure 11 the square wave voltage and the current are shown together but the transformer current is multiplied with 20 to make the current visible when plotted together with the higher amplitude voltage.

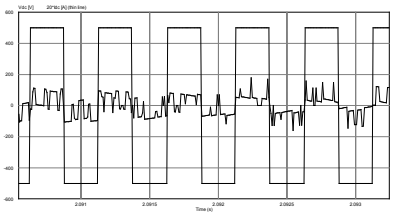

Fig. 11: Square wave voltage and associated current multiplied with 20

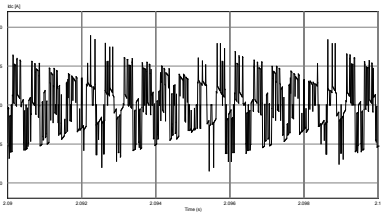

Fig. 12: The current input to the transformer

Simulations were also performed with a non-ideal transformer. The square wave voltage is then distorted, as can be seen in figure 13. A transformer from the PSIM library was used and it is believed that a better designed transformer will improve the operation.

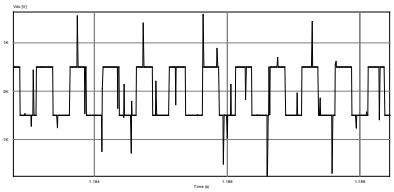

Fig. 13: Square wave voltage with non-ideal transformer

In order to characterize the nine-switch converter, the relation between the modulation index and the line to line three-phase voltage over half of the DC output voltage is shown in figure 14. It can be observed that for m=0.5, maximum ratio is achieved. The voltage ratio is shown both for standard PWM and for PWM with 3rd harmonic injection. The equation for the latter control signal is given in the following equation:

$$V_{ref} = m * K * (sin(2\pi f + \phi) + \frac{1}{6} sin(6\pi f + \phi)). \quad (5)$$

The equation is found in [9] and the factor K is calculated to be 1.155. This ensures that the full voltage range of the converter can be used as the peak of the modified control signal would else be only $\frac{sqrt(3)}{2}$ due to the 3rd harmonic injection.

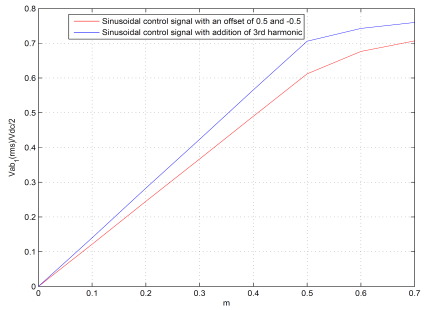

Fig. 14: Modulation index versus input line to line voltage over half the DC voltage

The losses in the RB-IGBTs are calculated by using a simplified method developed and verified by experiments in [10]. Equations describing the loss characteristics are implemented in a DLL-file connected to the simulation program. These equations are for a 600 V, 200 A RB-IGBT and for an equal rated IGBT for the fullbridge part. The simulation program uses ideal switches and calculates voltages and currents and these results are fed to the DLL-file. Five types of losses apply in the converter. Conduction, blocking, turn-on, turn-off and reverse recovery losses. The three latter ones are connected with the switching action while conduction is due to the resistance in the switch while it is conducting. The blocking losses are caused by leakage currents while the switch is blocking the voltages and are small compared to the others and thus neglected. [11] The loss calculations were done with induction generators working at a line-to-line voltage of 122.4 V and with an applied mechanical torque of 60 Nm. This was done as no control system had to be implemented for the induction generator setup. The DLL-file classifies which type that is occurring and calculates the losses by using the following equations [10]:

Conduction loss, P_{cond}:

$$P_{cond} = I_C \cdot V_{CE} \quad (6)$$

where I_C is from the simulation program and V_{CE} is calculated by equation 7.

$$V_{CE} = \frac{-b + \sqrt{b^2 - 4 \cdot a \cdot (c - I_C)}}{2a} \quad (7)$$

where $a = 22.789$, $b = 28.536$, $c = -32.091$ and I_C is the collector current.

Turn-on loss, E_{on}:

$$E_{on} = k_1 \cdot {I_C}^2 + k_2 \cdot I_C \, (mJ) \quad (8)$$

$$k1 = 8.14 \cdot 10^{-12} \cdot V_C + 1.78 \cdot 10^{-7} \cdot V_C \quad (9)$$

$$k_2 = 2.78 \cdot 10^{-7} \cdot V_C^2 + 1.32 \cdot 10^{-5} \quad (10)$$

Turn-off loss E_{off}

$$E_{off} = k_1 \cdot I_C^2 + k_2 \cdot I_C \, (mJ) \quad (11)$$

$$k1 = 4.77 \cdot 10^{-8} \cdot V_C + 4.92 \cdot 10^{-5} \cdot V_C \quad (12)$$

$$k_2 = -2.98 \cdot 10^{-9} \cdot V_C^2 + 2.11 \cdot 10^{-4} \quad (13)$$

Reverse recovery loss, E_{rr}

$$E_{rr} = k_1 \cdot I_C^2 + k_2 \cdot I_C \, (mJ) \quad (14)$$

$$k1 = -5.66 \cdot 10^{-11} \cdot V_C - 1.82 \cdot 10^{-7} \cdot V_C \quad (15)$$

$$k_2 = 3.73 \cdot 10^{-9} \cdot V_C^2 + 9.35 \cdot 10^{-5} \quad (16)$$

The switching losses are in mJand is converted to instantaneous values by equation 17.

$$dW = \frac{E \cdot dt}{1000} (Watt) \quad (17)$$

dW is then the instantaneous power loss found during the time step dt. The average value is found by summing up the

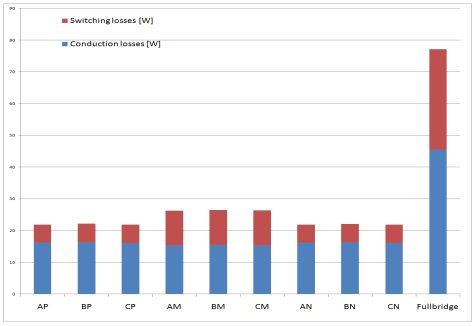

Fig. 15: Switching and conduction losses per switch in the nine-switch converter and total losses in the fullbridge converter

instantaneous losses for a chosen period and then dividing by this period as shown in 18.

$$W_{avg} = \frac{\sum dW}{T} \tag{18}$$

where W_{avg} is the average power loss and T is the period for which the summation is done. The period is here set to $0.02\,\mathrm{s}$ and corresponds to the period of the sine wave from the generators.

Reverse recovery losses in the diode is found in the curve for dissipated energy as a function of diode current in the diode data sheet. The calculated switching and conduction losses are shown in 15 and are given in watts for each switch in the nine-switch converter and for all four switches in the fullbridge converter. The efficiency of the converter is then found to be 97.4% of a total of $11.0\,\mathrm{kW}$.

V. Discussion

This paper has presented a new converter topology for a double-input system to be used for multiple-generator wind turbines. Simulations verify that a square wave is obtained by the switching scheme utilized. There are some notches in the current input to the transformer, which will cause power losses. By using this converter in a multiple-generator wind turbine, the total number of switches can be reduced compared to a conventional back-to-back converter. With this converter system and by using the high frequency square wave in the transformer the size and weight, and thus cost, can then be reduced. Further work will include investigation of the current notches and the parallel connection of two converters as proposed in the nacelle layout. A rating of the converter will also be performed. As the generators share the same square wave voltage the voltage rating of the switches has to be two times higher than in a conventional back-to-back converter. An application where this feature is not evident would be a system consisting of two generating systems not operating at full power at the same time. A generating system with a diesel generator and a wind turbine or another varying power source could successfully take advantage of the nine-switch converter for a low number of switches and with no DC-capacitor necessary. In this system each generator would be rated for the full load and the converter should operate the generators so that a constant load power is obtained.

References

[1] Clipper Windpower Plc, *T*he Liberty 2.5 MW Wind Turbine, http://www.clipperwind.com/pdf/Liberty_Brochure_2009_LR.pdf, 2006.

[2] A. Garcés and M. Molinas, *C*luster Interconnection of Offshore Wind Farms Using Direct AC High Frequency Links, IEEE, 2007.

[3] T. Kominami and Y. Fujimoto, *A* Novel Nine-Switch Inverter for Independent Control of Two Three-phase Loads, IEEE, 2007.

[4] J. Cotrell, *A* Preliminary Evaluation Of a Multiple-Generator Drivetrain Configuration for Wind Turbines, National Renewable Energy Laboratory, 2002.

[5] A.B. Mogstad, *N*ew switching pattern for AC/AC converters with RB-IGBTS for offshore wind parks, NTNU, 2008.

[6] Taltronics, *A*pplication technologies of reverse-blocking IGBT, http://www.eepublishers.co.za/images/upload/Taltronics\%20267.pdf, 2007.

[7] C. Klumpner and F. Blaabjerg, *U*sing reverse-blocking IGBTs in power converters for adjustable-speed drives, IEEE Transactions on Industry Applications, 2006.

[8] M. J. Bland, P. W. Wheeler, J. C. Clare, L. Empringham, *C*omparison of Bi-directional Switch Components for Direct AC/AC Converters, Annual IEEE Power Electronics Conference, 2004.

[9] J. A. Houldsworth and D. A. Grant, *T*he Use of Harmonic Distortion to Increase the Output Voltage of a Three-Phase PWM Inverter, IEEE Transactions on Industry Applications, 1984.

[10] A. Odaka, J. Itoh, I. Sato, H. Ohguchi, H. Kodachi, N. Eguchi and H. Umida, *A*nalysis of loss and junction temperature in power semiconductors of the matrix converter using simple simulation methods, Industry Applications Conference, 2004. 39th IAS Annual Meeting.

[11] Kharitonov, S.A. and Petrov, M.A. and Korobkov, D.V. and Maslov, M.A. and Zhoraev, T.Y., *A* principle of calculation dynamic and static power losses with hard-switching IGBT, International Siberian Workshop and Tutorials on Electron Devices and Materials, 2005.

Marta Molinas received the diploma of Electromechanical engineer from the National University of Asunción, Paraguay in 1992; MSc from Ryukyu University, Japan, in 1997, and Doctor of Engineering from Tokyo Institute of Technology, Japan, in 2000. She is now Professor at the Norwegian University of Science and Technology engaged in the research of renewable energy systems. Her focus is in FACTS and power electronics for harvesting renewable energy.

Kristian Prestrud Astad is currently finishing his Master's Thesis in Electric Power Engineering at the Norwegian University of Science and Technology under the supervision of Prof. Marta Molinas. In his thesis he is working with a feasibility study about an AC/AC converter for wind power applications. His other fields of interest include motor drives and electric machines.